FRACTURE OPTIMIZATION BASED ON GRADIENT DESCENT METHODOLOGY

by

Jiaheng Chen

A thesis submitted to the Faculty and the Board of Trustees of the Colorado School of Mines in partial fulfillment of the requirements for the degree of Master of Science (Petroleum Engineering).

Golden, Colorado

Date _____

Signed: _____

Jiaheng Chen

Signed: _____

Dr. Yu-Shu Wu

Thesis Advisor

Golden, Colorado

Date _____

Signed: _____

Dr. Erdal Ozkan

Professor and Head
Department of Petroleum Engineering

ABSTRACT

Knowing that determining the geometry of the hydraulic fractures with horizontal wells is demanding yet challenging for petroleum engineers, in this thesis we have developed a computer program to automatically optimize the length, the conductivity as well as the spacing of hydraulic fractures in unconventional reservoirs.

In our program, the cumulative discounted Net Present Value (NPV) is selected as the target function and the gradient descent methodology is adopted as the optimizer. Relying on the gradient information, gradient descent searches for the optimal solution along the steepest decent direction. A comprehensive reservoir simulator, MSFLOW, with gas adsorption/desorption and Klinkenberg effect coupled, is adopted to obtain the production rate and NPV at each searching step. Armijo rule is used to determine the searching step size.

With the developed workflow, we have investigated the optimal geometry of the fractures with single horizontal well as well as zipper-type wells. We have observed that gradient descent method is able to quickly converge to the optimal point. Moreover, we have preliminarily studied the sensitivity of the optimization parameters. Our work can be readily adopted by reservoir engineers to guide the fracturing strategies in unconventional formations.

TABLE OF CONTENTS

LIST OF FIGURES

LIST OF TABLES

ACKNOWLEDGEMENTS

First of all, I want to thank my supervisor Dr. Yu-Shu Wu for taking care of me carefully and patiently throughout all these years, not only in academic, but also in life. He offered me a great research environment to work on and led me into the fascinating world of reservoir simulation. With his help, I have learned how to work on research from the very beginning and the essentials to be a good researcher. All these achievements are impossible without his supports, inspirations and encouragements.

My sincere thanks also go to the rest of my committee members Dr. Luis E. Zerpa, Dr. Azra Tutuncu, and Dr. Xiaolong Yin for their time to read this thesis and provide several valuable comments and suggestions. What I learned from them are essentially beneficial for completing this thesis. And also I really appreciate the supports from the staff of Petroleum Engineering Department, especially from Denise Winn-Bower and Rachel McDonald.

My deepest gratitude goes to my family. My parents and wife's support, suggestion, encouragement, patience and love are the bedrock upon which the past one year of my life have been built. Without them, I am not able to study at Mines and finish my advanced education. In addition, I would like to thank my colleagues in Energy Modelling Group and friends for their helpful advice during the research process.

CHAPTER 1
INTRODUCTION

Over the past 10 years, unconventional gas resources have evolved into a significant resource play in United State and the world because of the advance of technologies and their large reserves. Hydraulic fracturing, as one of most crucial completion techniques to the booming of unconventional gas resources, greatly improves the low permeability conditions of unconventional gas reservoirs and has become the technique by which most natural gas is produced from unconventional reservoirs in the United States. EIA estimates that natural gas production from hydraulically fractured wells now makes up about two-thirds of total U.S. marketed gas production (Perrin and Cook 2016). Under this circumstance, hydraulic fracturing design has been a focus of attention of the petroleum industry. Hydraulic fracturing always has a strong influence on drilling and completion cost and thus affects companies' benefit. According to a study by the University of Pittsburgh, $2.5 million is needed for the portion of hydraulic fracturing of the $7.6 million to drill and complete a single Marcellus Shale gas well (Hefley et al. 2011). The main factors that determine the costs and benefits are fracture half-length, dimensionless fracture conductivity, and number of fracture stages (fracture spacing). Therefore, an optimal fracture design (combination of the three above factors that works best for a reservoir) is essential to achieve the maximum revenue.

Optimal fracture design is a challenging problem because of large uncertainty associated with a particular reservoir. Although we have experienced engineers who consider and analyze a lot of cases, in most scenarios, the cases that are delivered are far from the optimal one (Bangerth et al. 2006). Thus, an efficient automatic optimization method is needed. It provides a systematic way to search a broader set of conditions and automatically find optimal ones by a given period of reservoir production and reservoir scenarios. Combined with specialists, these algorithms provide a powerful guide for decision-making, fracturing design and operation.

A lot of published papers have investigated the problems in oil/gas field, such as recovery processes, planning, history matching, well placement and operation and so on, using optimization methods. For example, Bangerth et al. (2006) compared gradient-based methods

(SPSA, FDG) and gradient free method (VFSA) for well placement problem. Asadollahi and Naevdal (2009) used steepest descent and conjugate direction methods (gradient-based) to evaluate the reservoir waterflooding optimization problem. Hajizadeh et al. (2009) introduced a new stochastic approach (ant colony optimization algorithm) for automatic history matching problem. Chen et al. (2012) also investigated history matching problem by applying three derivative-free algorithms (Very Fast Simulated Annealing (VFSA), Simultaneous Perturbation and Multivariate Interpolation (SPMI) and Quadratic Interpolation Model-based (QIM). Bellout et al. (2012) solved well placement using derivative-free methods based on pattern search. Cui (2016) utilized the improved particle swarm optimization for the post-stack impedance inversion problem.

In the past, it is true that there are many published papers, which already studied, devised and analyzed the hydraulic fracturing optimization topic. However, in most cases, researchers just did the sensitivity analysis by changing a certain parameter, but keep other parameters same. Or researchers just investigated parameters that influence reservoir behavior by experiments or in case studies. They indicated the parameters that will affect the production and how strong they will as these parameters' value increases or decreases. For instance, Brake (2013) concluded that the longer fractures perform better in Wamsutter based on historical fracturing data, performance data, surveillance data, and field trials data. But no answer is given to the optimal length. Saldungaray and Palisch (2012) investigated hydraulic fracture optimization through case studies by focusing on fracture geometry and conductivity. Their paper took Barnett Shale case as an example to indicate that optimal spacing increased with increasing fracture conductivity relied on sensitivity analysis (Saldungaray and Palisch 2012).

Few papers investigated fracture optimization based on mathematical optimization programs as well as the real-time information obtained from a reservoir simulator directly and gave specific sets of fracture properties for a specific reservoir. Yu and Sepehrnoori (2013) used Response surface methodology (RSM) approach to investigate optimization of multiple hydraulically fractured horizontal wells. RSM can be considered as an optimization method, but strictly speaking it is a statistical method that uses reasonable experimental design method and experiments to obtain some data. A multivariate quadratic regression equation is then used to fit the functional relationship between factors and response value. Through analyzing the regression

equation, RSM can find the optimal process parameters and solve the multivariable problem (e.g. Yu and Sepehrnoori (2013) regarded NPV as a function of porosity, permeability, fracture half-length, fracture conductivity, fracture spacing and well distance). In a nutshell, Yu and Sepehrnoori (2013) have conducted some numerical simulations by designed hydraulic fracture optimization variables and some real reservoir data and obtain the NPV values. Then, by using the method of RSM, the relationship between these optimization parameters and NPV is fitted and also could be plotted through a graphical technique. And finally, the objective, to obtain best economic scenario, is achieved. This is an acceptable method; however, it has several disadvantages. First, the RSM model can only be linear or fully quadratic, which constrains the diversity of fit equations and accuracy of the results. Second, a massive numerical simulation should be run to get reliable results. Therefore, the idea to utilize the gradient descent methodology is brought forward.

In this paper, optimization algorithms, based on gradient descent methodology, are introduced to solve the fracturing optimization problem and the optimal solution will be determined. There are several main reasons why this method is selected. First of all, gradient descent methodology is based on real-time information in the application process, that is, according to the instantaneous gradient information to determine the next search direction. Second, there is no need to fit the equation among variables and objective functions. Third, gradient descent is a basic gradient-based algorithm. Many algorithms, such as conjugate gradient method, are based on this method. It's easy to be changed to another gradient-based algorithm for continuous study in the future. Fourth, they need less information but provide reasonable results. Only the first derivative information is needed, which decreases the number of simulations. Fifth, it is a method that can be mathematically proven. Sixth, few researchers utilized this method to solve fracture optimization problems. Although this optimization algorithm has a number of advantages, it has a weakness. It cannot be guaranteed to find the global solution if the problem and its constraints are nonconvex, which is a common problem for all optimization algorithms nowadays, either gradient-based or gradient-free type. Although gradient-free type algorithm could help avoid being trapped at local optimum, they cannot be mathematically validated since many gradient-free algorithms are heuristics and they only can find good answers if reasonable initial input, domain, iteration numbers, and other factors are set.

For gradient-based methods, if the problem and its constraints are convex, gradient-based method will find the local optimal solution for sure, which is also the problem's global solution. If the problem is nonconvex, algorithms could be restarted with various initial points and select initial points systematically to obtain better solutions. In general, the advantages outweigh the disadvantages and thus the gradient descent methodology is chosen.

In Chapter 2, the numerical simulator MSFLOW, developed by Dr. Yu-Shu Wu, is introduced. It is a modified version specifically for unconventional gas reservoir. The governing flow equation and constitutive relations are well described. Two significant effects for unconventional gas reservoirs, gas adsorption/desorption and Klinkenberg effect, are integrated into MSFLOW. This version MSFLOW has also incorporated geomechanics effect (Wu 2005), but it is not applied for this thesis. A modified mesh system is created and programmed for the needs of optimization and existence of hydraulic fractures, which is illustrated in detail in the final part of this chapter.

In Chapter 3, the background of optimization is first introduced and then optimization parameters are selected. The principle of gradient methodology and the code structure are explained. The objective function, cumulative discounted-net-present-value, is chosen based on real field's economic application. And finally, the evaluation parameters are pointed out in performance indicators section.

In Chapter 4, the optimization system is checked through validation and simplified model, one-half of hydraulic fracture, is applied to improve the efficiency of the process of optimization, which is also validated and compared with regular model (original model). Sensitivities are also conducted as in other previous papers. Finally several real reservoir cases are designed and the best economic scenario and its corresponding optimization parameters' values are determined.

In Chapter 5, conclusions and suggestions are made. Some thoughts for future research work inspired during the thesis work are also discussed.

CHAPTER 2
MATHMATICAL AND NUMERICAL MODELS

In this chapter, a modified version of the numerical simulator MSFLOW (multiphase subsurface flow model of unconventional gas in porous and fractured reservoir) will be introduced. The modified version is driven by the need of industry to effectively simulate the production of natural gas from unconventional resources. The original MSFLOW is a three-dimensional numerical reservoir simulator developed by Dr. Yu-Shu Wu for modeling three-phase flow of Newtonian and non-Newtonian fluids of oil, gas and water in multidimensional porous and fractured reservoir (Wu 1998). The modified MSFLOW is used to model two-phase flow of gas and water, especially for shale gas, in multidimensional porous and fractured. The model is based on isothermal condition of shale reservoirs based on the conclusion by Moridis et al. (2010) from their modeling studies. Moridis et al. (2010) concluded that inclusion of heat exchange in the gas production for shale or tight-sand does not have any advantages since the prediction of the model are practically identical. The modified version incorporates some of the characteristic and flow behavior recognized for controlling flow in unconventional gas reservoirs based on publications in the past few years. These flow behavior and physical processes include:

- Nonlinear and multiphase flow (Darcy and non-Darcy flow);
- Modified permeability due to Klinkenberg effect (gas slippage effect);
- Nonlinear gas adsorption/desorption
- Geomechanics effects on stress sensitive permeability of porous and fractured rock;

In addition, for the purpose of thesis research, the MESH system is also modified to model hydraulic fracture systems as a discrete fracture. Apart from these modifications, all the features of modified MSFLOW are the same to original MSFLOW, such as discretization techniques, code structure and so on. The necessary parts of the simulator are illustrated in this chapter. For more detailed information about the knowledge of simulation and the simulator refer to the book *Multiphase Fluid Flow in Porous and Fractured Reservoirs* by Dr. Wu (Wu 2015) and the MSFLOW manual (Wu 2005).

2.1 Introduction

Unlike reservoir simulators from CMG and Schlumberger, which have visual interfaces where users are able to type input parameters based on screen tips, users are supposed to utilize the specific input system when operating MSFLOW. The input system of MSFLOW adapts the data input conventions used by the TOUGH and TOUGH2 (Pruess 1987; Pruess 1991) and has the following features:

- all input data is organized in data blocks by keywords, such as ROCKS, ELEME, CONNE, GENER, INCON, PARAM, FLUID, PVTDA and so on;
- all input values will be read as fixed formats;
- SI units are adapted;
- Interfacing with several disk files.

All the keywords and their corresponding sub-information are arranged in order inside the input file and then will be read accordingly into MSFLOW to finish a simulation process. The keyword ROCKS is one of the most crucial parts, which includes constitutive relations, parameters for formation, Klinkenberg parameter, gas adsorption/desorption parameter and etc.

2.2 Mathematical Flow Model and Governing Equations

In general, a multi-phase flow model (gas-water flow), instead of a compositional model, is usually considered sufficient for most shale gas simulations since the most important thing that we are concerned with is to simulate the gas flow from the reservoir to well. Everything else is less significant excluding liquid phase flow. This is because the liquid phase flow is always occurring simultaneously with gas flow and will influence gas production. Liquid phase flow is supposed to be taken into consideration for the following conditions:

- in-situ connate water exists;
- aqueous hydraulic fracturing fluids exists;
- large amount of gas condensate may exist under in-situ reservoir pressure and temperature during production.

In this paper, we will mainly discuss two-phase (gaseous and aqueous phases) flow models for unconventional gas reservoir simulations. The model is assumed to be isothermal and

composed of two phases. For simplicity, the gas and water components are supposed to present only in their associated phases. Each phase flows will response to pressures, capillary forces and gravity based on the multiphase extension of Darcy's law or non-Darcy laws. To fully describe the flow system, two mass balance equations are needed. The mass balance equation (Equation 2-1) with adsorption term included for the two phases is written in an arbitrary flow region as follows:

$$\frac{\partial}{\partial t}\left(\phi S_\beta \rho_\beta + m_g\right) = -\nabla \cdot \left(\rho_\beta \overrightarrow{v_\beta}\right) + q_\beta \qquad (2\text{-}1)$$

where β represents different phases (β =g for gas phase and β =w for water phase); t is time; ϕ is the effective porosity of porous or fracture formation; S_β is the saturation of phase β ; ρ_β is the density of phase β ; m_β is adsorbed or desorbed gas mass per unit volume of formation; v_β is the volumetric velocity vector of phase β , which is determined by Darcy's law or non-Darcy laws and will be discussed below; and q_β is the sink/source term of phase β per unit volume of formation.

The governing partial differential equations for mass conservation equations of two-phase are discretized spatially by using integral finite difference (IFD) technique (Narasimhan and Witherspoon 1976; Pruess 1991). The time discretization is conducted by a backward, first-order finite difference method. The final discrete non-linear equations are then solved by Newton/Raphson iteration scheme fully implicitly to provide stability and large time step size or Adaptive Implicit Method (AIM) as an option to speed up the simulation time and reduce space storage requirement. The IFD method has been proven to be computationally efficient in handling highly non-linear flow problems and complicated geometry or irregularity of a reservoir domain. The detailed discretization information is attached in Appendix A.

2.3 Constitutive Relations

The governing equation (Equation 2-1) of mass conservation for two phases needs to be supplemented with constitutive equations. All these constitutive equations are expressed as functions of a set of primary thermodynamic variables of interest to completely describe the relationships for multiple phase flow through porous or fractured media.

2.3.1 Saturation Constraint

The saturation relationship between phases is constrained by equation:

$$S_w + S_g = 1 \tag{2-2}$$

2.3.2 Capillary Pressure Function

Capillary pressure function relates the pressure relationship between two phases. The function below shows the aqueous and gas phases pressure relationship; P_{cgw} represents the gas-water capillary pressure, which is assumed as a function of water saturation only. Generally, in MSFLOW, this kind of relationship is supplied by a table lookup.

$$P_w = P_g - P_{cgw}(S_w) \tag{2-3}$$

2.3.3 Relative Permeability Functions

The relative permeabilities are assumed as function of phase saturations only. The relative permeability to water phase is described as:

$$k_{rw} = k_{rw}(S_w) \tag{2-4}$$

to gas phase,

$$k_{rg} = k_{rg}(S_g) \tag{2-5}$$

Similar to capillary pressure data, the relative permeabilities are usually inputted as tables. However, when the relative permeabilities are not available, two functional forms of two-phase relative permeability are also provided as alternatives. The first function is Brooks-Corey type (Honarpour et al. 1986) and the two-phase relative permeability function form is:

$$k_{rw} = (\overline{S_w})^{2+\varphi} \tag{2-6}$$

$$k_{rg} = (\overline{S_g})^2[1-(\overline{S_w})^{\varphi}] \tag{2-7}$$

Another two-phase relative permeability function of the van Genuchten model is given by (Kaluarachchi and Parker 1989):

$$k_{rw} = (\overline{S_w})^{1/2}\{1-(1-(\overline{S_w})^{1/\gamma})^{\gamma}\}^2 \tag{2-8}$$

$$k_{rg} = (\overline{S_g})^{1/2}\{1-(\overline{S_w})^{1/\gamma})^{2\gamma} \tag{2-9}$$

where $\overline{S_w}$ is defined in Equation 2-10, $\overline{S_g}$ is defined in Equation 2-11, φ is defined in Equation 2-12, λ in the Equation 2-12 is the Brook-Corey pore size distribution index and γ is defined in Equation 2-13.

$$\overline{S_w} = \frac{S_w - S_{wr}}{1 - S_{wr}} \tag{2-10}$$

$$\overline{S_g} = \frac{S_g - S_{gr}}{1 - S_{wr}} \tag{2-11}$$

$$\varphi = 1 + \frac{2}{\lambda} \tag{2-12}$$

$$\gamma = 1 - 1/\beta \tag{2-13}$$

2.3.4 PVT Data, Fluid Viscosities and Porosity

The density of water under reservoir conditions could be treated as a function of formation volume factor (FVF) as Equation 2-14 shows:

$$\rho_w = \frac{(\rho_w)_{STC}}{B_w} \tag{2-14}$$

The density of gas is calibrated from ideal gas to real gas by Z factor, which is usually obtained directly from inputted PVT table or indirectly by interpretation based on PVT table. But it could be also calculated by any equation of states (EOS), such as Peng-Robinson EOS. Equation 2-15 shows the relationship of density with Zg factor, universal gas constant R, pressure P, temperature T and average molecular weight Mg.

$$\rho_g = \frac{Z_g M_g P}{RT} \tag{2-15}$$

Gas viscosity, if it is obtained based on a PVT table, is found similarly to the way that gas density is calculated (by interpolation or direct read). If not, the Lee, Gonzalez and Eakin (Lee et al. 1966) correlation will be used for gas viscosity calculation as Equations 2-16 to 2-19 show.

$$\mu_g = 10^{-4} K \exp(X \rho^Y) \tag{2-16}$$

where,

$$K = \frac{(9.379 + 0.01607 M_w) T^{1.5}}{209.2 + 19.26 M_w + T} \tag{2-17}$$

$$X = 3.448 + \left[\frac{986.4}{T}\right] + 0.01009 M_w \tag{2-18}$$

$$Y = 2.447 - 0.2224 X \tag{2-19}$$

and inside the equation, ρ and μ_g are density and gas viscosity at given temperature and pressure, the units of which are g/cm^3 and cp respectively. T is the temperature with unit $^\circ R$ and M_w is molecular weight of gas mixture with unit lb/lb-mole.

For effective rock porosity, it is assumed as a function of reservoir pressure and temperature as Equation 2-20 shows if geomechanics effect is not considered. Otherwise, correlations based on experiments will be used. Details about commonly used rock-property correlations and coupled geomechanics effect are presented in the MSFLOW manual (Wu 2005).

$$\phi = \phi^\circ (1 + C_r (P - P^\circ) - C_T (T - T^\circ)) \tag{2-20}$$

2.4 Incorporation of Klinkenberg effect

Gas flows are quite different from liquid in porous media because of its high compressibility and Klinkenberg effect (gas slippage effect). Klinkenberg effect might be significant to be neglected especially in low-permeability shale gas media with Nano-size pores and low reservoir pressure condition (Wu et al. 1998). Under these condition, the mean-free-path of molecules ($\bar{\lambda}$) is much larger than the characteristic dimension of conduit (Λ); the collision of the molecules with the conduit wall is more frequent than the collision with

themselves as Figure 2-1 shows. The “continuum hypothesis” and “no-slip” boundary condition cannot be applied anymore. Slip flow then happens and gas permeability is enhanced by “slip flow”. Thus, it is expected that Klinkenberg effect is the greatest in fine-grained, lower permeability porous media.

Figure 2-1 Low Velocity, Slip Flow (Klinkenberg effect)

In 1941, Klinkenberg observed that the apparent permeability to gas was dependent on the reciprocal of the mean flowing pressure (Klinkenberg 1941). And based on the molecular theory of Kundt and Warburg, Klinkenberg derived the following expression (Equation 2-21), which modified absolute permeability for the gas phase and was incorporated into MSFLOW:

$$k_g = k_\infty (1 + \frac{b}{P_g}) \tag{2-21}$$

where k_∞ is the absolute, gas phase permeability under very large gas phase pressure (when Klinkenberg effect is negligible); and b is the Klinkenberg factor, which depends on the pore structure of the medium and formation temperature for a given gas. Klinkenberg factor b is often determined by laboratory and treated either as constant or as a function of pressure (e.g., Ertekin et al. 1986) or Knudsen number.

The dynamic slippage model developed by Ertekin et al. (1986) is based on simultaneous flow resulting from viscous (Darcian) and diffusion (Fickian) flow processes and yields a pressure, composition and saturation-dependent (multiphase-flow) slippage factor (Ertekin et al. 1986). The factor is not constant anymore but a several-parameters-dependent value. The equation is given by:

$$b_a = \frac{D\mu c_g p}{k} \tag{2-22}$$

where c_g is gas compressibility and D is diffusivity coefficient.

2.5 Incorporation of Gas Adsorption and Desorption

Unconventional gas resources (shale gas) are distributed in large areas around the world and have an enormous potential for exploitation. Among shale gas reservoirs, gas exists in three forms: 1) as free gas in cracks, 2) as free gas in matrix pores, 3) as adsorption gas (Lane et al. 1989). Gas adsorption is usually closely related to the quantity of high organic matter or carbon-rich components, i.e. kerogen (Lu et al. 1995; Mengal and Wattenbarger 2011). Generally, shale reservoirs contain high organic matter as well as clay minerals. The pore structure of shale could provide large specific surface area, which enables the possibility of gas adsorption.

The phenomenon of gas adsorption has significant influence on the total gas reserves (20-80%), recovery rates and gas production resulting from gas desorption (absorbed gas is released as free gas) when reservoir pressure decreases with continuous gas production, thus it cannot be neglected in any analytical model or numerical model. Therefore, it is rather important to incorporate the gas adsorption or desorption term into mass conservation Equation 2-1 of our numerical model.

Based on International Union of Pure and Applied Chemistry (IUPAC) standard classification system (Sing et al. 1985), there exist six type diverse types of gas adsorption isotherms as shown in Figure 2-2. The detailed information about these adsorption isotherm classifications can be found in Sing et al. (1985). The shape of the curve is tightly related to pore-space geometry and the properties of adsorbate and solid adsorbent (Silin and Kneafsey 2012). Type I is the well-known Langmuir adsorption isotherm, which is widely accepted by academy and industry and so it will be used and incorporated into MSFLOW. The theory assumes there is a dynamic equilibrium between adsorbed and non-adsorbed gas at certain pressure and temperature (Langmuir 1918). According to Langmuir's isotherm (1918), the gas stored in shale is often described as:

$$V_E(P) = V_L \frac{P}{P + P_L} \tag{2-23}$$

where V_E is gas content in scf/ton (or standard volume adsorbed per unit rock mass), V_L is the Langmuir volume in scf/ton, P is the reservoir pressure in psi, and P_L is the Langmuir pressure in psi, the pressure at which one-half Langmuir volume of the gas is desorbed.

In order to incorporate the gas adsorption/desorption mass term into the mass balance equation, the transfer function is needed, and it is described as equation (Wu et al. 2012):

$$m_g(V) = \rho_k \rho_g f(P) \overline{S_k} V \tag{2-24}$$

where $m_g(V)$ is adsorbed gas mass in bulk formation volume V, ρ_k is kerogen density, ρ_g is gas density at standard condition, $\overline{S_k}$ is the average volume relative of kerogen in bulk volume and $f(P)$ is the adsorption isotherm function, which can be any correlation functions but in our model it is Langmuir isotherm function.

$$f(P) = V_E(P) = V_L \frac{P}{P + P_L} \tag{2-25}$$

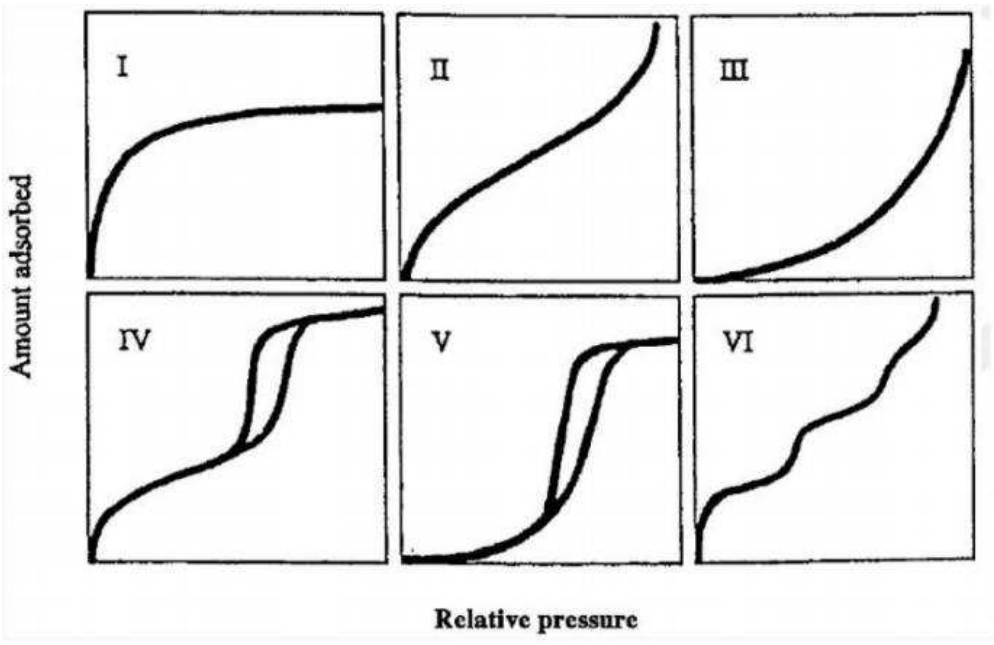

Figure 2-2 Six Types of Adsorption Isotherms according to IUPAC Classification (Sing et al. 1985)

2.6 Darcy's Flow and Non-Darcy Flow

The term v_β is the volumetric flow velocity in governing flow equation, which will be defined differently under various flow regimes or situations. Thus, it will be discussed in the following paragraphs.

When Darcy's law is applicable, the term v_β is defined as:

$$v_\beta = -\frac{kk_{r\beta}}{\mu_\beta}(\nabla\Phi_\beta) \tag{2-26}$$

$$\nabla\Phi_\beta = \nabla P_\beta - \rho_\beta g \nabla Z \tag{2-27}$$

where k is the absolute permeability for the porous or fractured media; if Klinkenberg effect is considered, permeability needs to be updated with Equation 2-21 for gas phase; $k_{r\beta}$ is relative permeability to phase β as described in Section 2.3.3; μ_β is the viscosity of phase β and is treated as Section 2.3.4 describes; and $\nabla\Phi_\beta$ is flow potential gradient defined as Equation 2-27; inside the Equation 2-27, P is the pressure of phase β, g is gravitational acceleration constant, and D is depth from a datum.

Except multiphase Darcy flow, nonlinear flow behavior of gas is also observed in shale gas reservoir, such as high velocity non-Darcy flow inside the continue (e.g. the flow near production well when reservoir is hydraulic fractured) in tight or shale gas reservoirs. Under this condition, the term v_β is described by using the multiphase extension of the Forchheimer equation (e.g., Wu 2002):

$$-\nabla\Phi_\beta = \frac{\mu_\beta}{k_{r\beta}} k v_\beta + \beta_\beta \rho_\beta v_\beta \mid v_\beta \mid \tag{2-28}$$

where the new term β_β is the effective non-Darcy flow coefficient for fluid β in unit m^{-1}.

2.7 Mesh System

Mesh or grid generation is one of the most significant steps before performing a simulation. MSFLOW adapts a meshmaker system from TOUGH2 code, which is able to

generate 1D or 2D radially symmetric R-Z grids or 1D, 2D or 3D cartesian (rectilinear) X-Y-Z grids under keyword RZ2D or XYZ. For naturally fractured reservoirs, the method of "Multiple Interacting Continua" (MINC) is generalized to permit a fully transient description of interporosity flow.

2.7.1 Modified Automatic XYZ Mesh

Due to existence of fractures, specifically designed grid systems are needed to model fractures explicitly. There are two ways to realize this goal. The first approach is local grid refinement (LGR) method, which refines structured meshes intersected by fractures at the scale of fractures width. This way, the fractures then become a set of small size and high permeability grids and thus improve numerical accuracy. Another approach is to insert fractures and treat these fractures as internal boundaries. The approach used in the thesis is the first one and the details as well as features are illustrated below.

The refinement is based on the original XYZ mesh system. The original mesh system can deal with grid increments but not automatically, which means specified grid increment values in X, Y or Z direction should be calculated and then typed into the input file. This is inconvenient and impossible for the goal of automatic fracture optimization. Thus, modified automatic XYZ mesh with logarithmic refinement is then created. The modified mesh system can create multiple hydraulic fractures at desired place with specific widths, lengths as well as heights and at the same time provide refinement. The hydraulic fractures are not necessarily uniform displayed. The refinement could be done in the direction of X, Y and Z through logarithmic function and the size of the mesh could be controlled by a parameter α. In order to accelerate the process of reservoir simulation and fracture optimization, the refinement is only conducted in the direction of X and tips of hydraulic fracture of the direction Y. The hydraulic fracture parts are handled by uniform spacing based on the hydraulic fracture half length.

Another feature of this modified mesh system is that it has an internal program to identify the different rock types (matrix, hydraulic fracture, well) based on their location information. In addition, the reservoir information, like length, width and depth, and the well information could be also taken into consideration. Following are three mesh systems created by the modified automatic XYZ system. Figure 2-3 shows a reservoir (1000 m*300 m*100 m) mesh with five

uniform-distributed hydraulic fractures. The hydraulic fracture grids have a width of 0.1 m and they are located at 100 m, 300 m, 500 m, 700 m and 900 m separately in X direction. They extend from 50 m to 250 m in Y direction and all through Z direction. Figure 2-4 shows a reservoir (1000 m*300 m*100 m) mesh with four non-uniform-distributed hydraulic fractures. The hydraulic fracture grids have a width of 0.1 m and they locate at 59.95 m, 199.95 m, 359.95 m, and 699.95 m separately in X direction. They also extend from 50 m to 250 m in Y direction and all through Z direction. Figure 2-5 shows a mesh sample with a reservoir (200 m*300 m*100 m) mesh with one hydraulic fracture located at the rightmost of X direction. The hydraulic fracture grids also have a width of 0.1 m and extend from 0 m to 60 m in Y direction and all through Z direction.

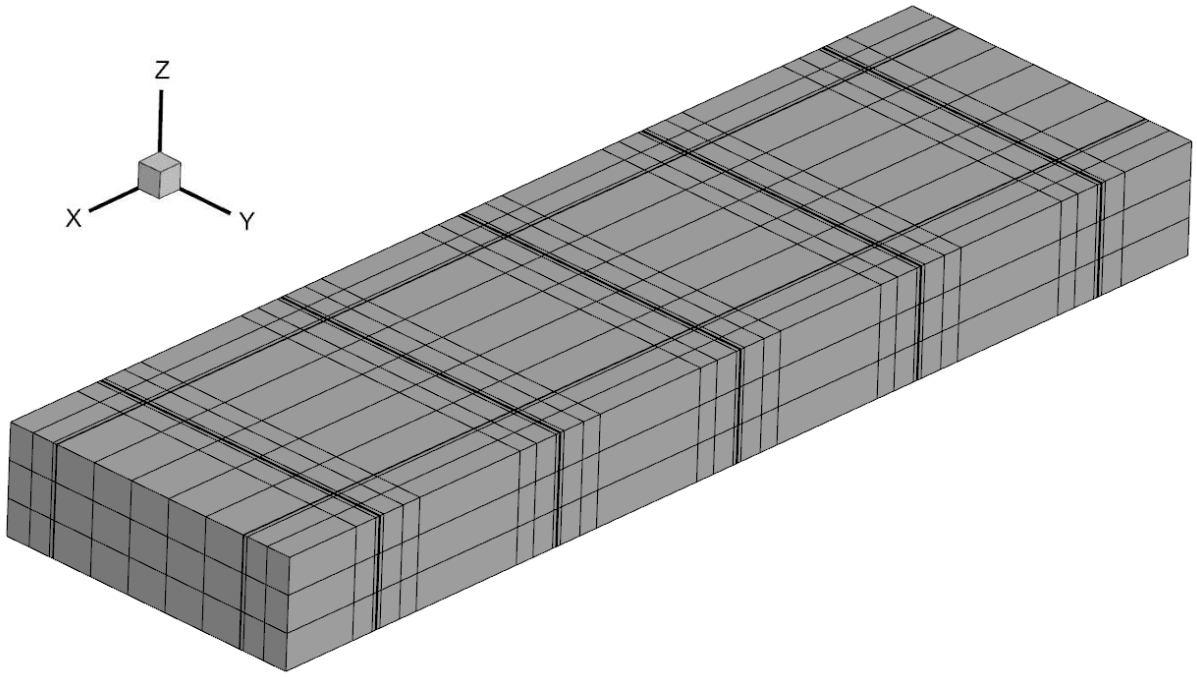

Figure 2-3 Mesh System with Five Uniform-distributed Hydraulic Fractures

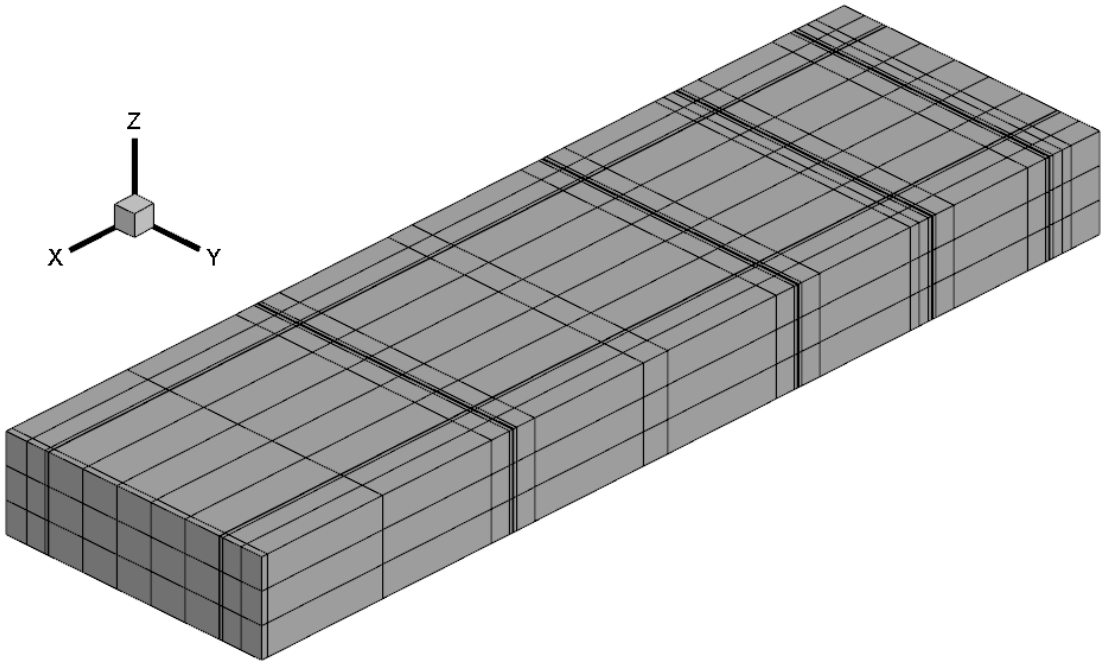

Figure 2-4 Mesh System with Four Non-uniform-distributed Hydraulic Fractures

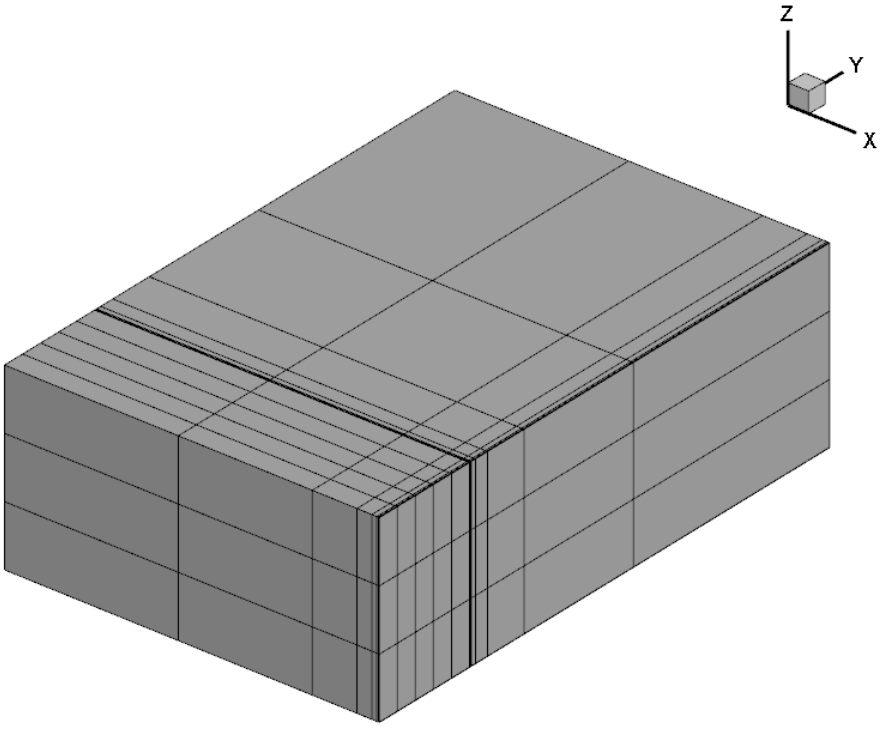

Figure 2-5 Mesh System with One Hydraulic Fracture (at the rightmost)

2.7.2 MINC Method for Handling Fractured Media

The MSFLOW applies a generalized multi-continuum approach to model fracture and porous matrix interaction and flow, which includes DP (double-porosity) method (Warren and Root 1963), the multiple porosity method (Wu and Pruess 1988), the dual-permeability method, and more general MINC method (Pruess and Narasimhan 1985).

The main function of MINC (Pruess 1983) is to sub-partition a "primary" porous medium grid into a "secondary" grid for fractured media. MINC method is much more rigorous than classical double-porosity approach, which is based on quasi-steady state flow assumption. The reason is because it describes gradients of pressure forces between matrix and fractures by appropriately sub-partition matrix block. MINC approach assumes that the change of fluid pressure will slowly invade the matrix block but propagate the fracture blocks rapidly, which means that the condition of matrix will be significantly determined by local distance between matrix and fracture. Based on the theory above, the fluid flow between porous media and fracture media can be treated as one-dimensional strings of nested grid blocks (Pruess 1991) and this conceptual model is shown in Figure 2-6.

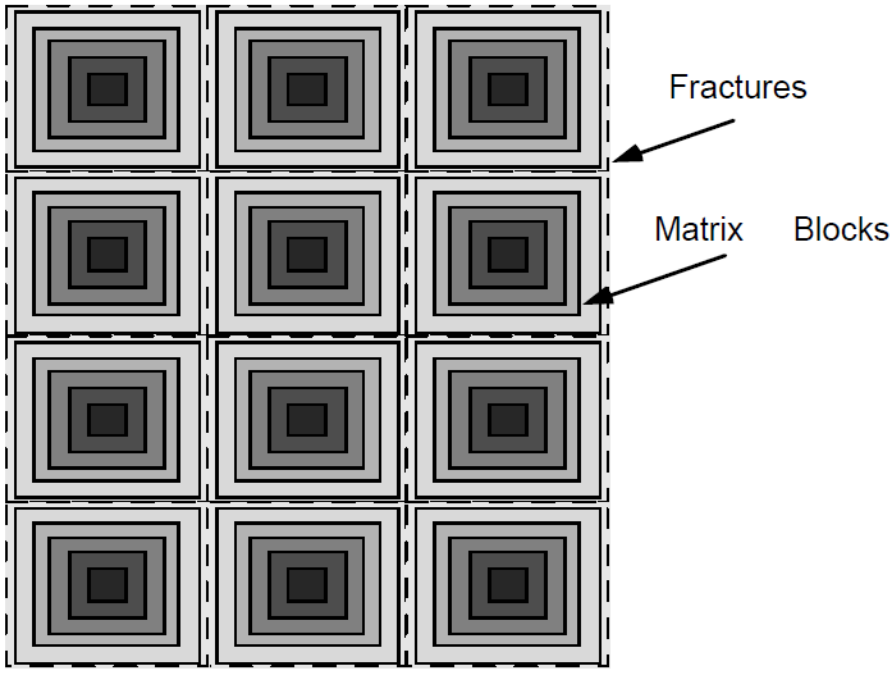

Figure 2-6 "Multiple Interacting Continua" (MINC) Subgridding (Pruess 1991).

MINC method can also consider “dual permeability” model but with certain accuracy sacrifice since both the matrix and fracture are approximated as one grid block and thus some quasi-steady state flow assumption should be made. However, the model will work fine under steady-state due to the minimal gradients around matrix surfaces. MINC method is applicable for most cases only if the reservoir fracture systems are not so sparse. Specifically, for a two continua case, the MINC method is the same as conventional double-porosity or dual-permeability model.

CHAPTER 3
OPTIMIZATION SYSTEM

In this chapter, the background of optimization is first introduced. The questions, such as what an optimization problem is, the application areas of optimization in oil and gas industry, the classification of optimization methods and so on, are answered. Then, the optimization system is explained. Basically, the optimization system is separated into five main parts: optimization parameters, optimization algorithms, reservoir simulator, objective function, and evaluation. Fracture half-length, dimensionless conductivity, and numbers of fracture stage (fracturing spacing) are chosen as fracture optimization parameters due to their significant effects on fracture behaviors. The optimization algorithm selected for the thesis topic is the gradient descent algorithm (also called steepest descent algorithm), which belongs to category of the gradient-based optimization methodology. The reservoir simulator MSFLOW is discussed in Chapter 2, so it will not be illustrated in this chapter. But one point to keep in mind is that it acts like a black-box or function and gives necessary information. The objective of this thesis is to realize the maximum profits for a given period and thus cumulative discounted-net-present-value (NPV) is picked as an indicator. The calculation of the NPV is based on how it operates in the real oil field. To the chapter end, three performance indicators of optimization algorithm are taken into consideration to evaluate the optimization method.

Generally, the optimization system is organized by the following steps regardless of types of objective functions: 1) Optimization algorithm is coded by MATLAB; 2) optimization starts with a or a set of initial guesses; 3) Input files and Mesh system are initialized based on initial guess; 4) reservoir simulator MSFLOW is run to obtain the required data (gas production and water production) for NPV and cumulative discounted-NPV calculation; 4) Cumulative discounted-NPV results are compared and next step of optimization parameters are updated according to the compared results; and 5) optimization system ends when a certain criteria or goal is achieved. Details of the gradient descent optimization algorithm will be expanded in the following sections.

3.1 Introduction

Optimization is always the core objective of our life and massive numbers of techniques have been developed since early ages of civilization. Starting from early 1950s, optimization techniques have been applied to oil and gas industry and are booming now. Applications have been reported for recovery processes, planning, history matching, well placement and operation, drilling, facility design and operation and so on. Optimization techniques employed in these applications cover almost all subfields in mathematical programming, such as linear programming, integer programming, stochastic programming and nonlinear programming (Wang 2003). Before these techniques are discussed, the definition of optimization problem will be clarified first. A simple optimization problem can be described as following:

Given f is a real valued function of several real variables $x_0, x_1, x_2, \ldots, x_n$. Then optimization problem or a mathematical programming problem is the problem that seeks to minimize (or maximize) $f(x_0, x_1, x_2, \ldots, x_n)$ subject to $x_0, x_1, x_2, \ldots, x_n \in \Omega$, where Ω is a subset of the domain of f. The function $f(x_0, x_1, x_2, \ldots, x_n)$ is called, an objective function, a loss function or cost function, while the set Ω is often termed as feasible solution and $x_0, x_1, x_2, \ldots, x_n$ are termed as control variables. A feasible solution that minimizes (or maximizes, if that is the goal) the objective function is called an optimal solution. Depending on the definition of Ω, the problem will be considered unconstrained or constrained. For example, if $\Omega = \{(x_0, x_1, x_2, \ldots, x_n) : each \ x_i \in R\}$, then problem is said to be unconstrained. But if the set Ω is defined by a system of equations or inequalities, then problem is said to be constrained. In petroleum, these constraints can be categorized into two types, capacity, safety and economic constraints (Asadollahi and Naevdal 2009). Oil production constrained by capacities of surface facilities is an example of capacity constraints. Safety constraints will be the problem such as limited pressure at the bottom of a well or some surface facility nodes and economic constraints will be the case like minimum flow rate to ensure the economic feasibility.

Generally, the objective in oil industry is to maximize the profit. The objective function is usually nonlinear and nonconvex due to the complex relations among control variables. Convex problem can be viewed as a special case of nonlinear programming. We always treat oil field

problems as nonconvex problems unless both the objective function and the feasible region are convex. The convex problem is simple since its local minimum or local maximum is also the global minimum. However, a nonconvex problem might have more than one local minimum or local maximum, which leads to the difficulty of searching global minimum or maximum. A large number of optimization techniques or algorithms have been developed for solving these nonlinear convex or nonconvex problems.

From prospective of whether a gradient is applied, the optimization can be into two categories (check below diagram): gradient based and gradient free optimization. For gradient based optimization, the common and frequent used methods include Newton's method, conjugate gradient method, Quasi-Newton method, gradient descent method and so on. For gradient free optimization methods, genetic, simulated annealing, direct, and Nelder-Meade algorithms probably are the most well-known.

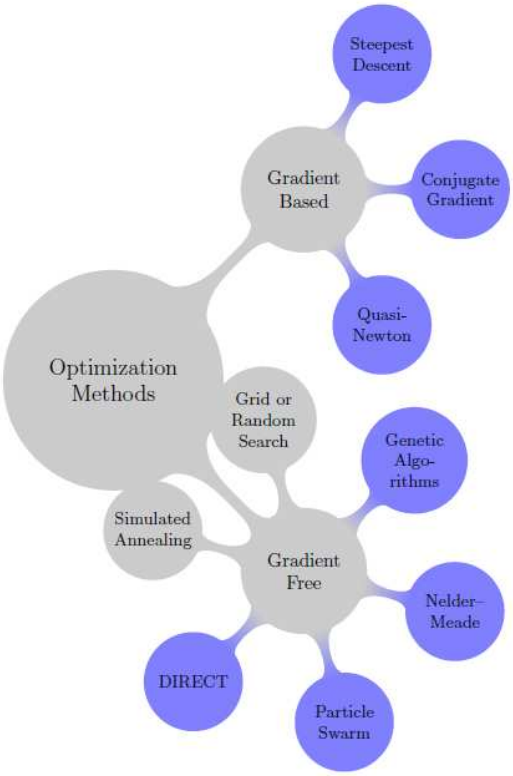

Figure 3-1 Optimization Methods for Nonlinear Problems (Martins et al. 2017)

Any optimization method substantially tries to find a set of the nearest or next best parameters from the initial parameters that will optimize the given function by terminating in a finite number of steps, or iterative methods that converge to a solution, or heuristics that may provide approximate solutions. In gradient based optimization, gradient is applied to get these parameters. The methods with gradient often require a large computation effort. The function is called at least N times each iteration if N variables are operated and only 1st derivatives (collected in Jacobian matrix) are needed. For methods that require 2nd derivatives (collected in Hessian matrix), each iteration will need N*N times function evaluation, which is really time consuming and cost overwhelming, especially for optimization problems that use a reservoir simulator. Reservoir simulator will act as the function or black box that needed to be run massive number of times. Since the gradient at any local minima or maxima is zero, there is a possibility that the optimal solution will be stuck in a local area and thus a global optimization will never be found. In addition, gradient based optimization algorithms have the following challenges: non-differentiable functions and/or constraints, disconnected and/or non-convex feasible space, discrete feasible space, mixed variables (discrete, continuous, permutation), multiple local minima (multi-modal) and multiple objectives. The graph below shows the problematic problems for gradient based optimization algorithms.

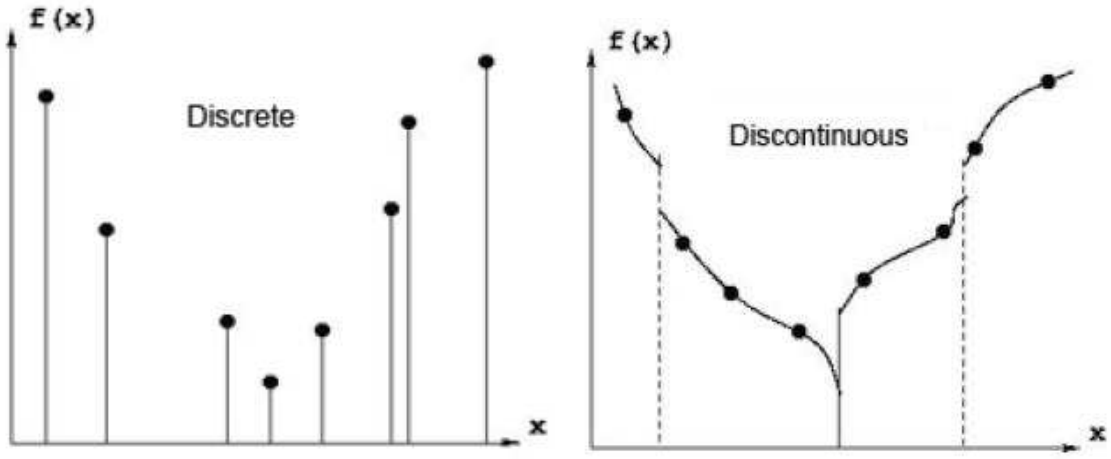

Figure 3-2 Problematic Problems for Gradient Based Optimization Algorithms (Martins et al. 2017)

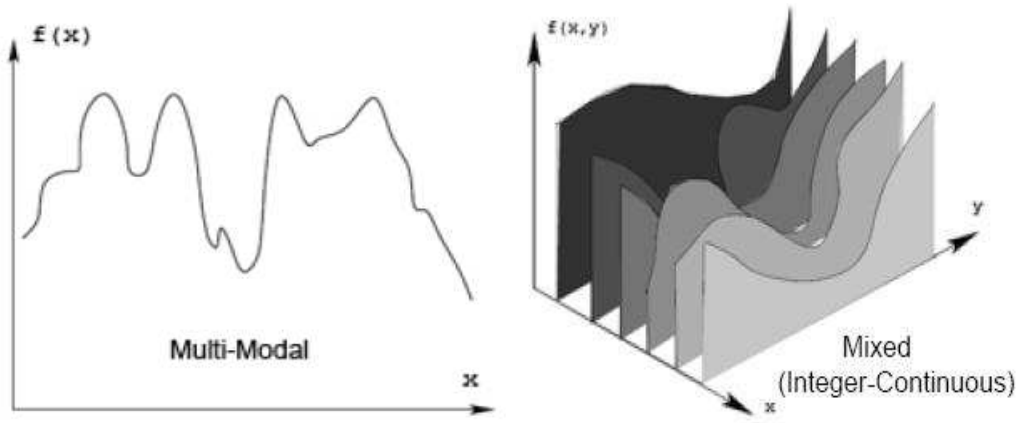

Figure 3-2 Continued

There are several ways to solve the questions above. First, start from multiple points for gradient based optimizer. Second, systematically search the design space. Third, use gradient-free optimizers. Most gradient-free methods mimic mechanisms that scientists observe from nature or use heuristics, such as Particle Swarm Optimization (PSO), which is inspired by a nature behavior of living organisms (a bird flock, fish school or ant colonies) searching for some targets (like food) and was developed by James Kennedy and Russel Eberhard for optimization process in 1995 (Kennedy and Eberhard 1995). Other similar gradient-free methods include Genetic Algorithms (GA), Simulated Annealing (SA) and so on. Gradient free methods are free from the "gradient faults" that are mentioned above and are able to find multiple local optima while searching for global optimum. However, unlike gradient-based methods, gradient free methods are not guaranteed to find true global optimal solutions and are not mathematically provable, but they are able to find many good solutions (the mathematician's answer vs. the engineer's answer) (Martins et al. 2017).

3.2 Optimization Parameters

A primary goal in unconventional reservoirs is to contact as much as rock as possible with a fracture or fracture network of appropriate conductivity. This objective is achieved by drilling horizontal wells and placing multiple transverse fracs along the lateral. Reservoir contact is typically optimized by defining the lateral length, the number of stages to be placed in the lateral, the fracture isolation technique and job size (Saldungaray and Palisch 2012). That's

why fracture half-length, dimensionless conductivity, and numbers of fracture stages (as a manner of fracturing spacing) are selected as fracture optimization parameters. And the sensitivity analysis in the Chapter 4 show their influences on gas production.

Optimization parameters have a boundary according to real conditions in the gas field. The numbers of fracture stages are controlled within two and fifty based on the average stages in Marcellus and Delaware gas field as Table 3-1 shows. Fracture half-length ranges from 0 m to 300 m and dimensionless fracture conductivity is set within 0 and 100.

Table 3-1 Average fracture stages number in real gas field (U.S. EIA 2016)

Year	Marcellus Average Stage	Delaware Average Stage
2010	12.93	8.62
2011	14.06	10.89
2012	18.91	11.12
2013	22.05	12.68
2014	27.89	16.25
2015	32.11	21.58
2016	35.00	22.92
2017	36.57	24.04
2018	38.24	24.89

Notice that, in the real process of optimization, the numbers of fracture stage will be replaced by fracturing spacing, which ranges from 20 m to 500 m. One reason is that the numbers of fracture stages cannot be displayed as decimals due to physical meaningless and thus they should be integers only. Another reason is that the integers values of fracture stages will led to the discontinuity of objective function and thus the function is not differentiable. Both of them will make the gradient descent methodology inapplicable. However, there is no problem when hydraulic fracture spacing is used.

In our optimization, one-half of a hydraulic fracture, represented by one fracture spacing length reservoir area, is simulated (as Figure 3-3 shows). The final production will be calculated by using the reservoir length to divide the hydraulic fracture spacing and then multiply by two as

Equation 3-1 shows. But, it is essential to point out that the prerequisite for doing this is that the hydraulic fracture is symmetrically distributed. This theory will be validated in Chapter 4.

$$prod_{total} = prod_{1/2} * \frac{Reservoir\ Length}{HF\ Spacing} * 2 \tag{3-1}$$

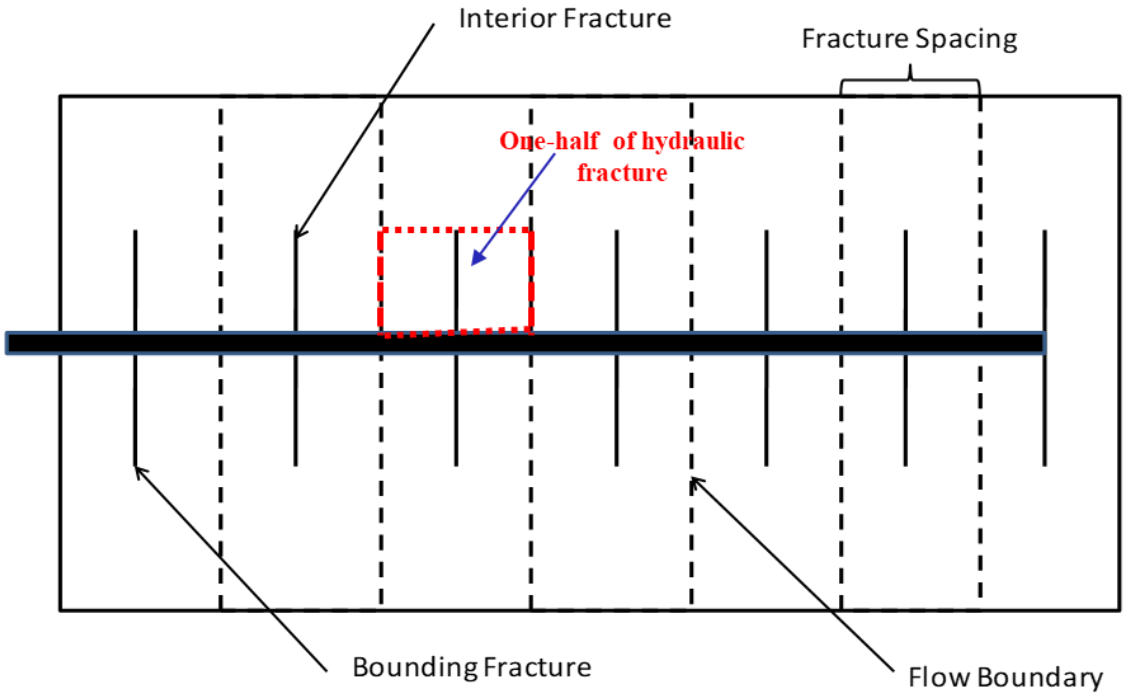

Figure 3-3 Simplified Model's Schematic Diagram

Another point I want to mention is that dimensionless fracture conductivity essentially changes the permeability of hydraulic fractures and thus affects reservoir productivity. The formula in optimization system is given by:

$$k_{f\_true} = \frac{F_{cd} * k_m * HFhl}{dfrac} \tag{3-2}$$

where k_{f_true} is the real hydraulic fracture permeability (corresponding hydraulic fracture permeability to grid width of hydraulic fracture $dfrac$), F_{cd} is real dimensionless fracture conductivity, and k_m matrix permeability.

3.3 Gradient Descent Methodology

Usually, among unconstraint optimization problems, different ways to determine the search direction or search step results in different algorithms. Method of gradient descent, also called steepest descent, is the simplest and oldest optimization algorithm to find the minimum of an unconstraint problem. Gradient descent gets its name since it is a first-order iterative method based on observation that descends by taking steps in the opposite gradient direction of the function at given point. Why opposite gradient direction? It is because that opposite gradient direction is the fastest direction that the value of the function changes. The explanation is following:

Suppose we have a continuous derivable function f, and now we discuss the changing of objective function value after a point in n-dimensional space moves to another point. Based on Taylor's expansion, we have:

$$f(x_k + \alpha d_k) = f(x_k) + \alpha g_k{}^T d_k + o(\alpha), \ \ \alpha > 0 \tag{3-3}$$

$$g_k{}^T d_k = \| g_k \| \| d_k \| \cos \bar{\theta}_k \tag{3-4}$$

Where,

x_k: Independent variable at k[th] point (a vector);

d_k: Search direction at k[th] point (a vector);

α: step size (a real number);

$g_k{}^T$: Gradient of objective function at x_k (a vector);

$o(\alpha)$: Higher-order infinitesimal of α;

$\bar{\theta}_k$: the angle between g_k and d_k.

The value of $o(\alpha)$ could be ignored. Thus, if we want to obtain the minimum value of $f(x_k + \alpha d_k)$, dot product of vector $g_k{}^T$ and d_k should be minimum. Obviously, only when

$\cos\bar{\theta}_k = -1$, which means $\bar{\theta}_k = \pi$ or d_k should be set as opposite direction of gradient, the minimum can be achieved.

3.3.1 Algorithm Realization and Flow Chart

The principle of gradient descent algorithm was introduced above. The specific details about how to conduct the gradient descent algorithm are divided into four steps and well-illustrated as follows.

Step 0: Pick initial point (first set of optimization parameters), initialize iteration k as 1, maximum iterations, and define calculation error ε;

Step 1: Calculate gradient g_k of the initial point ($g_k = \nabla f(x_k)$) and define search direction $d_k = -g_k$;

Step 2: Identify whether the value of d_k is smaller than error ε; if yes, break the program and print optimal parameters; otherwise, go to the step 3;

Step 3: Determine the step size α_k by Armijo inexact line search method (will be explained below), and use the step size found to upgrade the next step evaluation point by equation $x_{k+1} = x_k + \alpha_k d_k$;

Step 4: $k = k + 1$, go to step 1 until maximum iteration is reached. If $k > k_{\max}$, then also print results (specific termination condition could be add here based on the needs of different situations).

For better understanding of algorithm realization, the general flow chart of gradient descent algorithm is also given (shown in Figure 3-4).

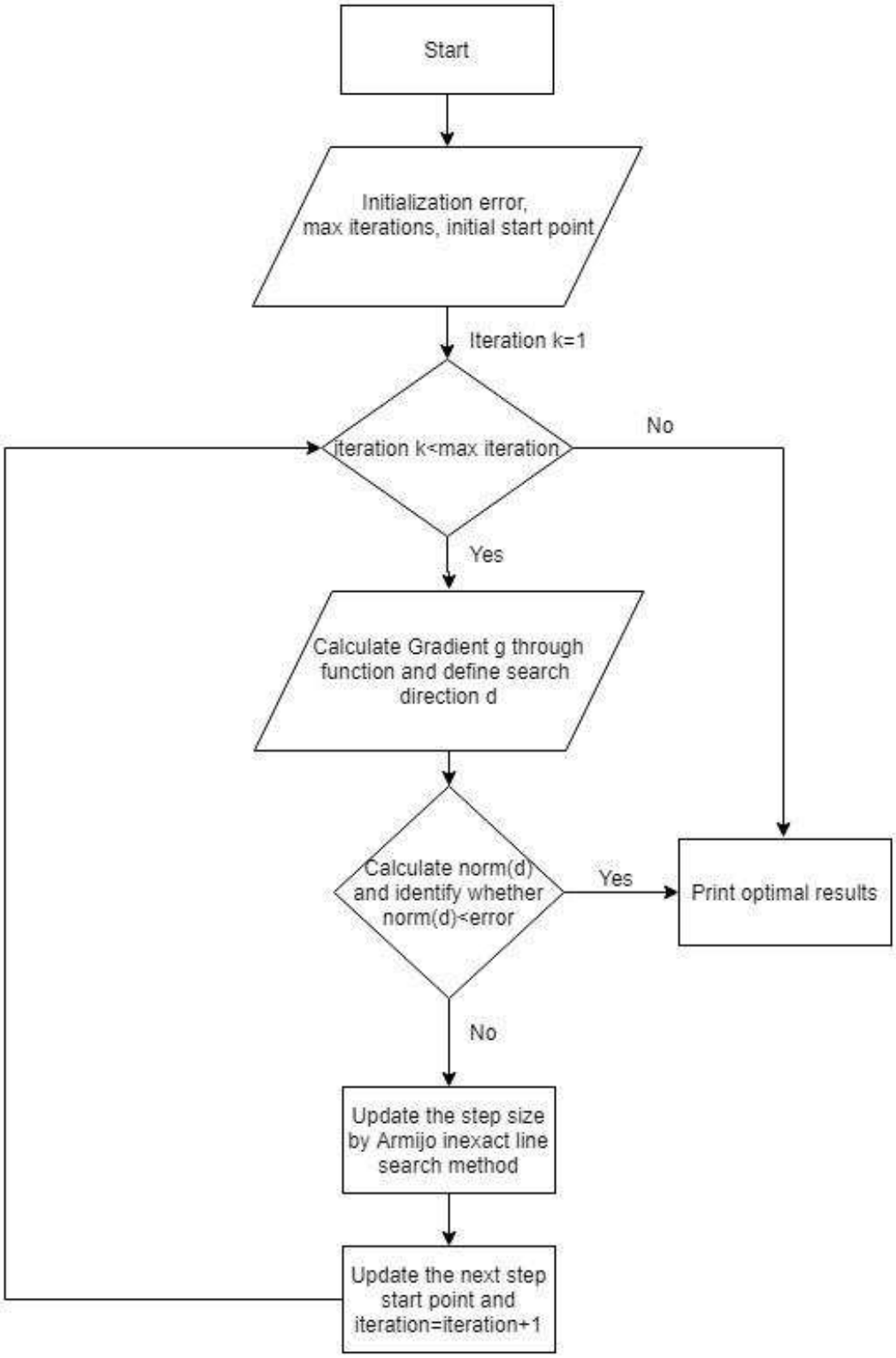

Figure 3-4 Gradient Descent Algorithm Flow Chart

3.3.2 Armijo Rule and Central difference

The most complex parts in the algorithm are the gradient calculation and updating issues of step size α_k. In fracture optimization problem, the cumulative discounted-NPV is calculated through MSFLOW simulator so that the relationship among objective cumulative discounted-NPV and variables is unknown, which means our objective function is implicit. In other words, suppose that a variable f relies on other variables $x_1, x_2 ..... x_n$, but we can only obtain the values f with input variables $x_1, x_2 ..... x_n$, as the data is from simulation. Therefore, the partial gradient information can't be obtained directly by differentiating function over a specific variable. The method of numerical differentiation should be applied to estimate the derivative information. There are three common numerical ways to get the derivative information, which are forward difference, back difference and central difference. Central difference will be used since the errors for the forward difference and backward difference tend to have opposite signs and averaging the two methods would give a better result than either alone (Young and Mohlenkamp 2009). The central difference Equation 3-5 is shown below:

$$\frac{\partial f}{\partial x_i} = \frac{f(x_i + h) - f(x_i - h)}{2h} \ (\textit{first derivative}) \tag{3-5}$$

The method that we used to solve the step size α_k problem is Armijo inexact line search. The Armijo principle is described as:

For given $\beta \in (0,1)$, $\sigma \in (0, 0.5)$, assume the step size as $\alpha_k = \beta^{m_k}$, where m_k is the minimum integer that satisfies the following inequality (Equation 3-6):

$$f(x_k + \beta^m d_k) \le f(x_k) + \sigma \beta^m {g_k}^T d_k \tag{3-6}$$

It can be proved that under the condition that $f(x)$ is a derivable continuous function and ${g_k}^T d_k$ is less than 0, there is always a positive σ such that a sufficiently large positive integer m will ensure the correctness of the above inequality (Equation 3-6).

By following Armijo principle, we are able to find the step size and then update the next search point. The algorithm step of Armijo principle is listed below:

Step 0: Initialize $\beta \in (0,1)$, $\sigma \in (0,0.5)$, Assume $m = 0$;

Step 1: if the inequality (Equation 3-6) above is true, then assign $m_k = m$, $x_{k+1} = x_k + \beta^{m_k} d_k$, otherwise go step 2

Step 2: $m = m+1$, go to step 1.

A graph is given for better understanding of Armijo rule as Figure 3-5 shows. The graph indicates an application of Armijo rule with starting point S.

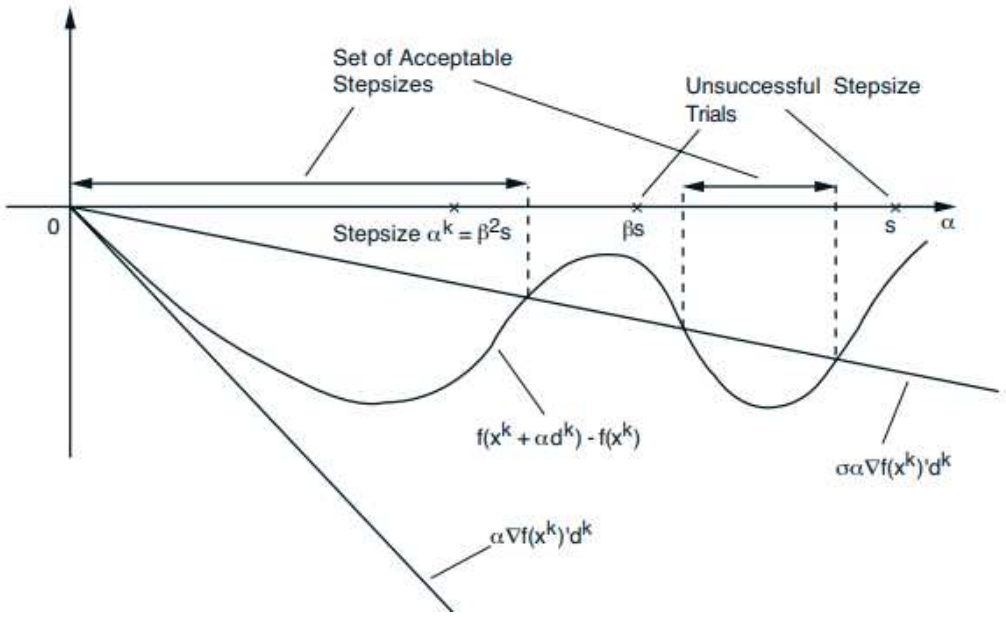

Figure 3-5 Application Schematic Diagram of Armijo Rule (Bertsekas 2005)

There is an issue that if the maximum m is reached but the smaller value compared to the previous one is not found, the loop will be forced to quit and the $m_k = 0$ will be used for new step size since it is not updated, which may cause the smaller new objective value. Thus, a termination could be added for identity if maximum m is reached. If maximum m is reached, the results could be outputted, and the gradient descent algorithm could be terminated. In this thesis, the maximum is set as 20, which is enough for determination and accuracy for new step size. There is another way of dealing with this issue, which is utilized in applications in Chapter 4. We do not stop the optimizer and keep it running. At this point, the optimizer starts optimizing

based on the new optimization variable value, so we can see if we can find a minimum value similar to the one we had before. And the optimization system will stop after reaching maximum iterations. By this way, the characteristics of fluctuations of gradient descent methodology can be observed and they are displayed in application in Chapter 4. Although optimizer's running time may therefore increase, it can be supplemented to verify the effectiveness of the optimization algorithm.

3.3.3 Euclidean Norm

Except gradient and step size, I want to attach the calculation of Euclidean norm of a vector, which is one of our algorithm termination criteria. The Euclidean norm is often known as the magnitude since it assigns to each vector the length of its arrow. The formula is:

$$\| \mathbf{x} \|_2 = \sqrt{\sum_{i=1}^{N} x_i^2} \tag{3-7}$$

The gradient method is powerful for convex problem; however, it has limitation for the nonconvex problem since it is relied on initial point. Different initial point might find different local optimal values. Therefore, it is significant to restart the algorithm with various initial points. By this way, we can find the better results and avoid some errors, but no one can guarantee the discovery of best results because we can't start with endless points.

3.4 Optimization Modules

The establishment of a set of automatic optimization system is actually to connect reservoir numerical simulator and optimization algorithm together. In order to achieve this goal, a variety of modules need to be established, including input module, output module, optimization module, objective function module, grid module, derivative module and extraction and calling module. This chapter explains in detail these modules and their functions.

The input module consists of four parts, which are economic input, fracture information, reservoir simulator input (called MSflow_input) and our optimization parameters. The input of economy includes investment information for the calculation of net present value, such as working interest, loyalty, burden, tax and so on. The fracture information part illustrates "reservoir length" (hydraulic fracture spacing in simplified model), "reservoir width" (half of

actual reservoir width), reservoir thickness, the number of hydraulic fracture, location of hydraulic fracture and the coefficient for LGR. The input of simulator MSFLOW includes information such as rock properties, fluids properties natural fractures/hydraulic fractures, reservoir initial conditions, PVT data, relative permeability data, simulation parameters and etc. Note, there are several parameter-modifier programs inside input module, which mean parts of inputs will be continuously updated. For example, the fracture information and input of simulator are changing during the process of optimization with the changing of three optimization parameters.

Output modules mainly include the information of gas production over time, reservoir gas pressure distribution, reservoir fluid pressure distribution (if fluid exists), cumulative discounted NPV, and optimization process and results.

Since the main program of optimization system is coded by MATLAB, MSFLOW, objective function module, and XYZ mesh, which are all programmed by Fortran, are converted to the application format (.exe) file to facilitate the MATLAB to call them. The main program, the optimization module, achieves the following functions: optimization algorithm parameter settings, determination of the next loop step as well as termination conditions of the program. The objective function module includes two evaluation functions: gas production and net present value. Gas production will be used in the next section to verify the correctness of the optimizer system. The cumulative discounted-NPV is described in detail in the following section 3.5 and will be used for actual reservoir applications in Chapter 4.

The grid module is used to automatically generate the grid system. To realize this goal, fracture information in the input module is changed first every time according to updated optimization parameters by programs written by MATLAB. And then the grid system is updated through the modified XYZ mesh program.

Derivative module is used to obtain the partial derivative value. And extraction and calling module is applied to call and run the above mentioned (.exe) format file and extract the information needed for optimization processes. Their relationships are made into Figure 3-6 and the arrow means they have information exchange.

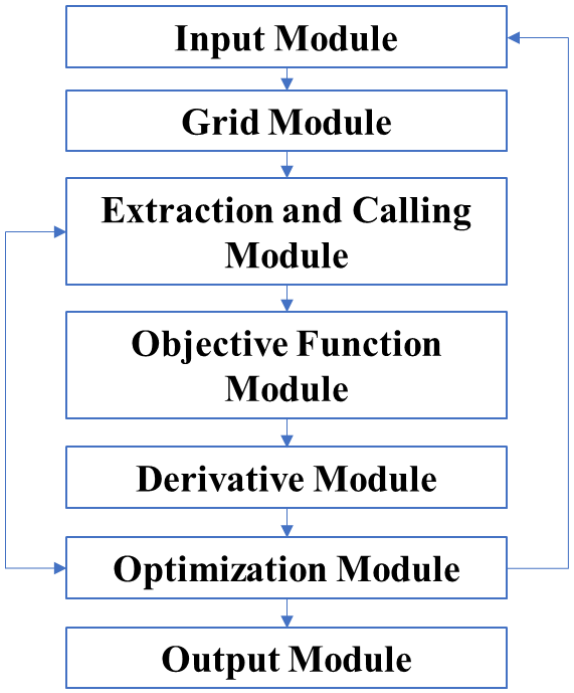

Figure 3-6 Diagram of Optimization Modules Relationships

3.5 Cumulative Discounted-Net-Present-Value

There are three common "models" which are used to determine profit. Each model (cash flow, financial, and tax) has a unique way of defining costs and thus results in a different calculated value of profit. The model we select for our economic analysis is cash flow model. The reason lies in the time value of money concept. In other words, money has a time value (Thompson and Wright 2015). For example, one hundred dollars received today is more valued than the one hundred dollars received five years later. Therefore, assigning the right "profit" to the right period is quite crucial in economic analysis. The money time value function is

$$P = \frac{F}{(1+r)^n} \tag{3-8}$$

Where P is present value, F is future value, r is the currency interest rate for a specific period, and n is the number of periods.

The detail cash flow diagram for a domestic oil property is shown as Figure 3-7. With all cash flows, NPV (Net Present Value) can be figured out by taking the sum of these cash flows

and discounting them to a specific time with a discount rate. And then the objective value could be calculated by adding these NPVs to an interested time, for instance, ten years cumulative discounted-NPV used in Chapter 4.

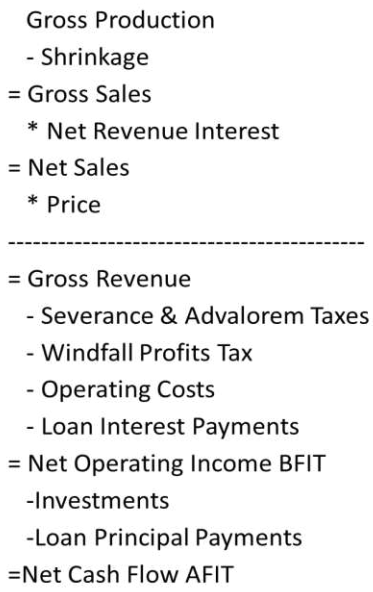

Figure 3-7 Gas Property Cash Flow Diagram (Thompson and Wright 2015)

Realistic objective function would include other factors or disregard some factors that would render it more complex, but the general form is same. Since various hydraulic fracturing designs have different costs, they are specifically separated out from other expense as an individual term, denoted as C_{hf} . General discounted form NPV function is shown below:

$$f_T(n_{stage}\,or\,HFsp, x_f, F_{cd}) = -\left(\int_0^T \left\{ \sum_{j=1}^{N_p} \left[(w_1 p_g q_g(t) - w_2 p_{w,disp} q_w(t)) \right] \right\} - \sum_{k=1}^{N} \left[w_3 C_{hf}(n_{stage}, x_f, F_{cd}) + w_4 C_{other}(t) \right] \right) (1+r)^{-n}\, dt \quad (3\text{-}9)$$

where q_g and q_w are the production rate for gas and water, the units of them in kg/s; the coefficient p_g is the price of gas price and $p_{w,disp}$ is the cost of disposing water; the term r as well as n represent currency interest rate and periods that costs need to be paid in front, the same

meaning as mentioned before; j represents different production sources; $C_{other}(t)$ is the drilling cost if the time is year one and is additional investment after year one; k represents multiple wells; $w_1, w_2, w_3 \; and \; w_4$ are the weighting factors based on their influence level (all set as 1 in this thesis, but it could be changed).

C_{hf} is the hydraulic fracturing costs based on the combination of different optimization parameters. It is not time dependent, but optimization parameters. This cost only occurs at the year one. C_{hf} is adapted from presentation of Dr. Gildin in Foundation CMG School 2017 and defined by Equation 3-10.

$$C_{hf} = \frac{C_{t@\max\#stage}}{n_{\max\#stages}} * n_{real\#stages} + a_1 * (1 + \frac{(a_2 * F_{cd} + 1000)}{1500}) * (2 * HFhl)^{a_3} \qquad (3\text{-}10)$$

where $C_{t@\max\#stage}$ means the cost of maximum stages, which is 50 in this thesis; $n_{\max\#stages}$ is the maximum stages; $n_{real\#stages}$ is the real stage numbers during the optimization process and it is equal to reservoir length divided by hydraulic fracture spacing; $HFhl$ is the hydraulic fracture half-length; $a_1 \, a_2 \, and \, a_3$ is coefficient to control the sensitivity of conductivity and $HFhl$ to the cost.

The discounted NPV function f_T is negative since our algorithms for optimization is to search for a minimum. With a negative sign, we can obtain maximum NPV and cumulative discounted-NPV. When we compare the cases for the same period, subscript T could be dropped but with various fracture half-length, dimensionless conductivity, numbers of fracture stage. Notice that $f_T(n_{stage} \, or \, HFsp, x_f, F_{cd})$ depends on fracture half-length, dimensionless conductivity, numbers of fracture stage in two ways. First, the pump schedule, which includes injection time, injection rate, injection volume, proppant type and size, and slurry concentration, and its associated cost, relies on the value of fracture half-length, dimensionless conductivity, numbers of fracture stage (fracture spacing). Second, the production rate and its associated cumulative production depend on the value of fracture half-length, dimensionless conductivity, numbers of fracture stage.

For most applications in Chapter 4, drilling cost is set as a constant and its value is \$2MM dollars based on Marcellus gas well cost as Table 3-2 shows. $a_1\, a_2\, and\, a_3$ is set as 10, 0.04 and 1.8 based on Dr. Gildin's presentation. $C_{t@\max\#stage}$ is set as \$2MM dollars too and so the total initial cost (fracturing cost and drilling cost at year one) is ranging from \$80M dollars to \$3.672MM dollars. However, these settings could be varied based on different engineers' experience.

Table 3-2 Reference for Drilling Cost (U.S. EIA 2016)

Formation	Drilling Cost (MM\$)
Marcellus Northeast Core	1.89
Marcellus Northeast Core	1.94
Marcellus SW Core	2.09
Marcellus SW Core	2.04
Marcellus Liquids RichAvg	1.76

3.6 Performance Indicators

To evaluate the performance of the optimization system, three main indicators will be considered. First, efficiency will be evaluated by checking the program running time and the times that reservoir simulator (MSFLOW) is called. Second, robustness will be evaluated by the values found by different initial points. Third, effectiveness will be evaluated by optimal objective function values. The meaning and boundary will be also considered for effectiveness evaluation.

Note, the three optimization parameters (hydraulic fracture spacing, hydraulic fracture half-length, and dimensionless fracture conductivity) in the tables of Appendix C, D, and E are only shown up to 4 digits after decimal point and thus if these approximate values are applied into MSFLOW for calculation, the objective value may be a little deviated. If the exact values are needed, please free to contact me. Program run time will be varied with different computer configurations and different MATLAB versions.

CHAPTER 4
VALIDATIONS AND CASE STUDIES

In this chapter, the concept and the reason for a simplified reservoir model is illustrated. The effectiveness of the simplified model is conducted by comparing the production and pressure distribution with the whole reservoir model. And the optimization system described as Chapter 3 will be validated through several methods. Results show that all of these methods give a good answer for the design case and some of the properties displayed by sensitivity analysis.

Real unconventional reservoir cases are designed and run through the optimization system. The results are analyzed to give a most suitable combination of optimization parameters for specific reservoir. The effects, such as gas adsorption/desorption and Klinkenberg effect, are taken into consideration when design the real cases.

In order to avoid some of the shortcomings of the gradient descent method discussed in Chapter 3, each study considered and calculated from different starting points. And we design these starting points relatively reasonable to make these starting points as possible cover a relatively large domain. Results due to different starting points are compared and the final best economic scenarios as well as values for fracture half-length, dimensionless fracture conductivity, and numbers of fracture stage at this condition are given.

4.1 Introduction

It is important and necessary to design validation for new created programs. Without validation, the results can not be trusted. Thus, validations are conducted before running any real reservoir cases.

4.2 Validations

In this section, the simplified model and optimization program will be validated. The simplified model is needed since during the optimization process, hundreds of simulation runs will be needed and will act as a black-box to obtain necessary information.

4.2.1 Validation of Simplified Model

Since the simulation of whole reservoirs (including all hydraulic fractures, called original model) is time-consuming, the simplified model, one-half of a hydraulic fracture (one fracture spacing length reservoir area) as mentioned in Chapter 3, is then proposed. The simplified model is based on the theory that the hydraulic fracture is symmetric. To validate the correctness of the simplified model, a case is then established for comparison. Only gas is produced from the reservoir for this case and the main parameters for simplified model are provided in Table 4-1.

Table 4-1 Simplified Model Parameters for Numerical Validation

Parameter	Value	Unit
Matrix porosity	$\phi_M = 0.06$	
Hydraulic fracture porosity	$\phi_{HF} = 0.5$	
Matrix permeability	$k_m = 9.87 \times 10^{-19}$	m^2
Dimensionless fracture conductivity	$F_{cd} = 20$	
Hydraulic fracture permeability	$k_{HF} = 3.948 \times 10^{-14}$	m^2
Hydraulic fracture half-length	$L_{HF} = 100$	m
Reservoir length	$L_R = 1000$	m
Reservoir width	$W_R = 600$	m
Reservoir thickness	$H_R = 100$	m
Initial reservoir pressure	$P_i = 4.14 \times 10^7$	Pa
Constant wellbore pressure (BHP)	$P_w = 1.0 \times 10^6$	Pa
Initial gas saturation	$S_g = 1$	
Gas density (standard)	$\rho_g = 0.668$	kg/m^3
Gas viscosity (standard)	$\mu_g = 5.955 \times 10^{-6}$	Pa*s
Klinkenberg coefficient	$b = 1.03 \times 10^6$	Pa
Langmuir's volume	$V_L = 2.2 \times 10^{-3}$	m^2 / kg
Langmuir's pressure	$P_L = 1.5759 \times 10^7$	m^3/day
Total compressibility of all media	$c = 1.0 \times 10^{-9}$	1/Pa
Reservoir temperature	$T = 50$	°C

Based on the above parameters, five hydraulic fractures are supposed to exist in the original model as Figure 4-1 shows. The original model has a length of 1000 m, a width of 600 m, and a thickness of 100 m. The total hydraulic fracture length is 200 m and is located between

200 m to 400 m in the Y direction. For simplified model, the simulation length is supposed to be 200 m, which is also the length of the hydraulic fracture spacing. The simulation width is supposed to be 300 m, half of reservoir width, and the simulation height is the same as the original model, which is 100 m. Figure 4-2 shows the grid system of the simplified model.

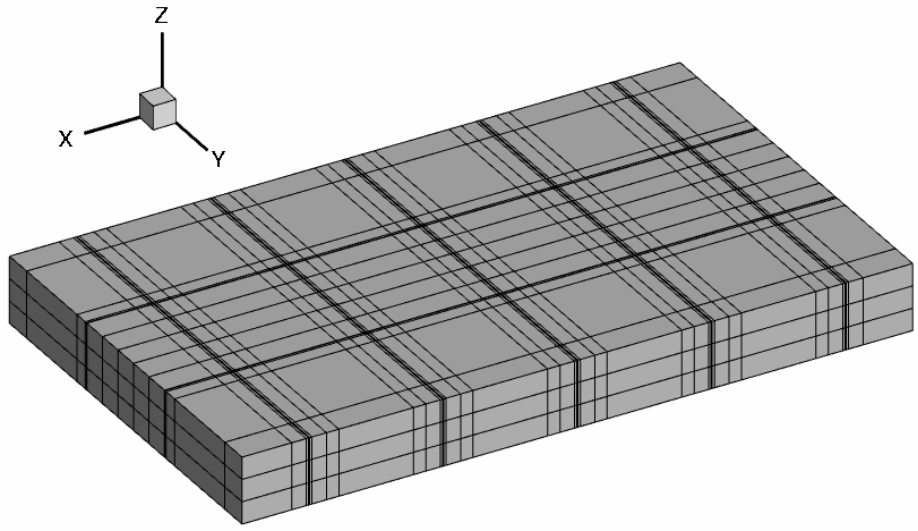

Figure 4-1 Original Model with Five Uniform-distributed Hydraulic Fractures for Validation

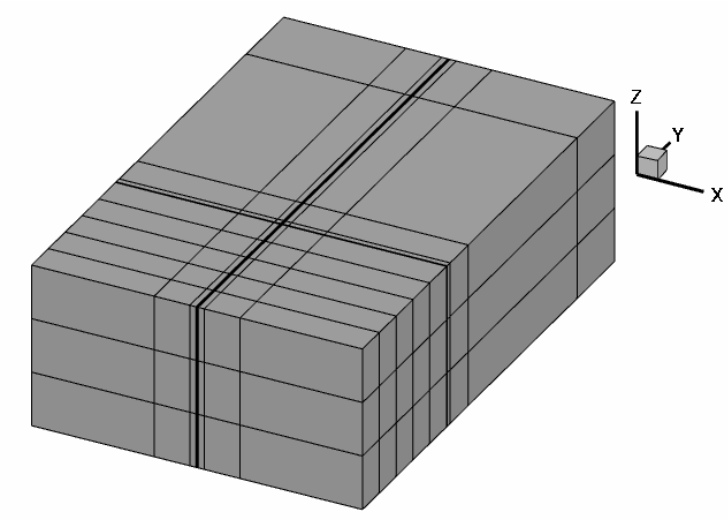

Figure 4-2 Simplified Model with One Centered Hydraulic Fracture for Validation

Simulation results show that it takes around 63.2334 seconds to finish the simulation of original model and 8.6415 seconds to finish the simulation of simplified model. It is obvious that the running speed of simplified model is much faster than original model, about 7.32 times faster

per simulator run. Although the speed of the simulation run is important, it is much more significant to check accuracy of simplified model. Thus, the results of gas production are listed as tables and plotted for the convenience of comparison.

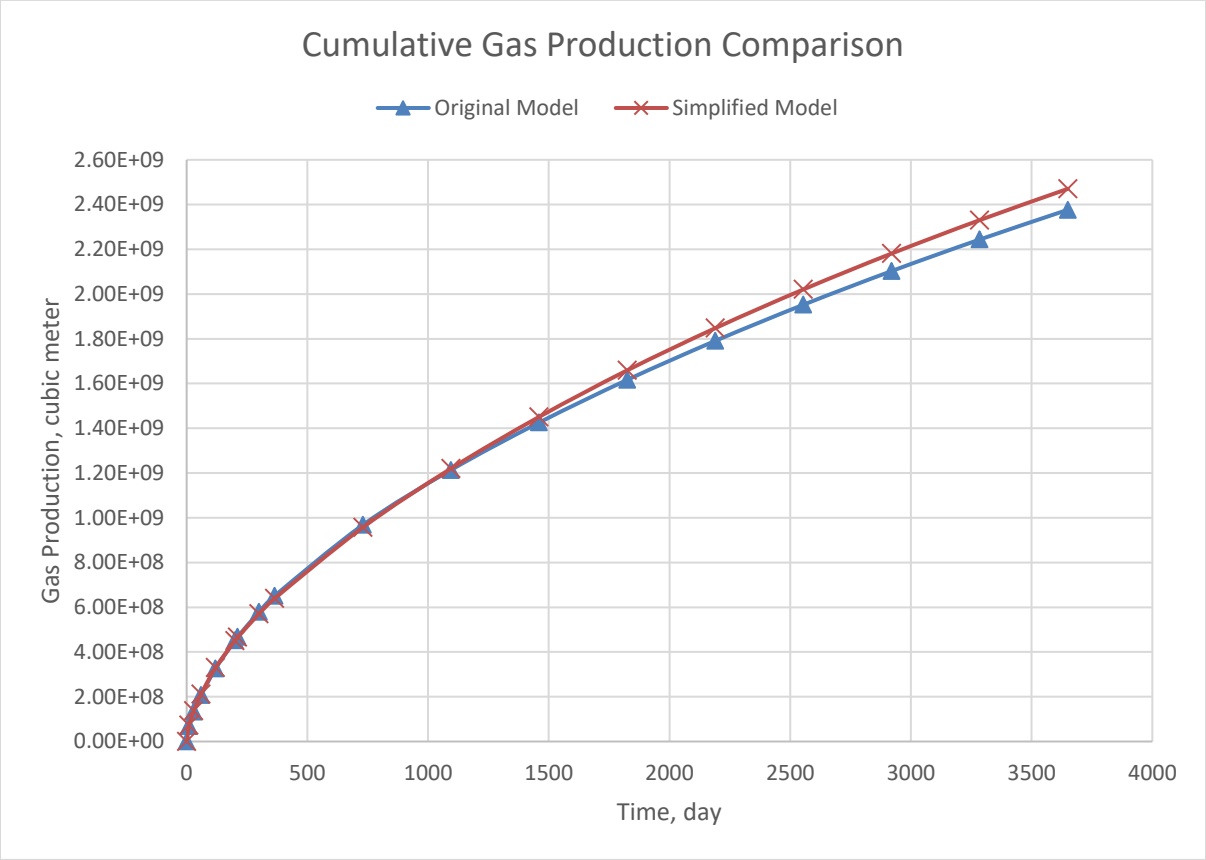

Figure 4-3 Ten-Years Cumulative Gas Production Comparison for Original Model and Simplified Model

The fixed cumulative gas production values of the simplified model are based on the Equation 3-1 in Chapter 3. Based on the comparison in Figure 4-3, deviations in the later time are observed and maximum deviation occurs at ten years. Thus, error identification is needed. The example error calculation of production at ten years is shown as below:

$$Error = \frac{Simplifed\ Model\ Gas_{prod@10\,yrs} - Original\ Model\ Gas_{prod@10\,yrs}}{Original\ Model\ Gas_{prod@10\,yrs}} = \frac{1.650207297\times10^{9} - 1.587540244\times10^{9}}{1.587540244\times10^{9}} = 3.95\% \quad (4\text{-}1)$$

Table 4-2 Data Table for Original Model and Simplified Model Comparison

Time(Day)	Original Model Cum Prod_gas (m^3)	Simplified Model Cum Prod_gas (m^3)	Fixed Simplified Model Cum Prod_gas (m^3)	Error
1.16E-39	0.00E+00	0.00E+00	0.00E+00	0.00%
1.00E+01	6.94E+07	7.28E+06	7.28E+07	4.84%
3.00E+01	1.34E+08	1.38E+07	1.38E+08	3.18%
6.00E+01	2.07E+08	2.12E+07	2.12E+08	2.41%
1.20E+02	3.26E+08	3.30E+07	3.30E+08	1.14%
2.00E+02	4.52E+08	4.51E+07	4.51E+08	0.29%
2.12E+02	4.68E+08	4.66E+07	4.66E+08	0.46%
3.00E+02	5.79E+08	5.71E+07	5.71E+08	1.40%
3.65E+02	6.51E+08	6.40E+07	6.40E+08	1.76%
7.30E+02	9.68E+08	9.57E+07	9.57E+08	1.12%
1.10E+03	1.21E+09	1.22E+08	1.22E+09	0.52%
1.46E+03	1.43E+09	1.45E+08	1.45E+09	1.78%
1.83E+03	1.62E+09	1.66E+08	1.66E+09	2.64%
2.19E+03	1.79E+09	1.85E+08	1.85E+09	3.17%
2.55E+03	1.95E+09	2.02E+08	2.02E+09	3.50%
2.92E+03	2.10E+09	2.18E+08	2.18E+09	3.73%
3.28E+03	2.24E+09	2.33E+08	2.33E+09	3.87%
3.65E+03	2.38E+09	2.47E+08	2.47E+09	3.95%
Average Error				**2.34%**

Based on the Table 4-2, the average error is only 2.34%, which is acceptable with 7.32 times simulation speed increased. Besides gas production, gas pressures are also plotted for original model as well as simplified model for different time periods as Figure 4-4, Figure 4-5, Figure 4-6 and Figure 4-7 show. Pressure decline is well observed at different time periods. Gas pressures are compared by these pressure distribution graphs and data lookup. Facts have proved that the pressure distributions of the two models at different times are very close, which is also verified with the result of production. Therefore, the simplified model could be used for optimization. In addition, the graphs also indicate the flow regime around hydraulic fractures (radial flow in the tip of hydraulic fracture and linear flow between matrix and hydraulic fracture), which leads to the elliptic-shape of pressure distribution.

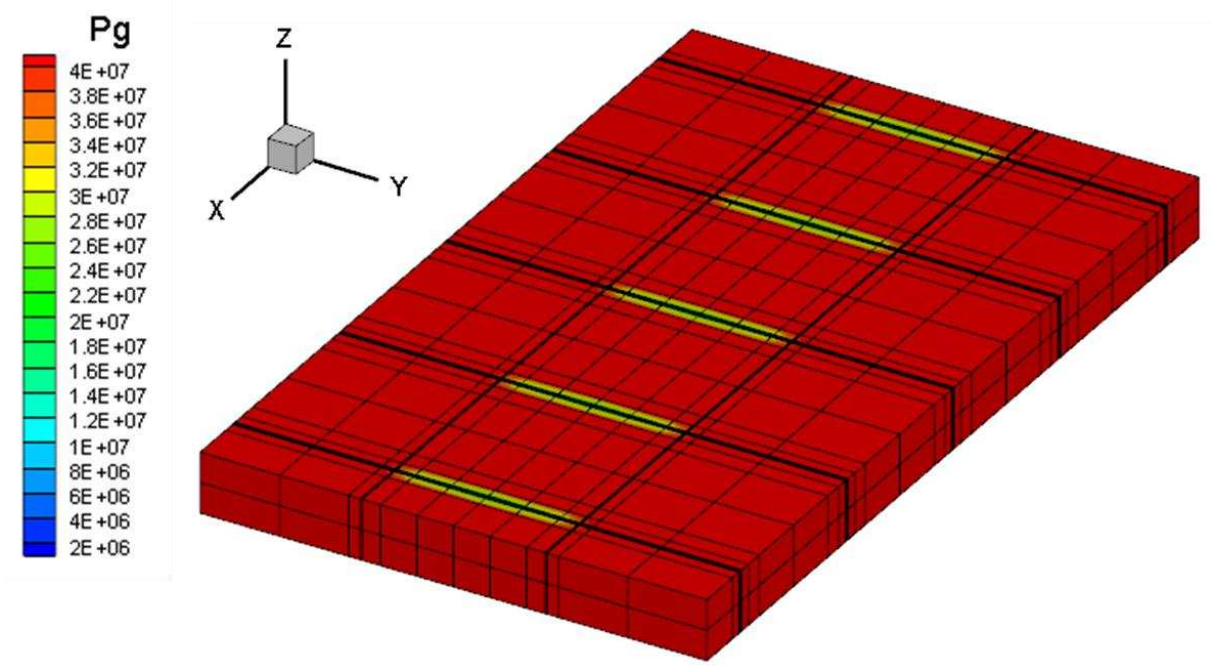

Figure 4-4 Gas Pressure distribution for whole reservoir at 10 days

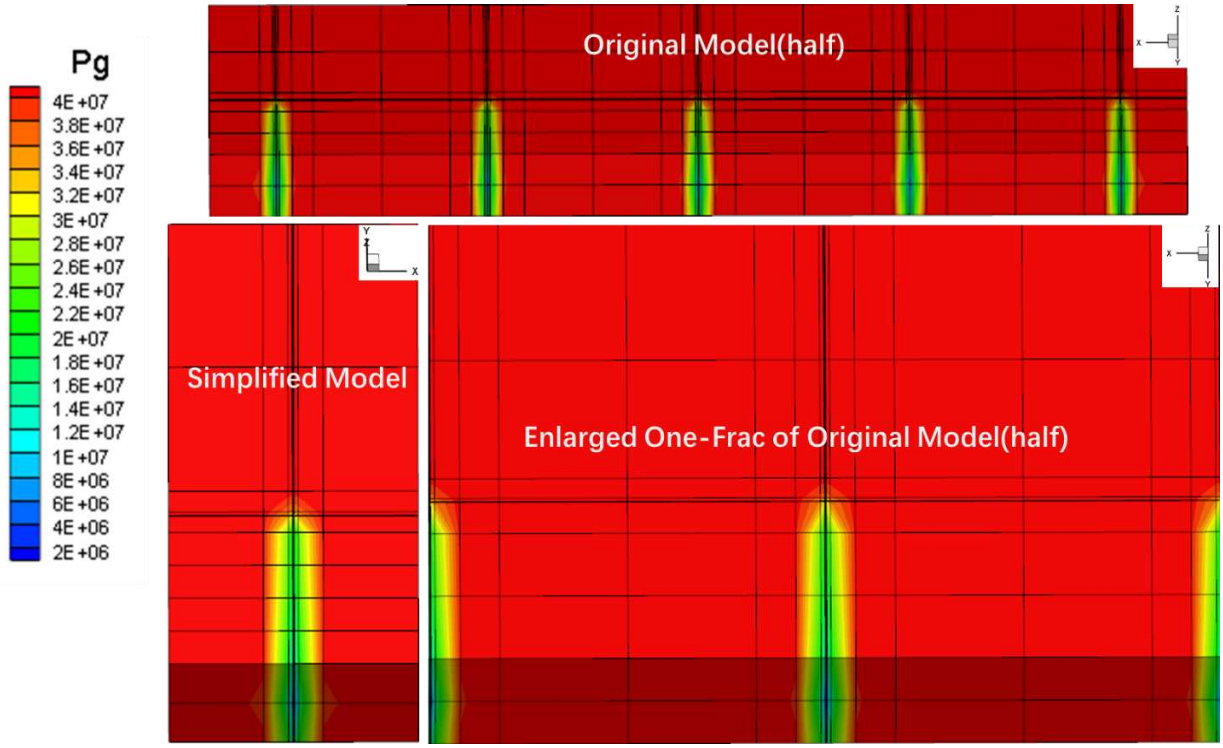

Figure 4-5 Comparison of gas pressure for original model and simplified model at 10 days

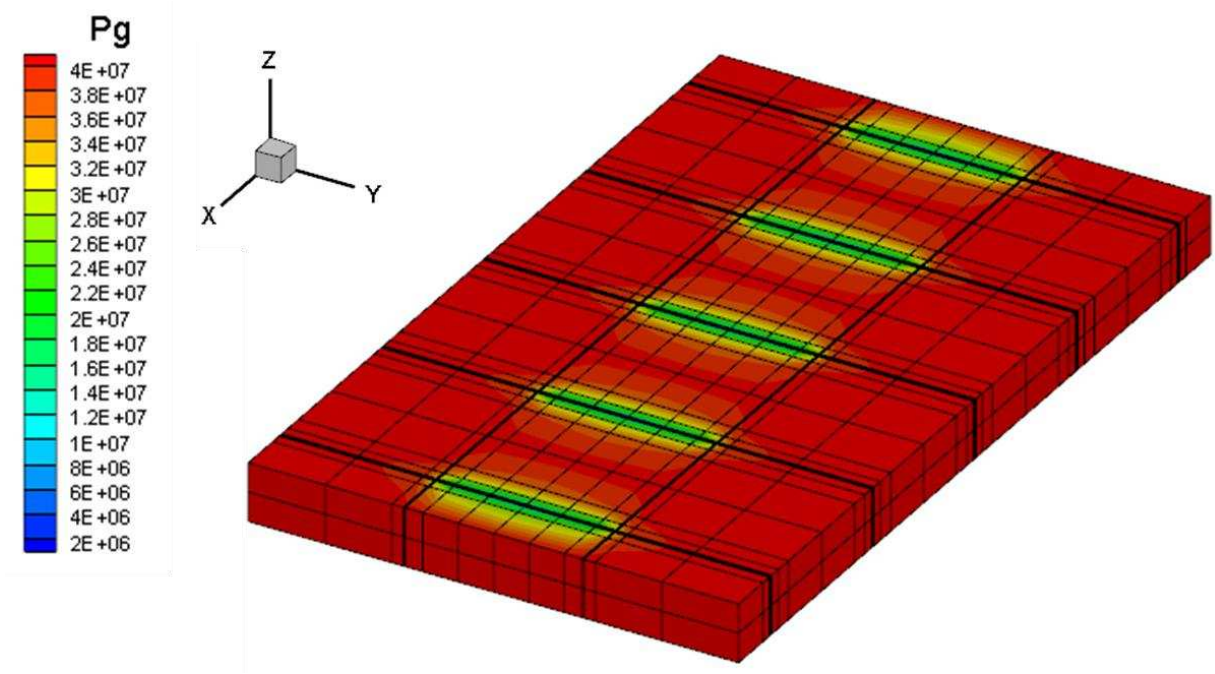

Figure 4-6 Gas Pressure distribution for whole reservoir at 120 days

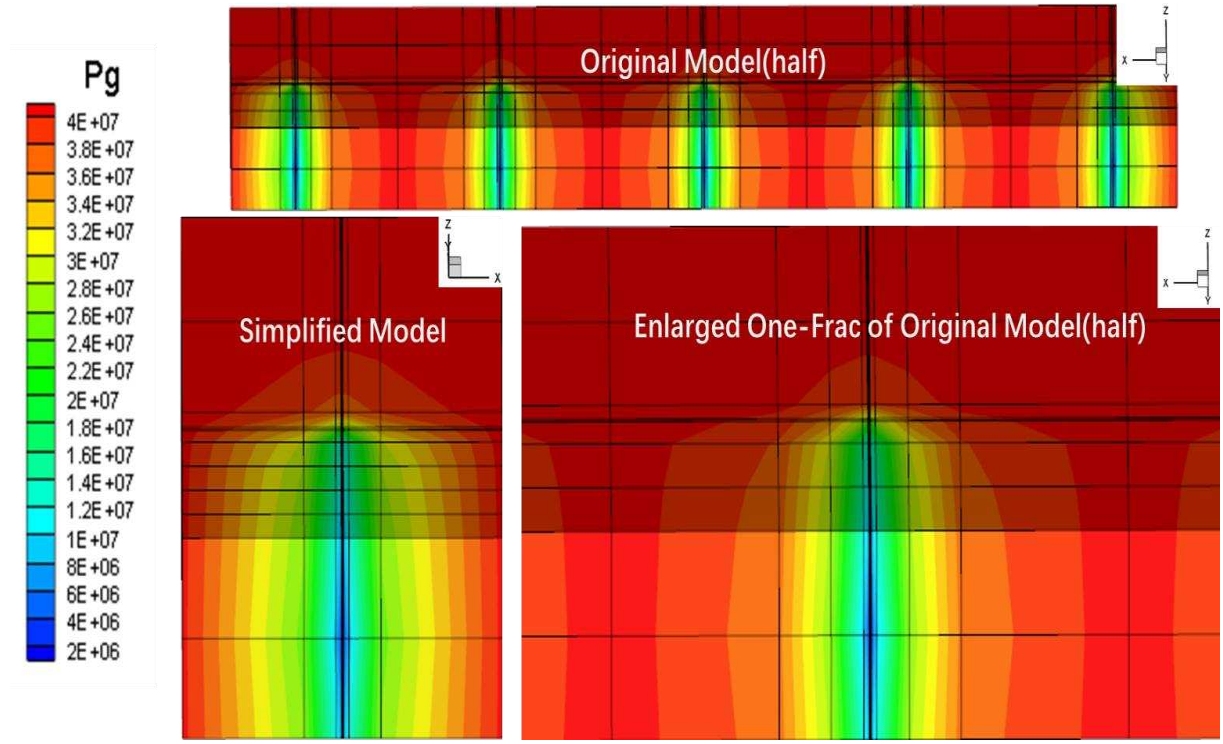

Figure 4-7 Comparison of gas pressure for original model and simplified model at 120 days

4.2.1 Validation of Optimization Program

The optimization program will be verified by two ways. For the first one, an explicit mathematical function with two variables is given. This mathematical function could be plotted and the minimum (optimal) value could be viewed from the graph. For the second one, a real fracture optimization case is designed. To verify the optimization program, the objective function is set as one year's cumulative gas production. The reason is that when the cost is not taken into consideration, gas production will be better with more hydraulic fracture stages, longer hydraulic fracture half-length, and higher dimensionless conductivity.

4.2.1.1 Verification Case One

A mathematical function with two variables is given by:

$$Z = 3x^2 + 4y^2 \tag{4-2}$$

It's obvious that this function has a minimum value 0 since x^2 and y^2 is always larger or equal to 0. The function graph is plotted as Figure 4-8 and the minimum value is reached at point (0, 0).

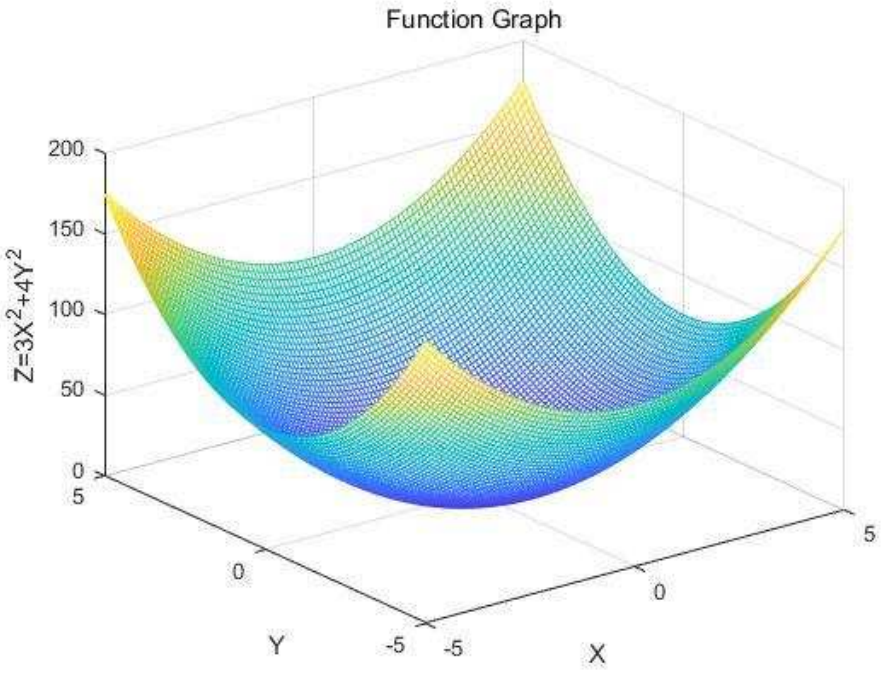

Figure 4-8 Graph of Explicit Function for Optimization Program Verification

The function then is coded into gradient descent optimization system. For gradient descent, different initial points were run and results are shown as below Table 4-3. No matter what the starting point is, the algorithm is able to find the minimum value with a few iterations.

Table 4-3 Optimization Program Verification Results Based on Explicit Function

Initial Point (x0)	#Iteration k	Objective Function Value
(-1, 1)	18	6.35E-22
(-10, 10)	20	2.48E-22
(-20.8, 30.42)	21	6.71E-23
(-150, 600)	22	2.18E-22
(1000, 3000)	23	6.06E-22

4.2.1.2 Verification Case Two

To verify the effectiveness of optimization systems for real reservoir cases, the explicit mathematical function is then replaced. The variables become our fracture optimization parameters: hydraulic fracture length, hydraulic fracture half-length, and dimensionless fracture conductivity. The reservoir simulator MSFLOW will act as a black-box function and "switch" three optimization parameters into the production values (objective). The reservoir properties are set as Table 4-1 and as discussed in Chapter 3, boundaries exist for our optimization parameters. The lower boundaries of hydraulic fracture spacing, hydraulic fracture half-length, and dimensionless fracture conductivity are 20 m, 0 m, and 0 separately, represented by [20 0 0]. And the upper boundaries of hydraulic fracture spacing, hydraulic fracture half-length, and dimensionless fracture conductivity are 500 m, and 300 m and 100 separately, represented by [500 300 100].

Then testing begins with a random initial point [400 150 5]. To visualize the changing process of three optimization parameters, their values are plotted versus the number of times that reservoir simulator MSFLOW called, production values, and program run times. Their values' table will not be listed in this section but in Appendix C for reference.

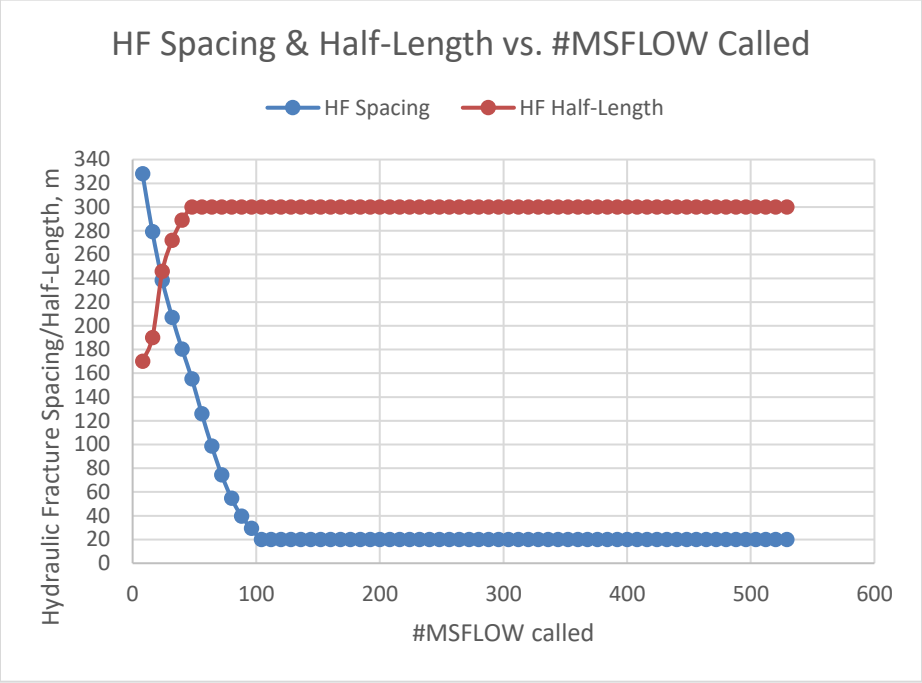

Figure 4-9 Hydraulic Fracture Spacing and Half-length vs. #MSFLOW Called when optimization starts from initial point [400 150 5]

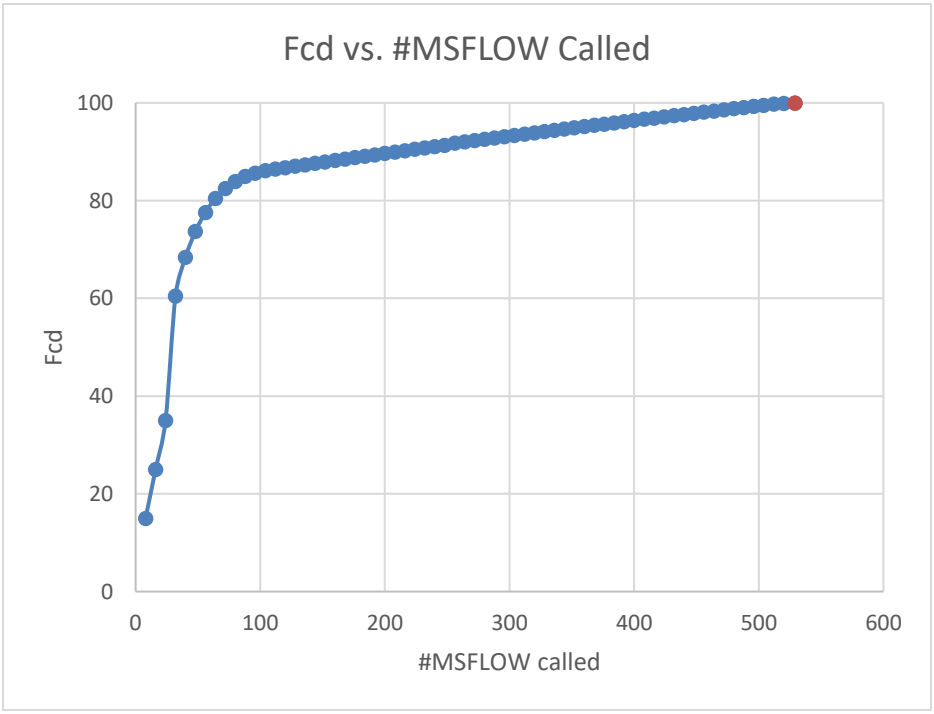

Figure 4-10 Dimensionless Fracture Conductivity vs. #MSFLOW Called when optimization starts from initial point [400 150 5]

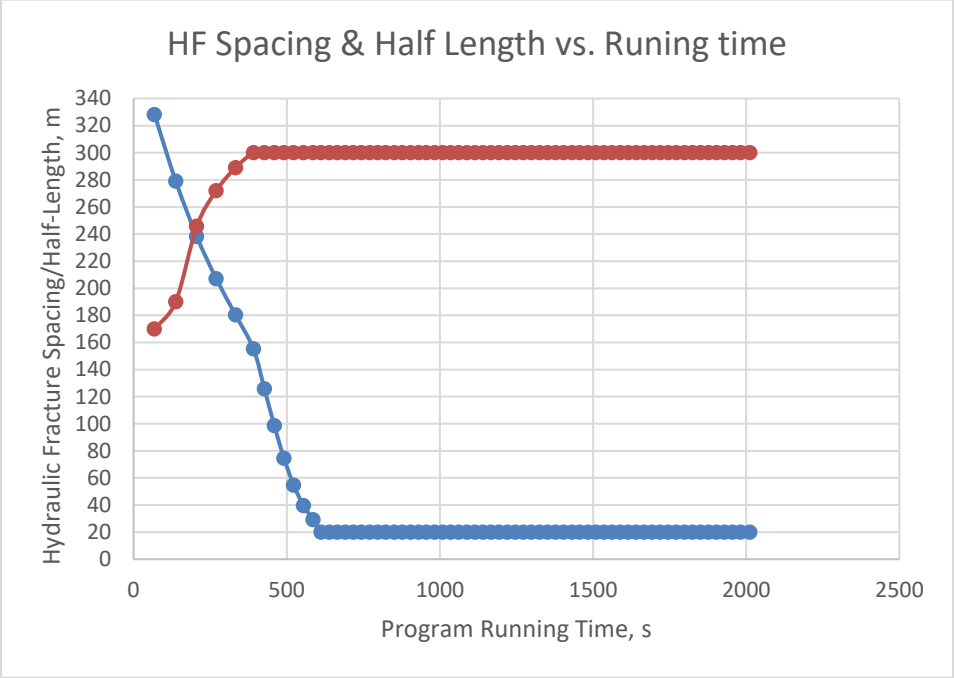

Figure 4-11 Hydraulic Fracture Spacing and Half-length vs. Optimization Program Running time when optimization starts from initial point [400 150 5]

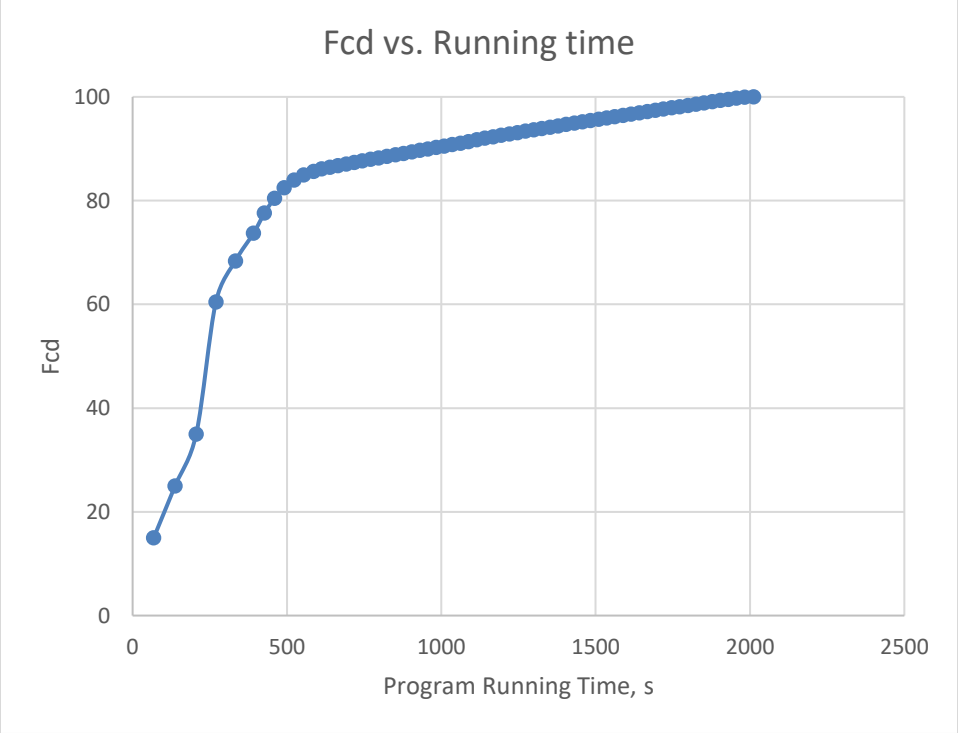

Figure 4-12 Dimensionless Fracture Conductivity vs. Optimization Program Running Time when optimization starts from initial point [400 150 5]

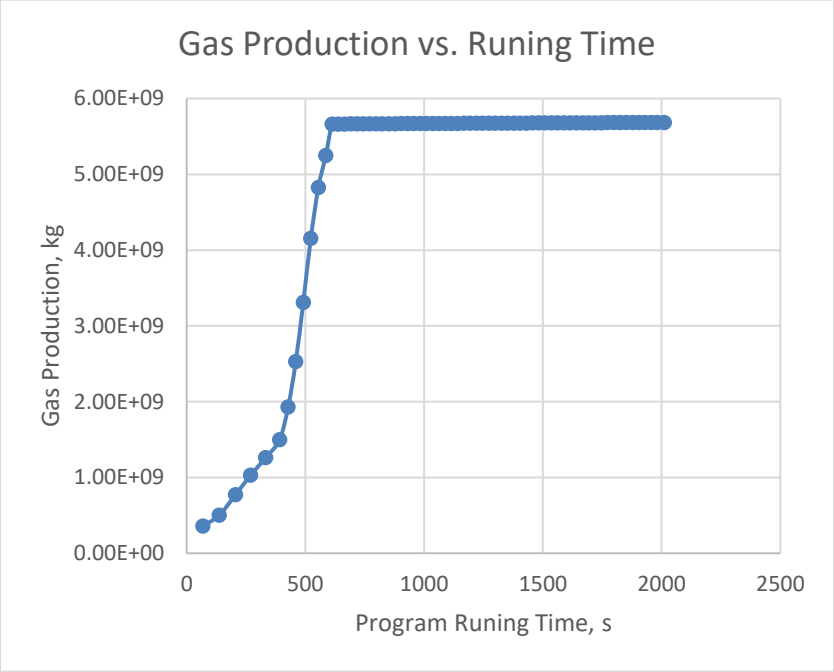

Figure 4-13 Gas Production vs. Optimization Program Running Time when optimization starts from initial point [400 150 5]

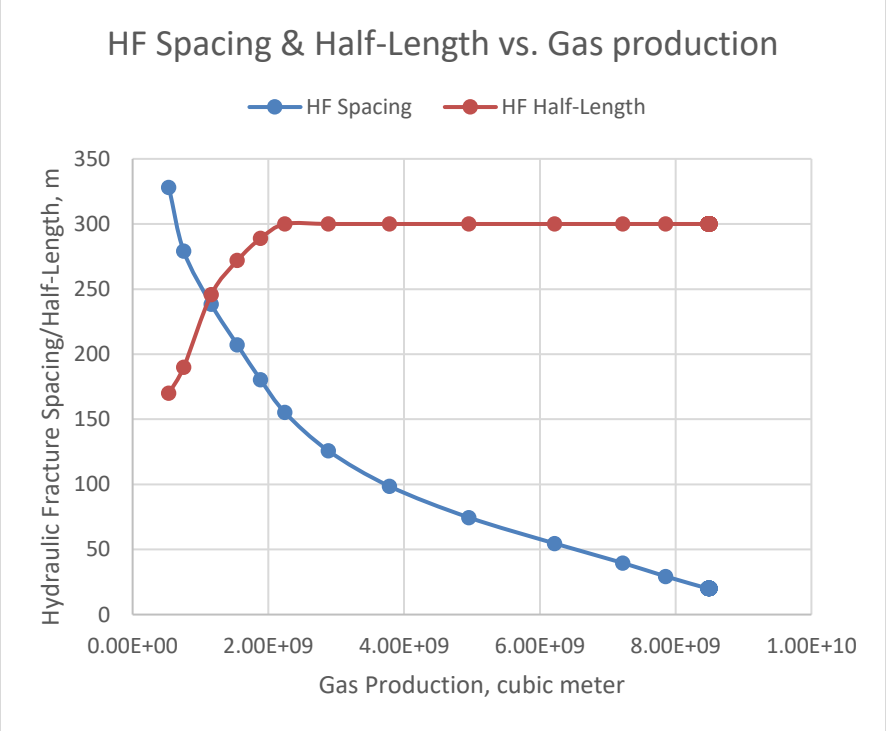

Figure 4-14 Hydraulic Fracture Spacing and Half-length vs. Gas Production when optimization starts from initial point [400 150 5]

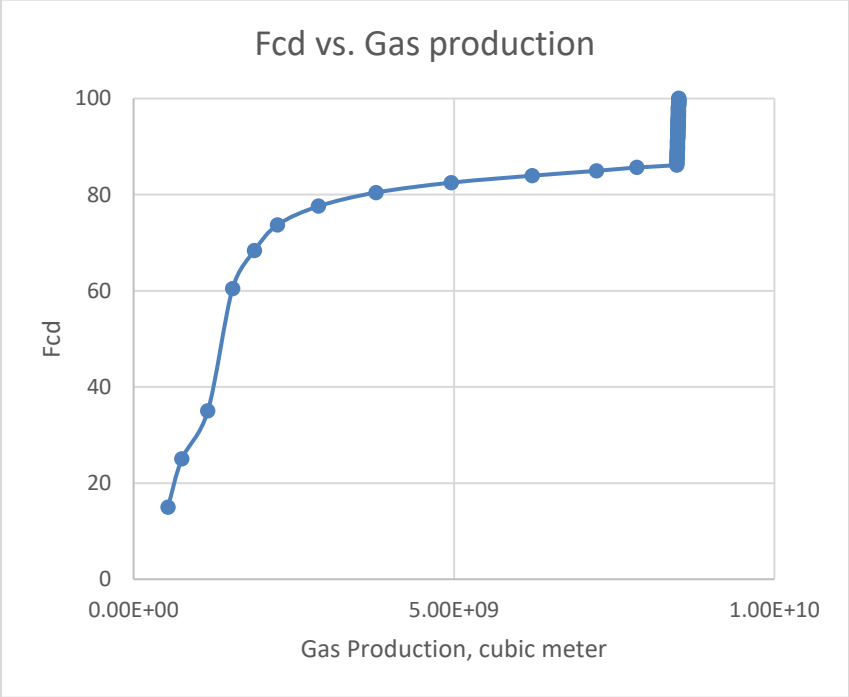

Figure 4-15 Dimensionless Fracture Conductivity vs. Gas Production when optimization starts from initial point [400 150 5]

Based on the above graphs and Appendix C table, we observed that the optimal or maximum gas production occurred when hydraulic fracture spacing, hydraulic fracture half-length, and dimensionless fracture conductivity are 20 m, 300 m, and 100 and its value is 8.5079×10^{9} m^3. In other words, hydraulic fracture spacing reaches its minimum value (maximum stage number) and hydraulic fracture half-length as well as dimensionless fracture conductivity reach their maximum value, which verify the common sense that when money is not a factor in oil/gas field, it will be better to have more stage numbers, longer hydraulic fracture half-length, and higher dimensionless conductivity.

Researchers may still doubt about the correctness of optimization programming since only one initial point is tried and gradient descent is likely to trap the target value at a local minimum/maximum. Thus, more random initial points were run to verify the validation of the optimization program. We found that these starting points finally found the same result as the previous result. It's impossible to list all results here so only another random initial point [200 50 30] result is shown. The similar result table and diagrams were shown in Appendix D for the

sake of layout beauty. In addition, we calculated some random parameter combinations not included in the optimization process to double guarantee the validity of our verification. The results are listed in the Table 4-4 and gas production values based on these combinations are found to be less than the optimal value found at [20 300 100].

Table 4-4 Random Optimization Parameter Combination for verification

HFsp (m)	HFhl (m)	Fcd	Gas Production (m^3)
20	100	100	3.23E+09
30	280	100	7.55E+09
40	200	80	5.05E+09
50	100	60	2.41E+09
80	10	40	2.66E+08
100	80	35	1.07E+09
150	250	70	2.01E+09
200	30	20	2.08E+08
260	290	5	7.73E+08
300	300	18	9.73E+08
345	130	96	4.84E+08
420	183	49	5.20E+08
450	50	10	1.25E+08
450	160	90	4.47E+08
500	300	100	7.11E+08

In summary, we can draw the following conclusions by carefully analyzing all of the result tables and figures:

- The optimization program is validated by the reservoir example with the objective function of gas yield.
- Gas production is a monotonic function of hydraulic fracture spacing, hydraulic fracture half-length, and dimensionless fracture conductivity; that is, gas production increases with decreasing hydraulic fracture spacing and increases with hydraulic fracture half-length and dimensionless fracture conductivity (based on Figure 4-9 to Figure 4-15).

- The optimal values of hydraulic fracture spacing and hydraulic fracture half-length were quickly found by the gradient descent method, but the optimal value of dimensionless fracture conductivity needs a long time to be found. This is due to the different sensitivity of these parameters to production, in other words, to the extent to which the impact on output is different. The sensitivity analysis in the next section is a good illustration of this problem. But all of them have a common feature in that they change rapidly in the early stages of optimization and change slowly in the middle and late stages, especially the dimensionless fracture conductivity. These can be seen by the relationship between these parameters and the number of simulation calls, running time, and gas production (based on Figure 4-9 to Figure 4-15).

4.3 Optimization Parameters Sensitivity Analysis

As most previous fracture optimization papers have done, optimization parameters sensitivity analysis will be done in this work through the simplified model too. There are two purposes for doing this: 1) proves that the three optimization parameters selected have a real and enormous influence on gas production and economics; 2) confirms with optimization program verification cases that the larger the value of the three optimization parameters in this paper, the higher the gas production, regardless of economic factors. Excluding these optimization parameters, the reservoir inputs will be set as similar values listed in Table 4-1 and the total simulation time is ten years for all sensitivity analysis cases.

4.3.1 Sensitivity of Hydraulic Fracture Stage Numbers

The hydraulic fracture stage numbers will be increased by ten from two to fifty (hydraulic fracture spacing will be increased from 20 m to 500 m correspondingly). The values of hydraulic fracture half-length and dimensionless conductivity will be kept the same when increasing hydraulic fracture stages numbers. They are set to 150 m and 20 separately and the total time for production is set to ten years. The gas production graphs and a few gas pressure distribution graphs are plotted to verify the effect of this parameter.

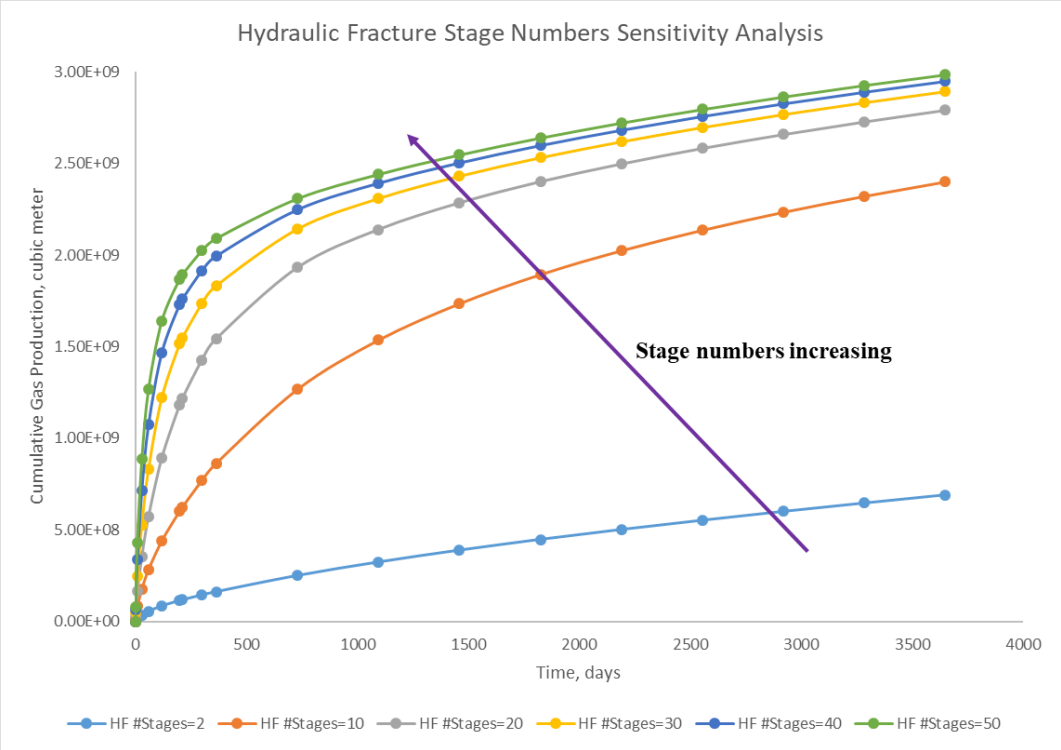

Figure 4-16 Hydraulic Fracture Stage Numbers Sensitivity Analysis

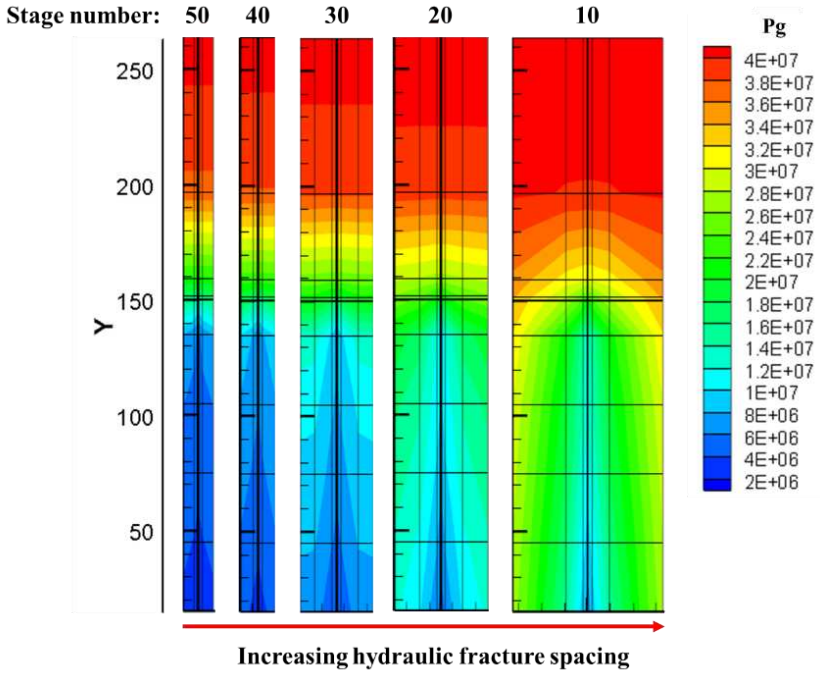

Figure 4-17 Gas Pressure Distribution Comparison for different Hydraulic Fracture Stage Numbers (t=365 days)

Based on cumulative gas production vs. time (Figure 4-16), it's obvious that hydraulic fracture stage number will greatly influence the gas production when they are increased from a relative small value. However, this trend will slow down after a certain hydraulic fracture stage number is reached, which is around 30 for the above sensitivity analysis case. X-Y gas pressure profiles (Figure 4-17) are also plotted under various hydraulic fracture stage numbers at t=365 days. They indicated the influence of stage numbers on production from prospective of gas pressure. Rapid gas pressure decline is observed with higher hydraulic fracture stage numbers, which have higher gas production.

4.3.2 Sensitivity of Hydraulic Fracture Half Length

The hydraulic fracture half-length will be increased by 50 m from 50 m to 250 m. And the values of hydraulic fracture stage numbers and dimensionless conductivity will be kept the same when increasing hydraulic fracture half-length. They are set to 20 and 20 separately and the total time for production is set to ten years. The gas production graphs and a few gas pressure distribution graphs will be also plotted to verify the effect of this parameter.

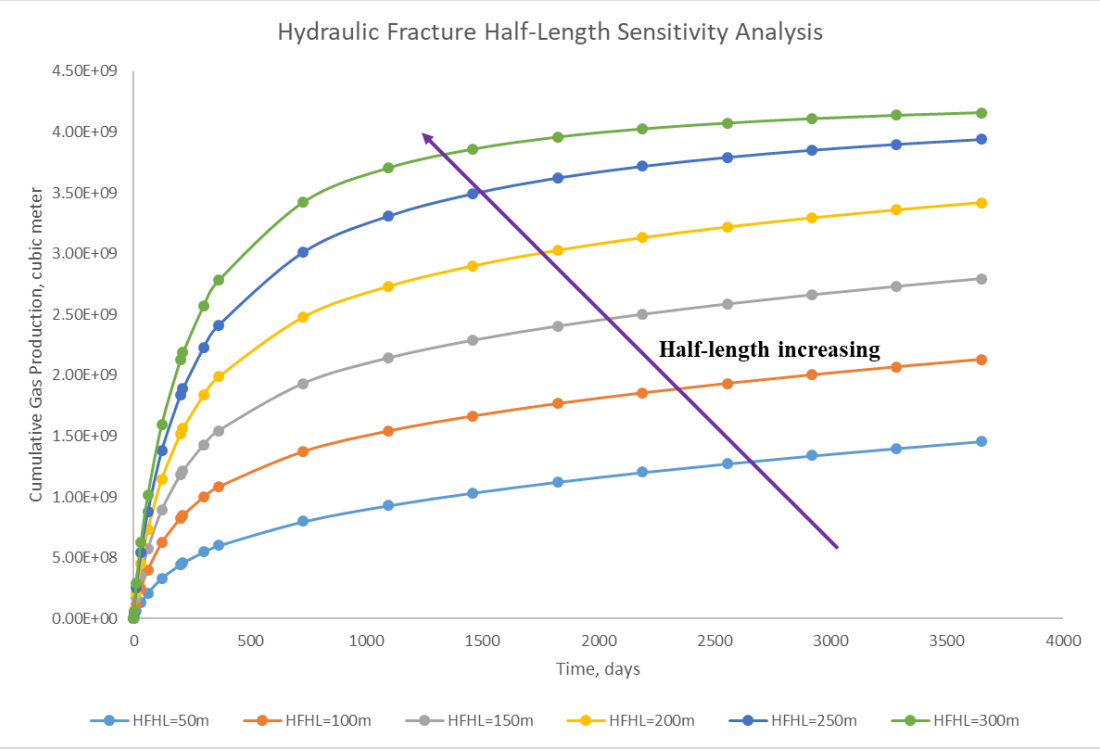

Figure 4-18 Hydraulic Fracture Half-length Sensitivity Analysis

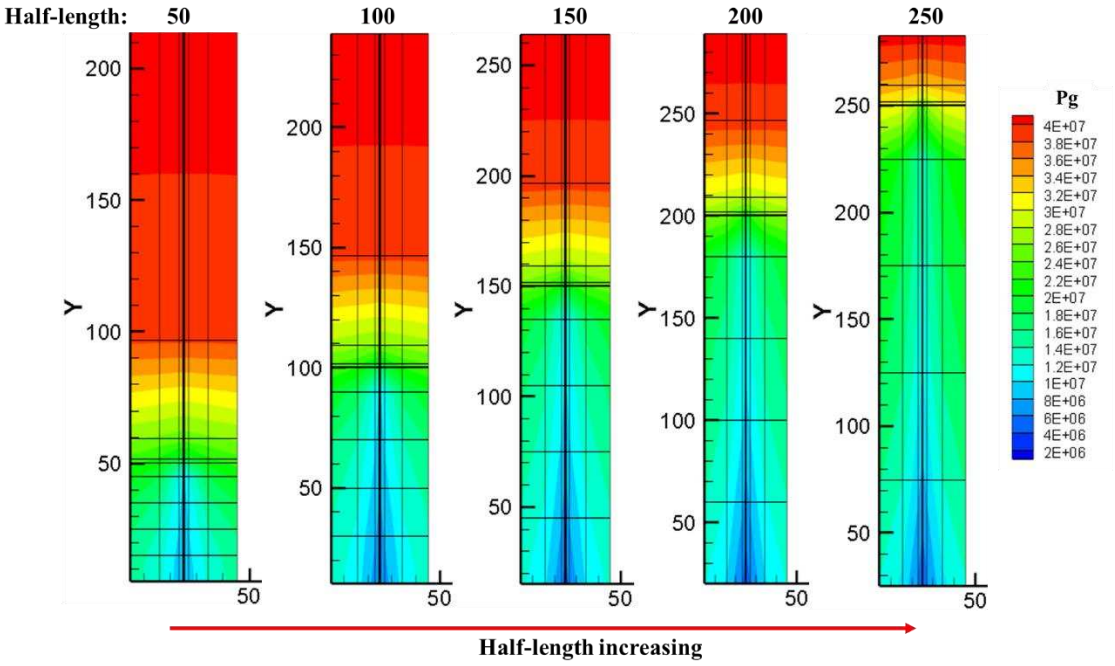

Figure 4-19 Gas Pressure Distribution Comparison for different Hydraulic Fracture Half-length (t=365 days)

Based on cumulative gas production vs. time Figure 4-18, it's clear that hydraulic fracture half-length has a significant effect on gas production. But the effect seems more even when the half-length is increased. Even though X-Y gas pressure profiles (Figure 4-19) have different scale in the Y direction due to LGR (hydraulic fracture area is refined evenly but with tips logarithm refined), a specific Y coordinate could be picked to view the influence of half-length. Thus, Y=100 m is selected. The color change (from red to light green and then to light blue, which represents more pressure decline gradually), is observed when half-length is increased.

4.3.3 Sensitivity of Hydraulic Fracture Dimensionless Conductivity

The dimensionless hydraulic fracture conductivity will be increased by 20 from 1 to 100. And the values for hydraulic fracture stage numbers and half-length will be kept the same when increasing dimensionless hydraulic fracture conductivity. They are set to 20 and 150 m separately and the total time for production is set to ten years. The gas production graphs and few gas pressure distribution graphs will be also plotted to verify the effect of this parameter.

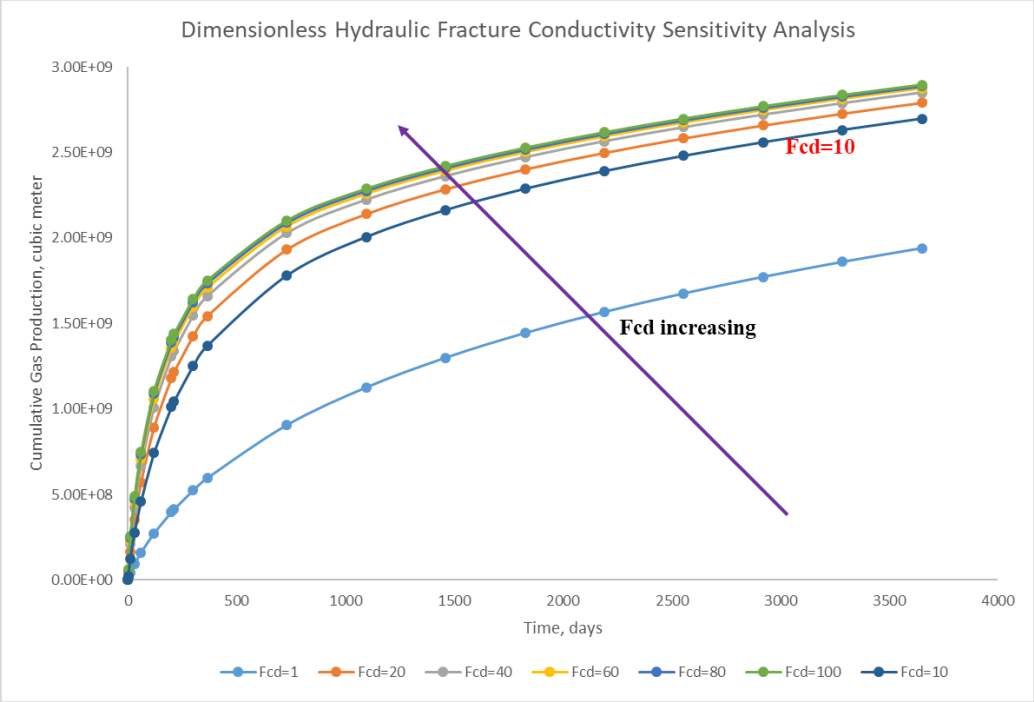

Figure 4-20 Dimensionless Hydraulic Fracture Conductivity Sensitivity Analysis

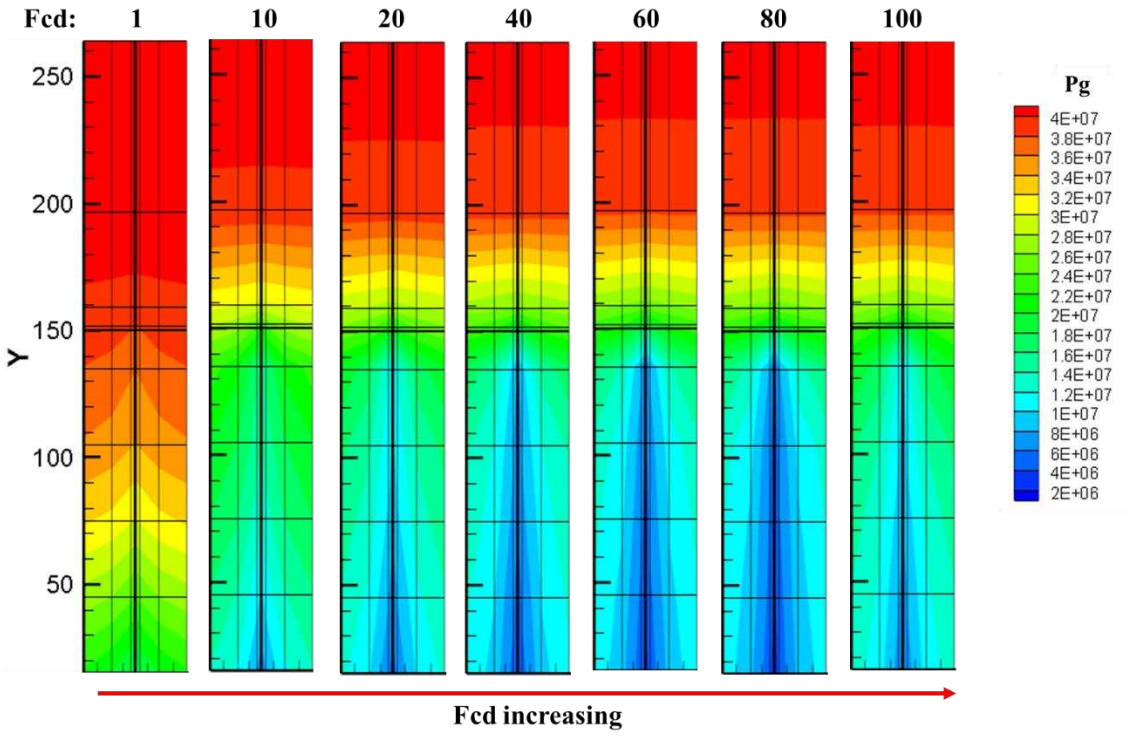

Figure 4-21 Gas Pressure Distribution Comparison for different Dimensionless Hydraulic Fracture Conductivities (t=365 days)

Based on cumulative gas production vs. time (Figure 4-20), a similar impact is showed for hydraulic fracture dimensionless conductivity as stage numbers increase. With dimensionless conductivity increased, gas production dramatically rises but after a certain value, which is 10 here, it increases slowly. This phenomenon could be noticed from X-Y gas pressure profile Figure 4-21. Starting from second plot of Figure 4-21, the color change (pressure change) in the outer area of Y direction is small and cause the slowdown of gas production.

4.3.4 Sensitivity Analysis Summary

Besides the conclusion mentioned above, a key point should be noticed. Even though these optimization parameters will influence gas production, they have different sensitivities to gas production. For example, when the stage number is increased from 2 to 50 (25 times enlargement), the gas production is only increased 4.26 times. But for half-length, when it is changed from 50 m to 300 m (6 times), the gas production increased 28.7 times. This phenomenon could be observed with gradient descent optimization method through the derivative value (gradient) calculated from numerical central difference method.

4.4 Influence of Gas Adsorption/desorption on Production

In Chapter 2, we discussed about the influence of gas adsorption/desorption on production. To display the effect explicitly, cases are designed. The reservoir inputs are also similar to Table 4-1, however, the Langmuir's volume will be set as $0\ m^2/kg$ (non-gas adsorption/desorption effect), $0.0022\ m^2/kg$, $0.005\ m^2/kg$ and $0.01\ m^2/kg$. Three optimization parameters are set to 20, 150 m and 20 separately and the total simulation time is also ten years. According to Figure 4-22, influence with and without gas adsorption/desorption is observed and this effect becomes bigger and bigger at later production periods or with bigger Langmuir's volume. This is because more adsorbed gas is released from solid phase to free gas phase as pressure decreases and contributes to the total production.

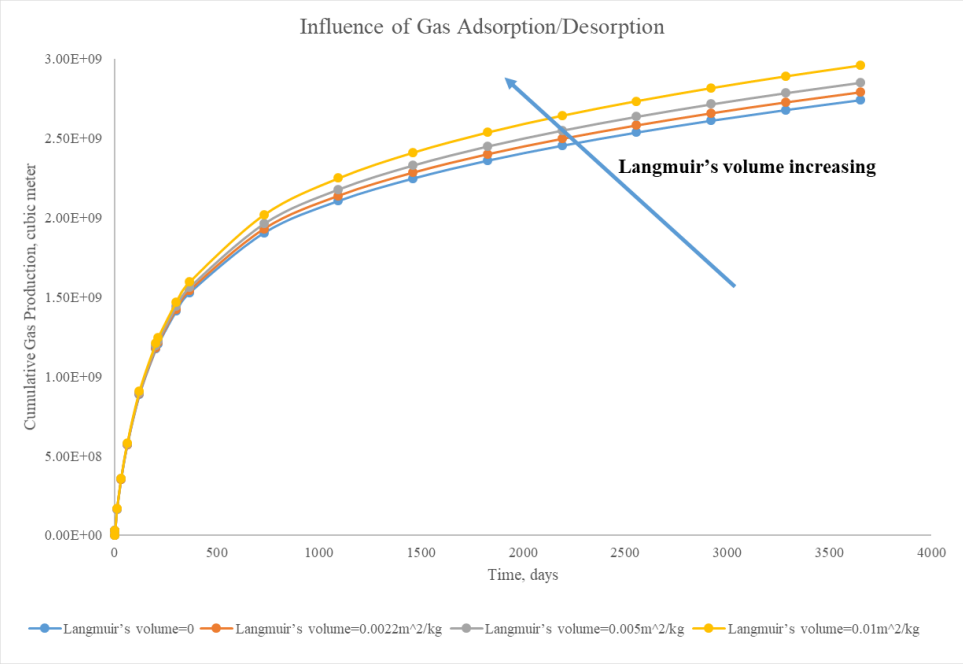

Figure 4-22 The Influence of Gas Adsorption/Desorption on Production

4.5 Influence of Klinkenberg Effect on Production

In Chapter 2, we also discussed about the influence of Klinkenberg effect on gas production. To visualize this effect, cases with and without Klinkenberg effect are simulated for ten years. Everything else is kept similarly as Table 4-1. The results are showed in Figure 4-23 and we do see the influence of Klinkenberg effect to the production, but not as much as gas adsorption/desorption.

4.6 Applications

The optimization program is proved to be effective above and so it will be applied to several real reservoir conditions. The objective function is changed from gas production to discounted cumulative-net-present value, which is already typed as Equation 3-10 in Chapter 3, and the simulation time is extended to ten years. These cases include: 1) basic unconventional gas reservoir case (same to verification case but use discounted cumulative-net-present value as objective function); 2) unconventional gas reservoir with nature fracture; 3) unconventional gas reservoir with Zipper-Fracking (without stress/geomechanics effect).

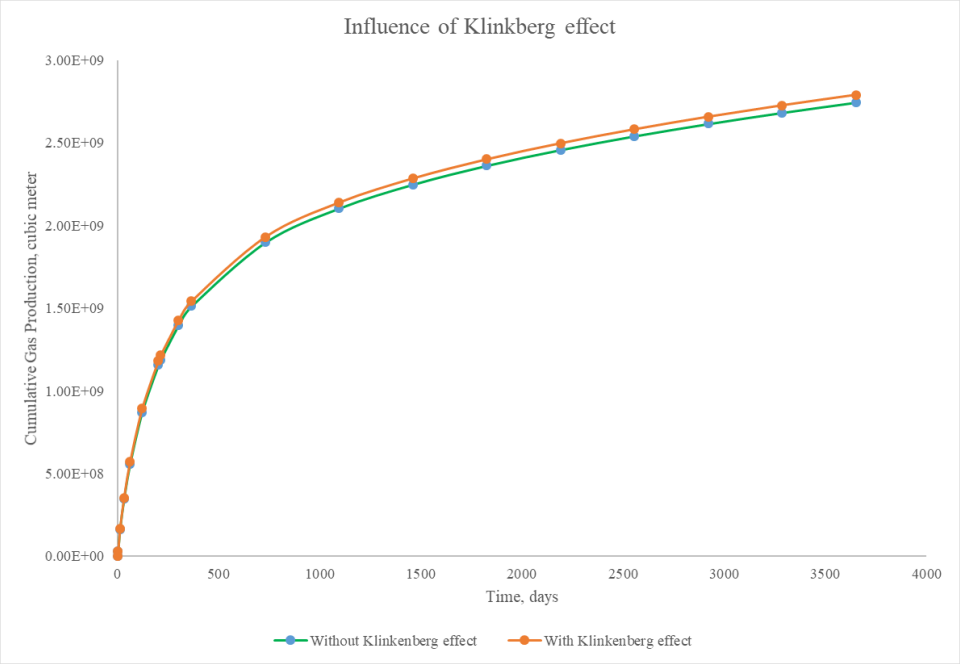

Figure 4-23 The Influence of Klinkenberg effect on Production

4.6.1 Regular Reservoir Case (Case#1)

The first real case setting is same to previous validation case's setting. Only hydraulic fractures are created in the reservoir system. The difference is that the objective function is switched to cumulative discounted-NPV. By applying coefficient into Equation 3-10, the discounted NPV function becomes:

$$C_{hf} = 40,000 * n_{real\#stages} + 10 * (1 + \frac{(0.04 * F_{cd} + 1000)}{1500}) * (2 * HFhl)^{1.8} \quad (4\text{-}3)$$

When the norm of the gradient is less than a very small number (5e-2), the changings of three optimization parameters between two steps are less than 0.00005 or the maximum iterations are reached, the optimization system will be terminated. Systematically initial points are designed so that larger domain could be covered, and the results for parts of combinations [300 150 5], [400 20 70], [100 50 60], [250 200 40], [25 200 40], [25 200 90] and [480 290 90] are displayed in Appendix D. The results (displayed as Table 4-5) showed that no matter what the initial point it is, the maximum cumulative discounted-NPV will be around 4.92 million dollars and its corresponding hydraulic fracture spacing, fracture half-length, and dimensionless fracture conductivity will be around 27~28 m, 293~294 m and 100. The best economic scenario

is found from initial point [400 20 70], which is $\$4.9206\times10^{6}$ and the corresponding HFhl, HFhl and Fcd values are 27.2695 m, 293.6781 m, as well as 100. To visualize the process of optimization, the values of hydraulic fracture spacing, fracture half-length, and dimensionless fracture conductivity for whole optimization processes with various initial points are plotted with gas production.

Table 4-5 Optimal Results by Starting from Various Initial Points for Case#1

Initial Points	HFsp (m)	HFhl (m)	Fcd	CDNPV ($)	#MSFLOW Called	Program Running Time (s)
[300 150 5]	27.0029	293.2596	100	4919317	1336	7994.24
[480 290 90]	27.1995	293.9436	100	4915165	452	3552.78
[400 20 70]	27.2695	293.6781	100	4920558	620	5118.65
[100 50 60]	27.3385	292.6629	100	4916353	806	4853.86
[250 200 40]	27.2320	293.8937	100	4915283	528	3239.79
[25 200 90]	27.1965	293.8291	100	4915511	666	3767.90

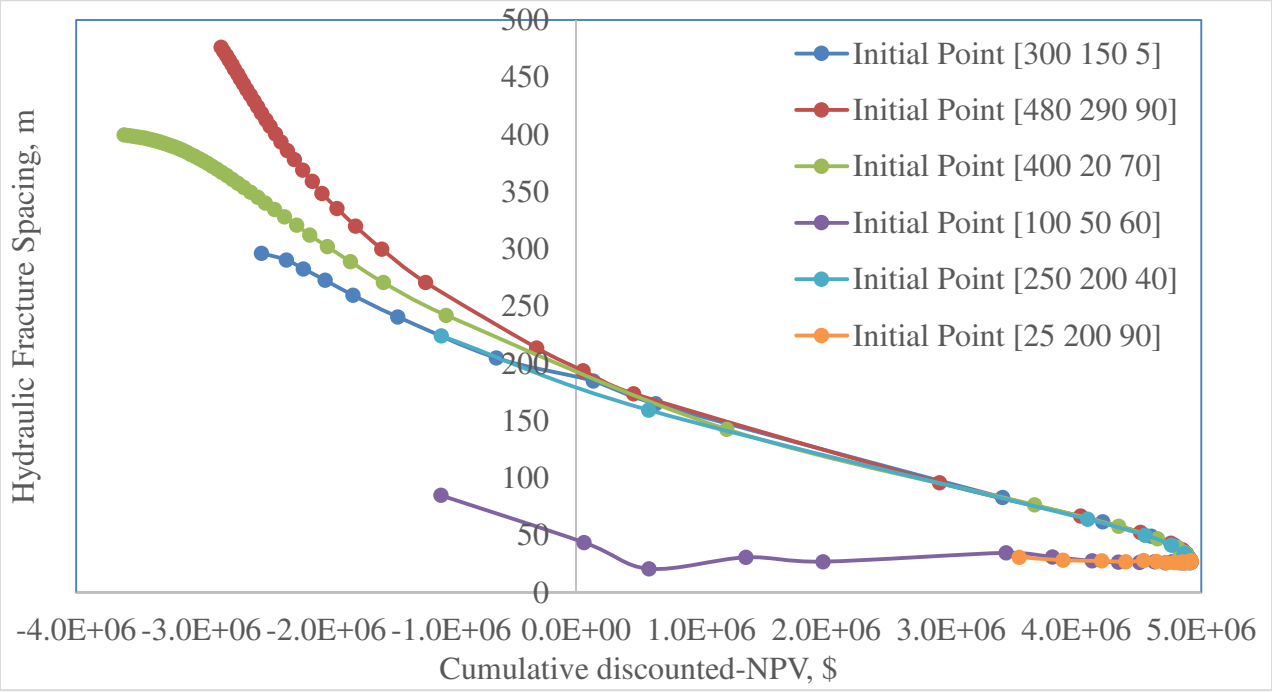

Figure 4-24 Optimization Process of Hydraulic Fracture Spacing vs. Cumulative discounted-NPV with different starting points

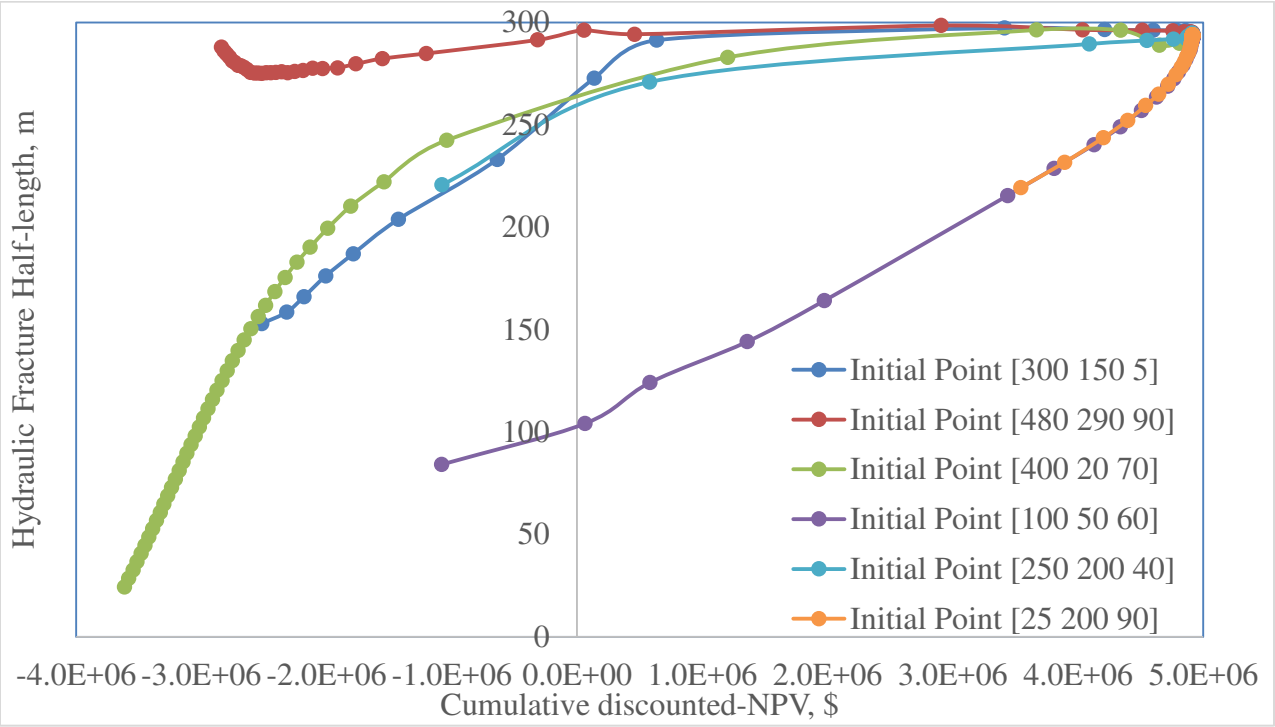

Figure 4-25 Optimization Process of Hydraulic Fracture Half-Length vs. Cumulative discounted-NPV with different starting points

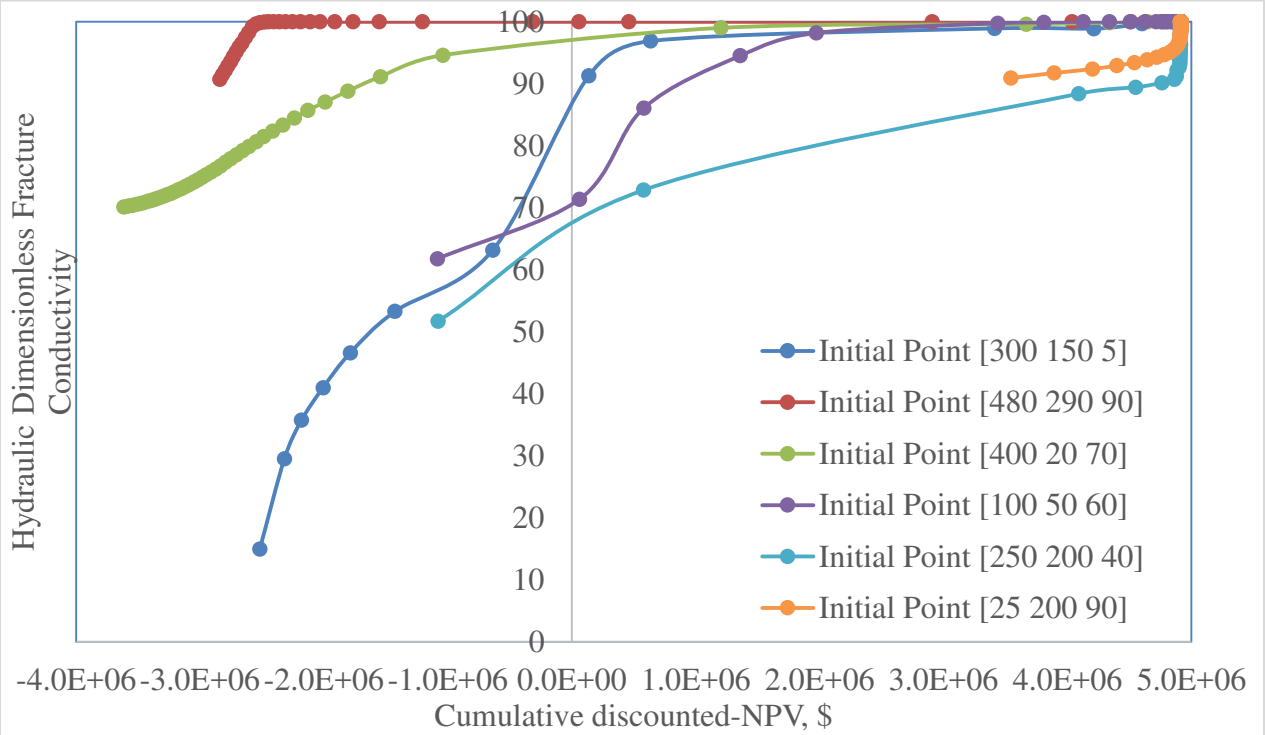

Figure 4-26 Optimization Process of dimensionless fracture conductivity vs. Cumulative discounted-NPV with different starting points

Based on the above graphs (Figure 4-24 to Figure 4-26) and result tables in Appendix D, we observed the evolution process of optimization and maximum cumulative discounted-NPV is around 4.92 million dollars no matter where the initial positions are. Its corresponding optimization parameters' values are reasonable since when economics is taken into consideration, the statement that it is better to have more hydraulic fracture stages (shorter hydraulic fracture spacing), longer hydraulic fracture half-length and higher dimensionless conductivity is no longer true. The reason that the value of dimensionless fracture conductivity stopped at the boundary is the small value setting of weight factors a_2, which means that increasing dimensionless fracture conductivity increases gas production and cash flow by a higher amount than the cost of the investment. This condition will be changed based on how experienced engineers designed its value. In addition, a phenomenon described in Chapter 3 is observed: when the three optimization parameters are closer to their optimal values, some fluctuations occur around optimal values. This is due to the characteristic of gradient descent method as Figure 4-27 shows. And this phenomenon could be also seen in case #2. Since the fluctuations here are small and not easy to be seen, they are not plotted in this case but will be showed in case #2.

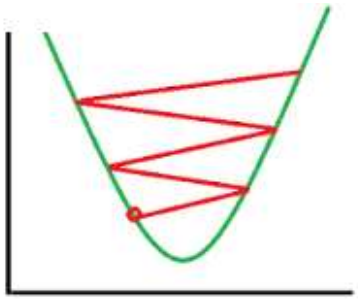

Figure 4-27 "Fluctuations" Characteristic of Gradient Descent Method

4.6.2 Reservoir Case with Natural Fractures (Case#2)

The presence of natural fractures will no doubt contribute to unconventional gas production and improve revenue. To better understand the contribution and the influence of natural fractures to the optimization parameters, this case is designed. The global flow is assumed to occur only through the fracture continuum, while rock matrix and fractures will interact locally by means of "inter-porosity" flow (double-porosity model).

The generation of a mesh system is different to previous cases because of natural fractures. To create the mesh system with natural fractures, the MINC method is used to sub-partition a "primary" porous medium into a "secondary" mesh for fracture media. In a nutshell, MINC made a copy of previous mesh system and assign the natural fractures' properties to these copied blocks. To realize this function, one extra step with the simulator is added to the optimization system; that is, MSFLOW will run one time with keyword "MINC" but without simulation run. The parameter settings of MINC and properties of natural fractures are given in Table 4-6.

Table 4-6 Additional Parameters for Nature Fracture Case

Parameter	Value	Unit
Nature fracture permeability	$k_{NFx} = k_{NFy} = k_{NFz} = 9.87 \times 10^{-16}$	m^2
Nature fracture porosity	$\phi_{NF} = 0.4$	
MINC type	THRED	
MINC volume fraction	0.000001	

The termination criteria are similar to Case #1. Systematically initial points are designed so that larger domain could be covered, and the results for parts of combinations [250 50 50], [100 200 35], [400 120 22], [500 180 90], [22 280 5], [310 250 1] and [50 20 72] are displayed in Appendix E. The results (displayed as Table 4-7) show that starting from these initial points, the maximum cumulative discounted-NPV is founded to be around 6.28 million dollars and its corresponding hydraulic fracture spacing and fracture half-length are around 100-103 m and 73-76 m. The best economic scenario is found from initial point [100 200 35], which is $\$6.2812 \times 10^6$ and the corresponding HFhl as well as HFhl are 101.272m and 74.7094 m. The above values are reasonable when we compared them with the results of Case #1 since we know that the existence of natural fractures will absolutely contribute to our benefits and less fracture stages numbers (more fracture spacing) as well as less fracture half-length will be needed. The dimensionless fracture conductivity is needed to be modified due to the existence of a specific phenomenon displayed as Figure 4-28. We found out that the dimensionless fracture conductivity fluctuates within a certain value finally no matter what the initial points are, which indicates that it has been trapped. In other words, due to the existence of natural fractures, the hydraulic fracture conductivity is likely to have negligible effect on production after a certain characteristic value. Therefore, the dimensionless fracture conductivity needs to be re-

determined. To determine the range of this certain value, random fracture conductivity values were tried but with the same hydraulic fracture spacing and fracture half-length value. Followings are results tables (Table 4-8 and Table 4-9) and figures (Figure 4-29 and Figure 4-30).

Table 4-7 Optimal Results by Starting from Various Initial Points for Case#2

Initial Points	HFsp (m)	HFhl (m)	Fcd	CDNPV ($)	#MSFLOW Called	Program Running Time (s)
[250 50 50]	102.9212	73.3237	49.2561	6280992.6	1092	16556
[100 200 35]	101.2720	74.7094	38.6753	6281189.5	1150	15457
[400 120 22]	100.7716	75.5512	41.0406	6281017.1	1130	15778
[500 180 90]	102.2372	73.3213	88.6908	6280462.2	1010	15760
[22 280 5]	101.2858	76.7118	0.9232	6280976.0	1282	18535
[310 250 1]	103.6265	76.0125	0.4901	6280952.5	772	9675
[50 20 72]	100.4351	73.9687	71.9127	6280938.1	252	3231

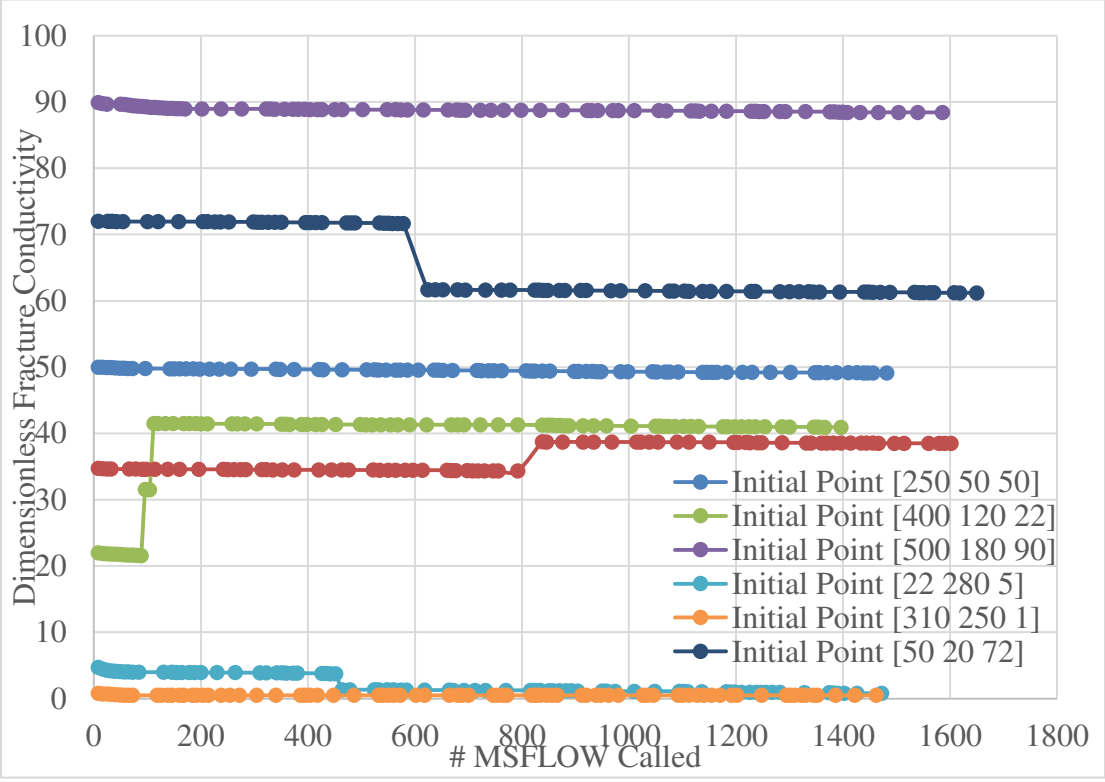

Figure 4-28 Dimensionless Fracture Conductivity vs. #MSFLOW Called for Nature Fracture Case when optimization starts from various initial points

Table 4-8 Fcd vs. Cumulative discounted-NPV for Optimal Results

Fcd	CDNPV1 (HFsp=102.9212m, HFhl=73.3237m)	CDNPV2 (HFsp=101.272m, HFhl=74.7094m)	CDNPV3 (HFsp=100.7716m, HFhl=75.5512m)
0.00E+00	6281057.08	6281241.79	6281073.82
1.00E-03	6281057.66	6281242.35	6281074.48
0.1	6281057.68	6281242.29	6281074.23
0.2	6281057.54	6281242.17	6281073.99
0.5	6281057.22	6281241.84	6281073.75
1	6281056.58	6281240.97	6281072.94
10	6281044.45	6281228.86	6281060.44
30	6281018.24	6281201.38	6281032.61
60	6280978.53	6281160.48	6280990.69
100	6280925.48	6281105.66	6280934.73

Table 4-9 Fcd vs. Cumulative discounted-NPV for Random Values

Fcd	CDNPV4 (HFsp=250m, HFhl=50m)	CDNPV5 (HFsp=450m, HFhl=20m)
0.00E+00	5952755.28	4923415.66
1.00E-03	5952756.05	4923420.61
0.1	5952755.64	4923419.69
0.2	5952755.61	4923417.38
0.5	5952755.29	4923416.55
1	5952754.89	4923416.37
10	5952749.01	4923415.56
30	5952735.60	4923412.65
60	5952716.53	4923408.42
100	5952689.44	4923403.84

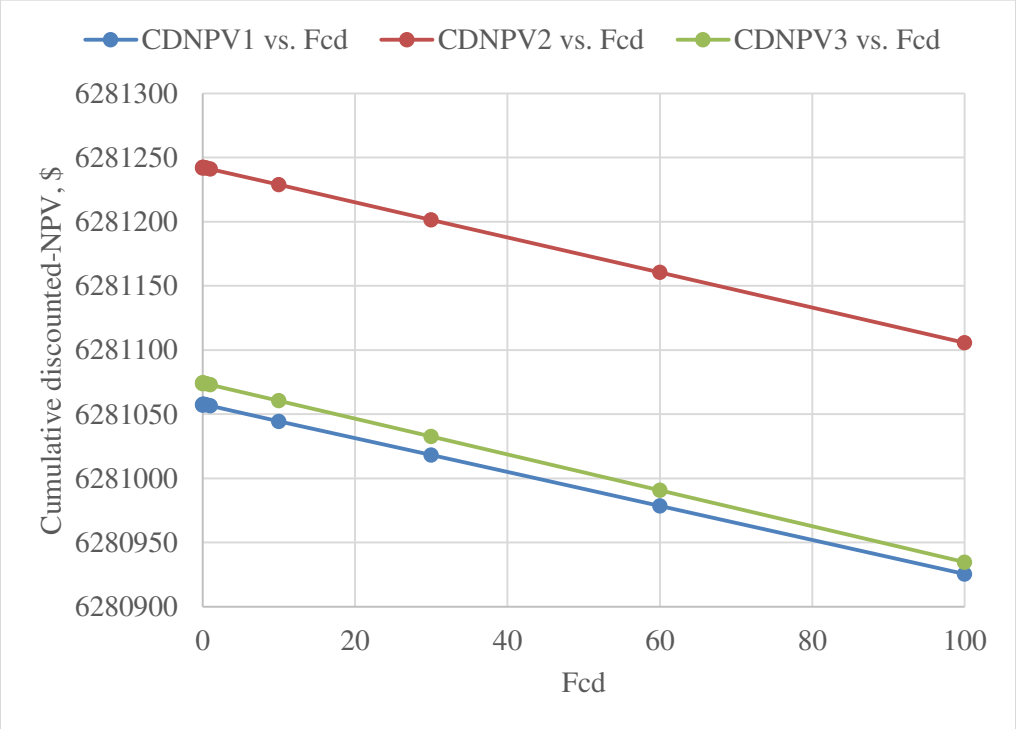

Figure 4-29 Fcd vs. Cumulative discounted-NPV for Optimal Results

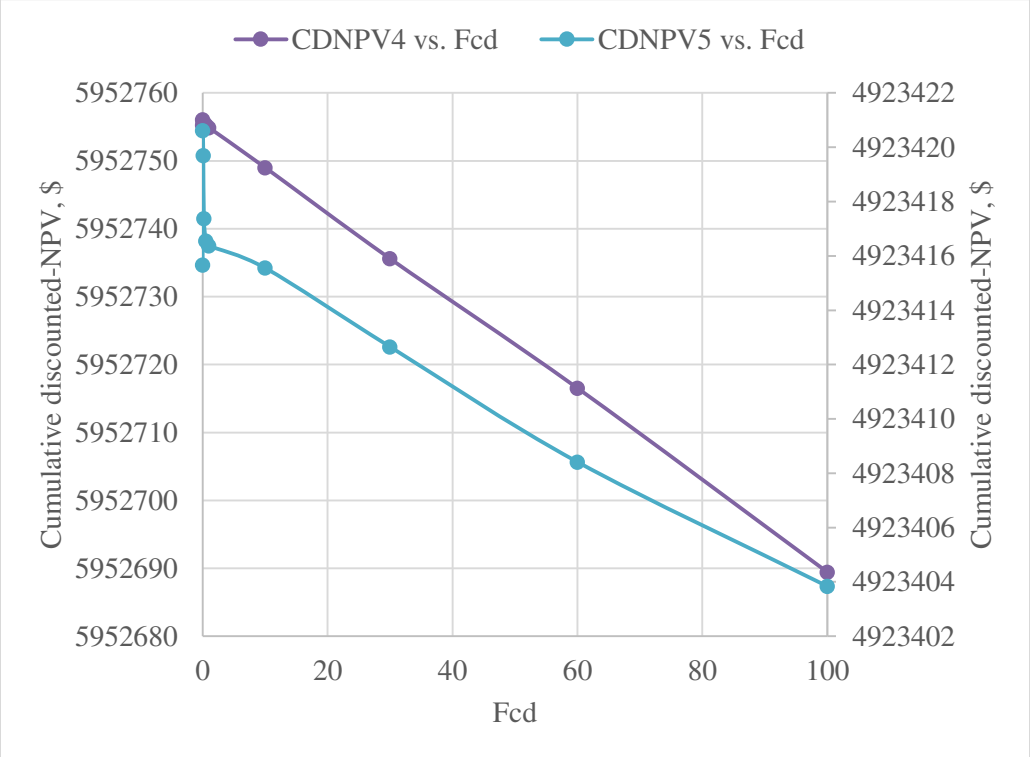

Figure 4-30 Fcd vs. Cumulative discounted-NPV for Random Values

Based on the above tables and diagrams, we found they have similar trends. Cumulative discounted-NPV will increase first and then decrease after a certain value. And by looking into the tables (Table 4-8 and Table 4-9), we found that this dimensionless fracture conductivity value for all the cases are below 0.2, which is pretty small because of the large values of nature fracture permeability. With updated fracture conductivity, the maximum CDNPV is changed to $\$6.2812\times10^{6}$ when HFhl, HFhl and Fcd are 101.272 m, 74.7094 m, and 0.001.

To visualize the fluctuations that I discussed in Case#1, the three optimization parameters could be plotted with number of function calls or program run time. We select the number of function calls for the case with different initial points. We observed, even though we started from different initial points, their final values fluctuate within a small range of our optimal values.

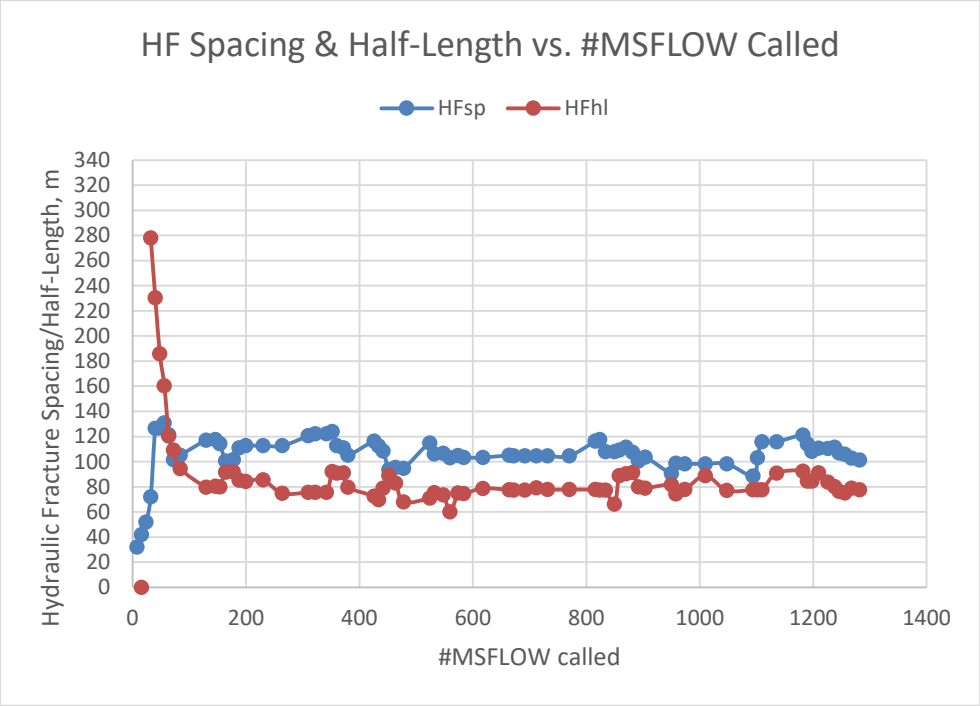

Figure 4-31 The Fluctuations Features of Hydraulic Fracture Spacing and Half-length when optimization starts from initial point [22 280 5]

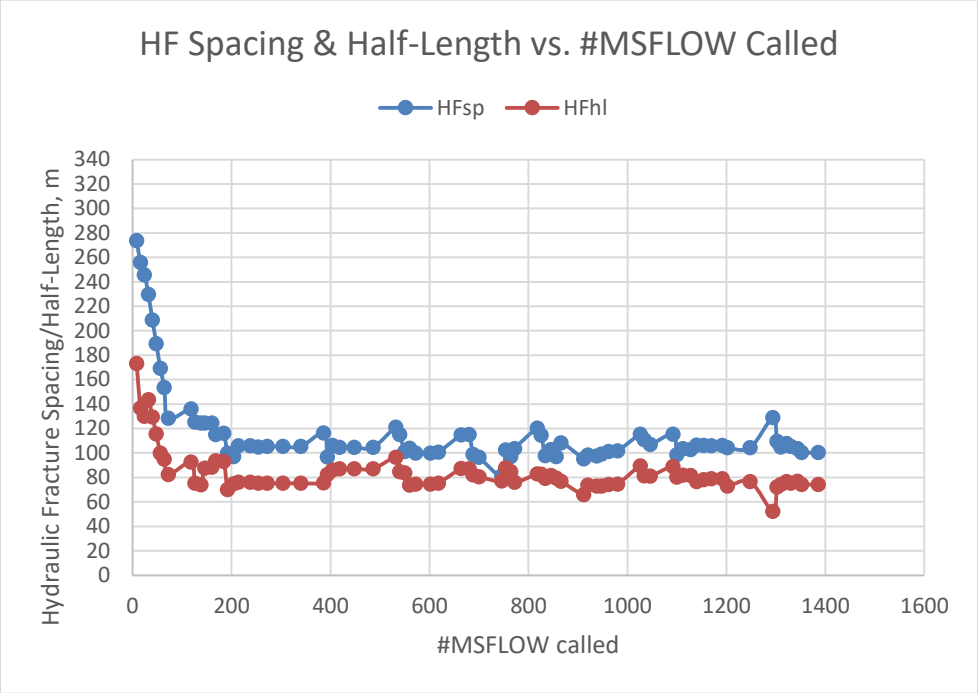

Figure 4-32 The Fluctuations Features of Hydraulic Fracture Spacing and Half-length when optimization starts from initial point [310 250 1]

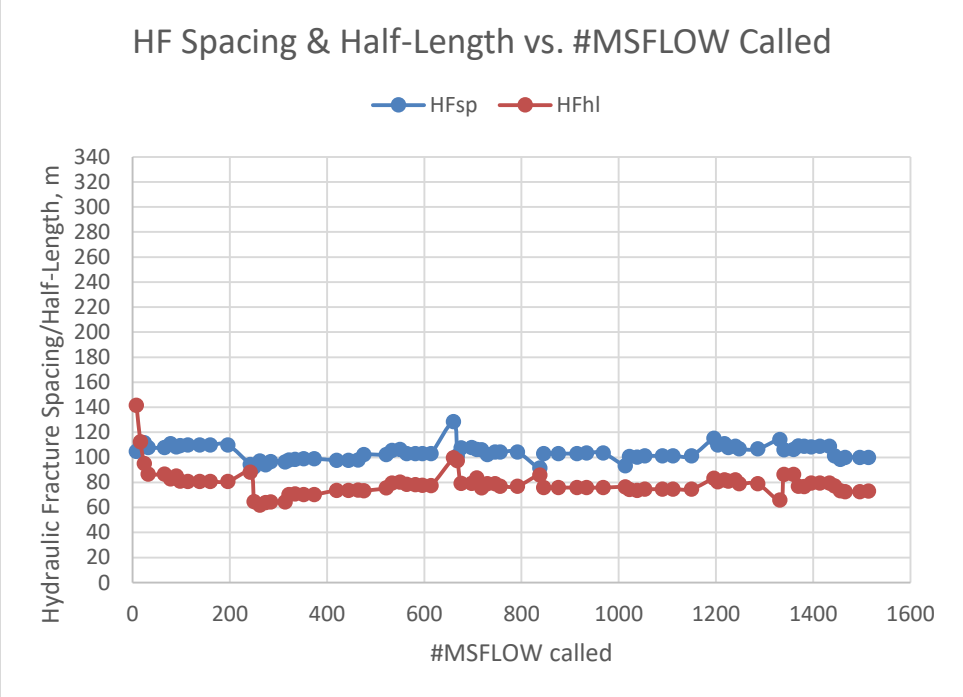

Figure 4-33 The Fluctuations Features of Hydraulic Fracture Spacing and Half-length when optimization starts from initial point [100 200 35]

4.6.4 Reservoir Case with Modified Zipper Frac (Case#3)

Zipper Frac, as Figure 4-34 displays, is a successful completion strategy for organic shale, which was originally designed to reduce cycle times between fracture stages and enhance general operational efficiency. But many companies have reported increased production rates after applying zipper frac technology (Algarhy et al. 2017). Thus, researchers started to investigate into this field and they found that the modified zipper frac has a better influence on reservoir behaviors. Modified Zipper Frac (MZF) does nothing more than arrange the frac stages of two or more adjacent wells so that each well's frac stages will be located in the middle zones between the frac stages of other well (as Figure 4-36 shows). However, what should be the spacing, fracture half length, and dimensionless fracture conductivity when economics and reservoir conditions (like heterogeneity) are considered? Our optimization system is able to figure out these problems. Zipper frac or modified zipper frac cases are supposed to be simulated with original model since the way that hydraulic fracture distributed due to zipper frac will cause the asymmetry if the simplified model is selected. The zipper frac cases are similar with Case#1 and programs are easy to be modified. The only difference is that it has a different fracturing cost function compared to previous cases because of the added wells and frac stages. Thus, the optimization process and the format of results will be similar. Due to the case similarity and time-consuming issues (original model will be needed), it will not be run. However, the gas production for cases with zipper frac or MZF will be compared.

The reservoir length and thickness have been modified into 1100 m and 120 m for this case for the convenience of designing the location of hydraulic fracture. But other parameters are kept same as Table 4-1. The results (Figure 4-37) show that the ones (red and green) with MZF has a greater impact on gas production when compared with the one (blue) with zipper fac.

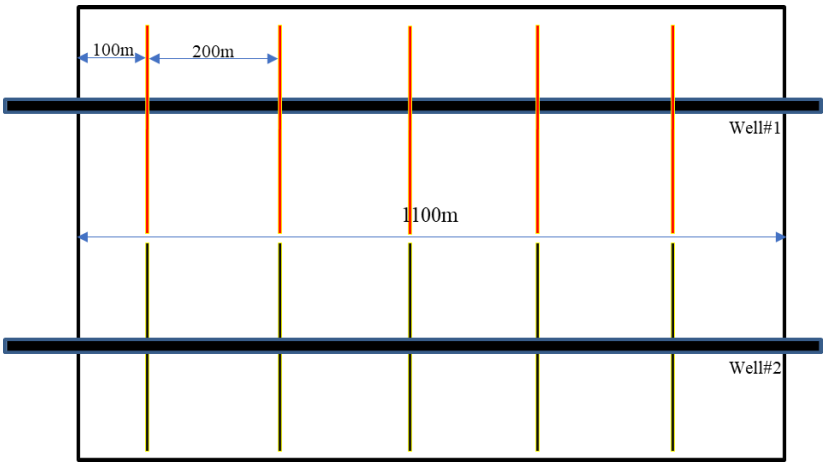

Figure 4-34 Zipper Frac

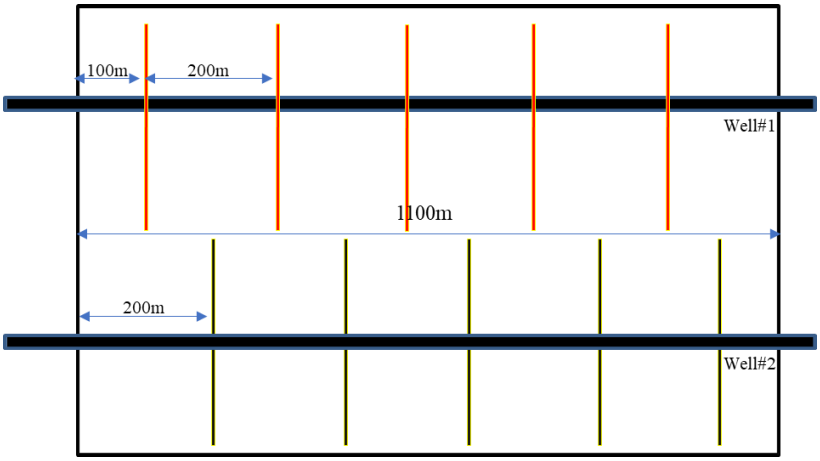

Figure 4-35 Modified Zipper Frac (non-staggered)

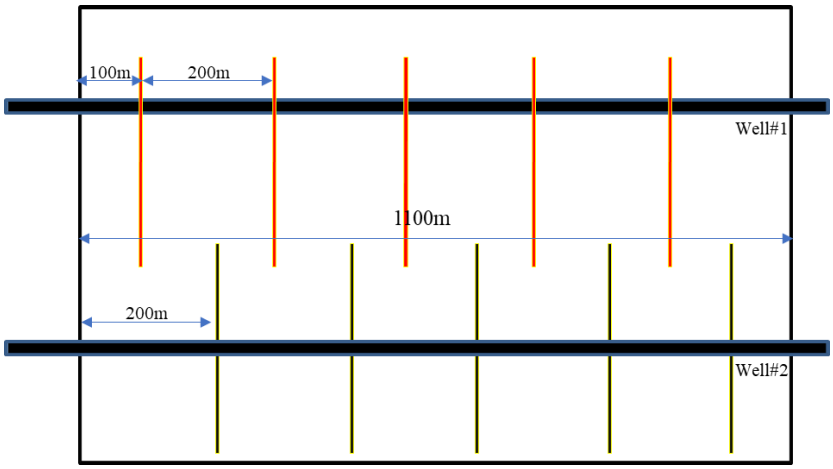

Figure 4-36 Modified Zipper Frac (staggered)

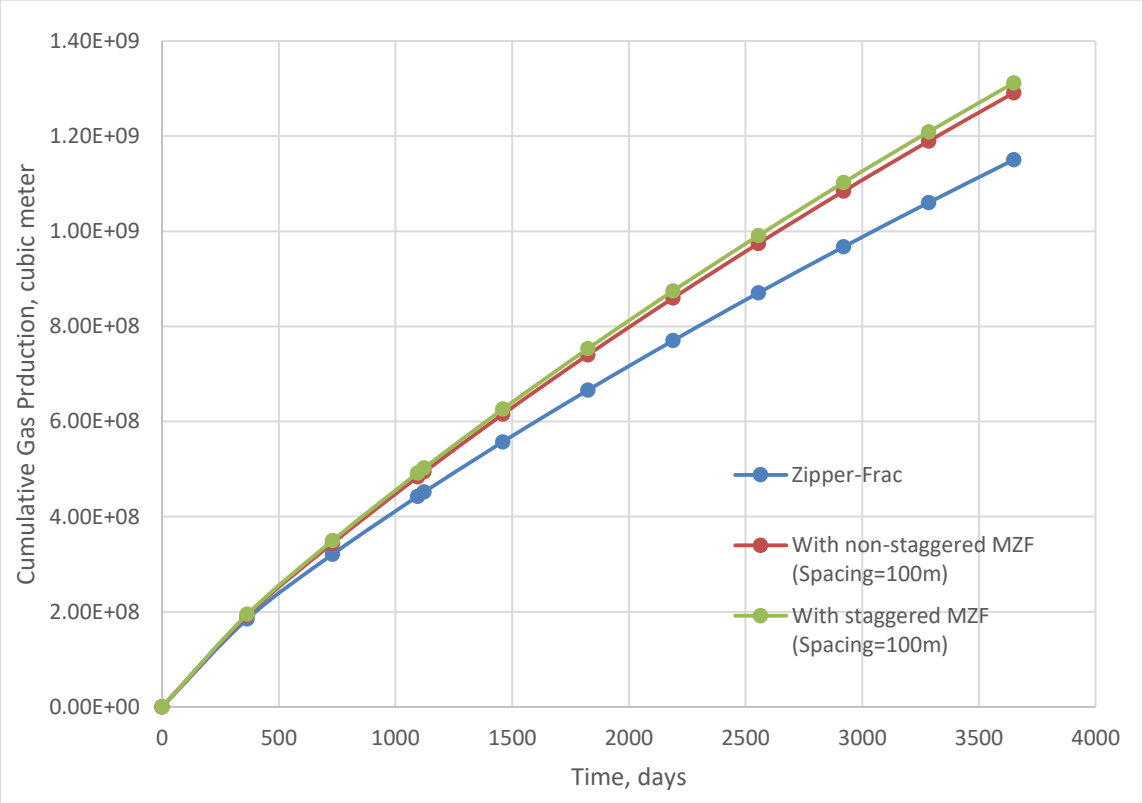

Figure 4-37 Cumulative gas production with Zipper Frac or Modified Zipper Frac

CHAPTER 5
CONCLUSIONS AND RECOMMENDATIONS

In this chapter, we summarize the research results of this thesis with several conclusions and recommendations at the end.

5.1 Summary and Contributions

This thesis develops a hydraulic-fracture optimization system specifically for unconventional gas reservoirs. The optimization system is validated and is shown quite useful. On the one hand, with different reservoir cases and reservoir inputs, the systems are able to give a relative good result and accuracy. Based on these optimization results, engineers could identify the best scenario for their project by combining their field experience. Based on various applications, we observed the influence of reservoir properties and economic effect on fracture optimization parameters. On the other hand, the algorithm of optimization system could be easily changed into any gradient based methodologies for future studies and comparison. Also the optimization system could be easily modified to investigate other field questions since the principles are similar for most optimization problems, such as well placement, history matching and so on, by changing optimization parameter as well as objective functions.

5.2 Conclusions

Based on the research of this thesis, we find that different reservoir characteristics, different economic effects, and different optimization objectives lead to the diversity of optimized results. Therefore, in practical applications, we need to adapt to local conditions. Based on the reservoir characteristics in this thesis and the characteristics of fracturing operational costs, we can draw the following conclusions:

- When we don't consider the hydraulic fracturing cost, gas production will be better with more hydraulic fracture stage number, longer hydraulic fracture half-length and higher dimensionless conductivity, which means gas production is a monotonic function of hydraulic fracture spacing, hydraulic fracture half-length, and dimensionless fracture conductivity. However, after a certain threshold value is reached, the influence these optimization parameters are relatively negligible. [20

300 100] is the best combination scenario and the corresponding largest cumulative gas production for a year is $8.5079\times10^{9}\ \mathrm{m}^{3}$.

- When economy and natural fractures are taken into consideration, it is not good to have more hydraulic fracture stage number, longer hydraulic fracture half-length and higher dimensionless conductivity. [27.2695 293.6871 100] is the best combination scenario and the corresponding largest cumulative discounted-NPV for ten years is $\$4.9206\times10^{6}$.
- The existence of natural fractures will contribute the gas production and reduce the needs of bigger hydraulic fracture stage numbers, hydraulic fracture half-length and dimensionless conductivity. The degree that influences the three optimization parameters above will be determined by the value of its permeability. [101.272 74.7094 0.001] is the best combination scenario and the corresponding largest cumulative discounted-NPV for ten years is $\$6.2812\times10^{6}$.
- Distinct types of Zipper-Frac are observed to have a different influence on gas production and so economy. And the influence is determined whether it is staggered or not, or the spacing between multiple well's hydraulic fractures. The case of Zipper-Frac is not conducted since its similarity to Case#1.

5.3 Recommendations

In the course of my research, I learned about the gradient-free optimization approach through further understanding of optimization. Many of the gradient-free methods are heuristic, and their advantage is that the algorithms do not need gradient information, which greatly improves the efficiency of the multi-parameter optimization problems, especially, for the cases that treat reservoir numerical simulators as a black box. In other words, if there are N optimization parameters in the objective equation, using the gradient based methods require 2 × N reservoir numerical simulator operations (central difference) or more if it is a multi-order derivative gradient-based method. But, gradient-free heuristic optimization requires less computation. Its downside is that these gradient-free heuristic optimization methods cannot be mathematically proven to be correct, although in many cases they will find a number of good engineering results.

Therefore, if we can combine the two methods together, we can greatly improve the efficiency and the accuracy of results by avoiding the issues of local-trapping. The idea of this combined approach is to:

- Initialize the starting values of any gradient algorithms by using a gradient-free heuristic algorithm and then search for the local optimum value by a specific gradient algorithm;
- The local optimal value is substituted into the gradient-free algorithm to initialize the initial value of the gradient algorithm again;
- By iterating for multiple times, not only can the "local-trapping" issue be avoided, but it also increases the optimization efficiency, which is the future research direction.

Another idea is to combine this system with fracture operating optimization system, which is already realized by Frac-CSM designed by our Energy Modeling Group (EMG). By using the results obtained from the fracture optimization system in the paper as input values for Frac-CSM to get a set of operating solution; if the operating solutions can not be obtained, the optimization system in this paper is supposed to be run again and again by increasing the limitations for fracture optimization until a set of possible operating plan is acquired. By this way, we are able to design a fracture operating solution that creates the most suitable hydraulic fractures for a particular reservoir.

LIST OF SYMBOLS

Symbol	Description
A_{ij}	the common interface area between control volumes i and j
a_i	sensitivity coefficient
b	gas slippage factor
c	compressibility for all media
C_T	thermal expansion coefficient of formation rock
c_g	gas compressibility
C_{hf}	hydraulic fracturing costs
d_i	distance from the geometric center of i to interface
d_k	search direction at kth point
D	diffusivity coefficient or depth from a datum
f	function
F_{cd}	dimensionless fracture conductivity
F_{ij}	flow going through area A_{ij} between control volume i and j
g_k^T	gradient of objective function at x_k
H_R	reservoir thickness
k	absolute permeability
k_{HF}	hydraulic fracture permeability
k_m	matrix fracture permeability
$k_{r\beta}$	relative permeability of phase β
k_∞	absolute, gas phase permeability under very large gas phase pressure
L_R	reservoir length
m_g	adsorbed or desorbed gas mass per unit volume of formation
m_k	the iteration number when a smaller function value is found

M_w	molecular weight of gas mixture
n_{stage}	numbers of fracture stage
$o(\alpha)$	Higher-order infinitesimal of α
P	pressure
P°	reference pressure
P_β	pressure of phase β
P_{cgw}	gas-water capillary pressure
P_L	Langmuir's pressure
P_i	initial pressure
P_w	wellbore pressure
q_β	sink/source rate of phase β
R	gas constant
S_β	the saturation of phase β
S_{wr}	residue water saturation
$\overline{S_k}$	average volume relative of kerogen in bulk volume
T	formation temperature
T°	reference temperature
v_β	Darcy velocity of phase β
V	bulk volume
V_i	element volume of the element i
V_E	Langmuir's volume
V_L	Langmuir's volume at state L
W_R	reservoir width
w_i	weight factor for i
x_k	independent variable at kth point
x_f	fracture half-length

$\| \mathbf{x} \|_2$	Euclidean norm
Z_g	gas compressibility factor

Greek Symbols

α	step size
β_β	effective non-Darcy flow coefficient for fluid
μ_g	gas viscosity
λ	Brook-Corey pore size distribution index
$\bar{\lambda}$	mean-free-path of gas molecules
Λ	dimension of conduit
$\bar{\theta}_k$	the angel between g_k and d_k
ϕ	the effective porosity
$\phi°$	the effective porosity of formation at reference pressure
ϕ_M	matrix porosity
ϕ_{HF}	hydraulic fracture porosity
Φ_β	flow potential of phase β
ρ_β	the density of phase β
ρ_k	kerogen density
Γ	system boundary
σ	parameter for Armijo rule

Abbreviation

AIM	adaptive implicit method
BHP	bottom hole pressure
CMG	computer modeling group
CDNPV	cumulative discounted-NPV
DP	double porosity

EIA	energy information administration
EOS	equation of state
EMG	energy modeling group
FDG	finite difference gradient
FVF	formation volume factor
GA	genetic algorithms
HF	hydraulic fracture
HFhl	hydraulic fracture half length
HFsp	hydraulic fracture spacing
IFD	integral finite difference
IUPAC	international union of pure and applied chemistry
LGR	local grid refinement
MINC	multiple interacting continua
MSFLOW	multiphase subsurface flow model
MZF	modified zipper frac
NPV	net present value
PDE	partial differential equation
PR-EOS	Peng-Robinson equation of state
PSO	particle swarm optimization
QIM	quadratic interpolation model-based
RSM	response surface methodology
SA	simulated annealing
SPMI	simultaneous perturbation multivariate interpolation
SPSA	simultaneous perturbation stochastic approximation
TOUGH	transport of unsaturated groundwater and heat
VFSA	very fast simulated annealing

REFERENCES CITED

Asadollahi, M. and Naevdal, G. 2009. Waterflooding Optimization Using Gradient Based Methods. Presented at the SPE/EAGE Reservoir Characterization and Simulation Conference, Abu Dhabi, UAE, 19-21 October. SPE-125331-MS. http://doi:10.2118/125331-MS.

Aloulou, F. and Zaretskaya, V. 2016. Shale gas production drives world natural gas production growth, https://www.eia.gov/todayinenergy/detail.php?id=27512 (accessed 20 February 2018).

Algarhy, A., Soliman, M., Heinze, L., et al. 2017. Increasing Hydrocarbon Recovery from Shale Reservoirs Through Ballooned Hydraulic Fracturing. *Unconventional Resources Technology Conference.*

Bangerth, W., Klie, H., Wheeler, M., Stoffa, P., et al. 2006. On optimization algorithm for the reservoir oil well placement problem. *Computational Geosciences* **10**: 303–319. http://doi:10.1007/s10596-006-9025-7.

Bellout, M.C., Echeverría Ciaurri, D., Durlofsky, L.J. et al. 2012. Joint optimization of oil well placement and controls. *Computational Geosciences* **16**: 1061. https://doi.org/10.1007/s10596-012-9303-5.

Bertsekas, D. 2005. Nonlinear Programming Lecture 4 Convergence Analysis of Gradient Methods, http://web.mit.edu/6.252/www/LectureNotes/6_252%20Lecture04.pdf (accessed 20 February 2018).

Brake, A. C. 2013. Fracture Optimization in a Giant Gas Field. Presented at the SPE Unconventional Gas Conference and Exhibition, Muscat, Oman, 28-30 January. SPE-164029-MS. https://doi:10.2118/164029-MS.

Chen, C., Jin, L., Gao, G., et al. 2012. Assisted History Matching Using Three Derivative-Free Optimization Algorithms. Presented at the SPE Europec/EAGE Annual Conference, Copenhagen, Denmark, 4-7 June. SPE-154112-MS. https://doi:10.2118/154112-MS.

Cui, X. 2016. Poststack impedance inversion using improved particle swarm optimization. Society of Exploration Geophysicists. https://doi.org/10.1190/segam2016-13877269.1.

Donnez, P. 2007. Reservoir Fluid Properties. In *Essential of Reservoir Engineering*, first edition, Chap. 2, 150-151. Paris: Editions Technips.

Ertekin, T., King, G. A., and Schwerer, F. C. 1986. Dynamic Gas Slippage: A Unique Dual-Mechanism Approach to the Flow of Gas in Tight Formations. *SPE Form Eval* **1**(1): 43-52. SPE-12045-PA. https://doi:10.2118/12045-PA.

Hajizadeh, Y., Christie, M. A., and Demyanov, V. 2009. Ant Colony Optimization Algorithm for History Matching. Presented at the EUROPEC/EAGE Conference and Exhibition,

Amsterdam, The Netherlands, 8-11 June. SPE-121193-MS. https://doi:10.2118/121193-MS.

Hefley, W.E., Seydor, S.M., Bencho, M.K., et al. 2011. The economic impact of the value chain of a Marcellus Shale Well. Working paper, Katz Graduate School of Business, University of Pittsburgh. http://d-scholarship.pitt.edu/10484/.

Honarpour, M., L. Koederitz and Harvey, A. H. 1986. Relative permeability of Petroleum Reservoirs. *CRC Press, Inc.*, Boca Raton, Florida (1986).

Kaluarachchi, J. J. and Parker, J. C. 1989. An Efficient Finite Element Method for Modeling Multiphase Flow. *Water Resources Research*, **25** (1): 43–54.

Kennedy, J. and Eberhart, R.C. 1995. Particle Swarm Optimization. *Proc. IEEE Int. Conf. on Neural Networks*, **4**, 1942–1948. Piscataway, NJ: IEEE Service Center.

Klinkbenberg, L.J. 1941. The Permeability of Porous Media to Liquids and Gases. *Drill. & Prod. Prac.*, API (1941) 200-13.

Kundt, A. and Warburg, E. 1875. Ueber Reibung und Waermeletiung verduennter Gase. Ann. Physik, Poggendorf **155**: 337-65.

Lane, H.S., Watson, A.T., and Lancaster. D.E. 1989. Identifying and estimating desorption from Devonian shale gas production data. Presented at the SPE annual technical conference and exhibition, Society of Petroleum Engineers, San Antonio, Texas, 8–11 October, pp.1–8. SPE-19794-MS. https://doi.org/10.2118/19794-MS.

Langmuir, I. 1918. The Adsorption of Gases on Plane Surfaces of Glass, Mica and Platinum. *J. Am. Chem. Soc.* **40**: 1403-1461.

Leahy-Dios, A., Das, M., Agarwal, A., and Kaminsky, R. D. 2011. Modeling of Transport Phenomena and Multicomponent Sorption for Shale Gas and Coalbed Methane in an Unstructured Grid Simulator. Presented at the SPE Annual Technical Conference and Exhibition, Denver, Colorado, USA, 30 October-2 November. SPE-147352-MS. http://doi:10.2118/147352-MS.

Lee, A. L., Gonzalez, M. H., and Eakin, B. E. 1966. The Viscosity of Natural Gases. *J Pet Technol* **18**(8). SPE-1340-PA. http://doi:10.2118/1340-PA.

Lu, X.C., Li, F.C. and Watson, A.T. 1995. Adsorption measurements in Devonian shales. *Fuel* 74(4): 599-603. https://doi.org/10.1016/0016-2361(95)98364-K.

Martins, J.R.R.A., Ning, A. and Hicken, J. 2017. Multidisciplinary Design Optimization, http://flowlab.groups.et.byu.net/me575/textbook/MDO.pdf (downloaded 20 November 2017).

Mengal, S.A. and Wattenbarger, R.A. 2011. Accounting for Adsorbed Gas in Shale Gas Reservoirs. Presented at the SPE Middle East Oil and Gas Show and Conference held in

Manama, Bahrain, 25–28 September. SPE-141085-MS. https://doi.org/10.2118/141085-MS.

Moridis, G. J., Blasingame, T. A., and Freeman, C. M. 2010. Analysis of Mechanisms of Flow in Fractured Tight-Gas and Shale-Gas Reservoirs. Presented at the SPE Latin American and Caribbean Petroleum Engineering Conference, Lima, Peru, 1-3 December. SPE-139250-MS. http://doi:10.2118/139250-MS.

Narasimhan, T. N. and Witherspoon, P. A. 1976. An Integrated Finite Difference Method for Analyzing Fluid Flow in Porous Media. *Water Resources Research* **12** (1): 57–64.

Peng, D. Y. and Robinson, D. B. 1976. A New Two-Constant Equation of State. *Industrial and Engineering Chemistry: Fundamentals* **15**: 59–64. http://doi:10.1021/i160057a011.

Perrin, J. and Cook, T. 2016. Hydraulically fractured wells provide two-thirds of U.S. natural gas production, https://www.eia.gov/todayinenergy/detail.php?id=26112 (accessed 20 February 2018).

Pruess, K. 1983. GMINC - A Mesh Generator for Flow Simulations in Fractured Reservoirs, Research Report No. LBL-15227, Lawrence Berkeley Laboratory, Berkeley, CA.

Pruess, K. 1987. TOUGH User's Guide, Research Report No. LBL-20700, Lawrence Berkeley Laboratory, Berkeley, CA.

Pruess, K. 1991. TOUGH2 - A General Purpose Numerical Simulator for Multiphase Fluid and Heat Flow, Research Report No. LBL-29400, Lawrence Berkeley Laboratory, Berkeley, CA.

Saldungaray, P. M., and Palisch, T. T. 2012. Hydraulic Fracture Optimization in Unconventional Reservoirs. Presented at the SPE Middle East Unconventional Gas Conference and Exhibition, Abu Dhabi, UAE, 23-25 January. SPE-151128-MS. http://doi:10.2118/151128-MS.

Silin, D. and Kneafsey, T. 2012. Shale Gas: Nanometer-Scale Observations and Well Modeling. *Journal of Canadian Petroleum Technology* **51**(6): 464-475.

Sing, K.S.W., Everett, D.G., Haul, R.A.W., et al. 1985. Reporting Physisorption Data for Gas/Solid Systems with Special Reference to the Determination of Surface Area and Porosity (Recommendations 1984). *Pure Appl. Chem.* **57**(4): 603-619.

Thompson, R. and Wright, J. 2015. *Oil and Gas Property Evaluation*, 2015 edition. Golden, Colorado: Thompson-Wright Associates.

U.S. Energy Information Administration (EIA). 2016. Trends in U.S. Oil and Natural Gas Upstream Costs, https://www.eia.gov/analysis/studies/drilling/pdf/upstream.pdf (accessed 20 October 2017).

Wang, P. 2003. Development and Applications of Production Optimization Techniques for Petroleum Fields. PhD thesis, Stanford University, Stanford, California.

Wang, S., Lukyanov, A. A., Wang, L., Wu, Y. S., Pomerantz, A., Xu, W., and Kleinberg, R. 2017. A non-empirical gas slippage model for low to moderate Knudsen numbers. *Physics of Fluids*, 29(1), 012004.

Wang, S., Pan, Z., Zhang, J., et al. 2017. On the Klinkenberg Effect of Multicomponent Gases. Presented at SPE Annual Technical Conference and Exhibition, San Antonio, Texas, 9–11 October. SPE-187065-MS. https://doi.org/10.2118/187065-MS.

Warren, J.E. and Root, P. J. 1963. The Behavior of Naturally Fractured Reservoirs, *Soc. Pet. Eng. J., Trans., AIME* **228**: 245-255.

Wu, Y.S. 2002. Numerical Simulation of Single-Phase and Multiphase Non-Darcy Flow in Porous and Fractured reservoir. *Transport in Porous Media* **49**(2), 209-240. https://doi.org/10.1023/A:1016018020180.

Wu, Y.S. 2005. Multiphase Subsurface Flow Model of Oil, Gas and Water in Porous and Fractured Reservoirs Documentation and User's Guide.

Wu, Y.S., Pruess K., and Persoff. 1998. Gas Flow in Porous Media with Klinkenberg Effects. *Transport in Porous Media* **32**(1), 117–137. https://doi.org/10.1023/A:1006535211684.

Wu, Y.S. and Pruess, K. 1998. A Numerical Method for Simulating non-Newtonian Fluid Flow and Displacement in Porous Media. *Advances in Water Resources* **21**: 351-362. https://doi.org/10.1016/S0309-1708(97)00004-3.

Wu, Y.-S., Wang, C., Li, J., et al. 2012. Transient Gas Flow in Unconventional Gas Reservoir. Presented at the SPE Europec/EAGE Annual Conference, Copenhagen, Denmark, 4-7 June. SPE-154448-MS. http://doi:10.2118/154448-MS.

Wu, Y.-S. 2015. *Multiphase Fluid Flow in Porous and Fractured Reservoirs*, first edition. Netherlands: Gulf Professional Publishing.

Wikipedia. 2018. *Equation of State (20 January 2018)*, https://en.wikipedia.org/wiki/Equation_of_state#cite_note-12 (accessed 10 February 2018).

Yu, W., and Sepehrnoori, K. 2013. Optimization of Multiple Hydraulically Fractured Horizontal Wells in Unconventional Gas Reservoirs. Society of Petroleum Engineers. http://doi:10.2118/164509-MS.

Young, T. and Mohlenkamp, M.J. 2009. Introduction to numerical methods and Matlab Programming for Engineers. Lecture 27: 101-103. Ohio University Department of Mathematics, OH.

APPENDIX A
TIME AND SPACE DISCRETIZATION OF MASS BALANCE EQUATION

The mass balance equation needs to be discretized:

$$\frac{\partial}{\partial t}\left(\phi S_\beta \rho_\beta + m_g\right) = -\nabla \cdot \left(\rho_\beta \overrightarrow{v_\beta}\right) + q_\beta \tag{A-1}$$

Firstly, integrate the flow equation with respect to a control volume V_i:

$$\iiint_{V_i} \frac{\partial}{\partial t}\left(\phi S_\beta \rho_\beta + m_g\right) dV_i = -\iiint_{V_i} \nabla \cdot \left(\rho_\beta \overrightarrow{v_\beta}\right) dV_i + \iiint_{V_i} q_\beta dV_i \tag{A-2}$$

given that:

(1) volumetric integral $\iiint_{V_i} \frac{\partial}{\partial t}\left(scalar\right) dV_i = \frac{\partial}{\partial t}\left(\iiint_{V_i} \left(scalar\right) dV_i \right)$

$$\begin{aligned} &\iiint_{V_i} \frac{\partial}{\partial t}\left(\phi S_\beta \rho_\beta + m_g\right) dV_i = \frac{\partial}{\partial t}\left(\iiint_{V_i} \left(\phi S_\beta \rho_\beta + m_g\right) dV_i \right) = \frac{\partial \left(\phi S_\beta \rho_\beta + m_g\right)_i}{\partial t} V_i \\ &= \left\{ \left[\phi S_\beta \rho_\beta + m_g\right]_i^{n+1} - \left[\phi S_\beta \rho_\beta + m_g\right]_i^{n} \right\} \frac{V_i}{\Delta t} \end{aligned} \tag{A-3}$$

(2) volumetric integral $\iiint_{V_i} \left(\nabla \cdot \left(vector\right)\right) dV_i$ can be transformed to a surface integral with respect to the closed surface of the control volume, by $\iiint_{V_i} \left(\nabla \cdot \left(vector\right)\right) dV_i = \iint_{\Gamma_i} \left(vector \cdot \vec{n}\right) d\Gamma_i$, in which $\vec{n}$ is the normal vector of a surface.

Then, approximate the integral using $\iiint_{V_i} \left(scalar\right) dV_i = scalar_{average} \cdot V_i$ and $\iint_{\Gamma_i} \left(vector \cdot \vec{n}\right) d\Gamma_i = \sum_j A_{ij} F_{ij}$, in which:

i. $scalar_{average}$ is average quantity to represent the properties of the whole control volume;

ii. A_{ij} is the area connected to the other control volumes j, summing all connected adjacent control volumes gives total amount of flow;

iii. F_{ij} is the flow going through area A_{ij} between control volume i and j.

$$-\iiint_{V_i} \nabla \cdot \left(\rho_\beta \overrightarrow{v_\beta}\right) dV_i = -\iint_{\Gamma_i} \left(\left(\rho_\beta \overrightarrow{v_\beta}\right) \cdot \vec{n}\right) d\Gamma_i$$

$$= -\sum_j A_{ij} \left(\rho_\beta \overrightarrow{v_\beta}\right) = \sum_j A_{ij} \rho_\beta \frac{k k_{r\beta}}{\mu_\beta} \left(\nabla P_{\beta,ij} - \rho_\beta g \nabla D_{ij}\right) \tag{A-4}$$

(3) Discretize the equation in using Backward Finite Difference method for time stepping: $\frac{dM_i}{dt} = \frac{M_i^{n+1} - M_i^n}{\Delta t}$ and evaluate all flow terms (and parameters) on the time level of n+1.

Incorporate Darcy velocity of mass: $F_{ij} = \left(\rho_\beta v_\beta\right)_{ij}$ into the discretization obtained from and evaluate absolute permeability, gas density, viscosity and relative permeability at interface Γ_{ij} and time level of n+1, evaluate the gas pressure gradient using $\left(\nabla P_\beta\right)_{ij} = \frac{\partial P_\beta}{\partial d_{ij}} = \frac{P_{\beta,j} - P_{\beta,i}}{d_i + d_j}$ in which d_i is the distance from the geometric center of i to the interface Γ_{ij}. And the then final discretization is:

$$\left\{\left[\phi S_\beta \rho_\beta + m_g\right]_i^{n+1} - \left[\phi S_\beta \rho_\beta + m_g\right]_i^n\right\} \frac{V_i}{\Delta t}$$

$$= \sum_j \left(\rho_\beta \frac{k_{r\beta}}{\mu_\beta}\right)_{ij+\frac{1}{2}}^{n+1} \frac{A_{ij} k_{ij+\frac{1}{2}}}{d_i + d_j} \left[\left(P_{\beta j}^{n+1} - \rho_{\beta j}^{n+1} g D_j\right) - \left(P_{\beta i}^{n+1} - \rho_{\beta i}^{n+1} g D_i\right)\right] + Q_{\beta i}^{n+1} \tag{A-5}$$

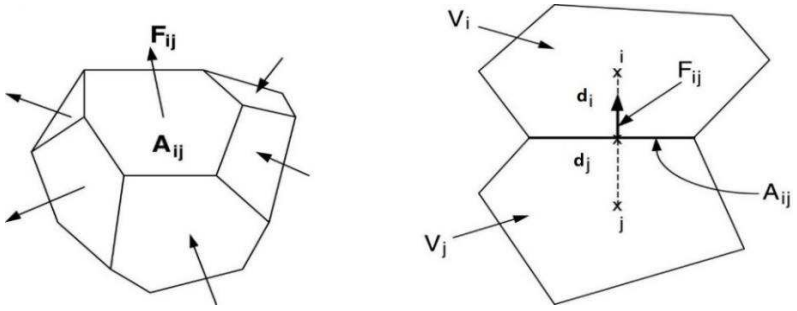

Figure A- 1 Schematic Diagram of Surface Integral and Related Parameters

By rearranging the discretization equation above, we can get residue form as below:

$$R_i^{\beta,n+1} = \left\{ \left[\phi S_\beta \rho_\beta + m_g \right]_i^{n+1} - \left[\phi S_\beta \rho_\beta + m_g \right]_i^{n} \right\} \frac{V_i}{\Delta t}$$
$$- \sum_j \left(\rho_\beta \frac{k_{r\beta}}{\mu_\beta} \right)_{ij+\frac{1}{2}}^{n+1} \frac{A_{ij} k_{ij+\frac{1}{2}}}{d_i + d_j} \left[\left(P_{\beta j}^{n+1} - \rho_{\beta j}^{n+1} g D_j \right) - \left(P_{\beta i}^{n+1} - \rho_{\beta i}^{n+1} g D_i \right) \right] - Q_{\beta i}^{\ n+1} = 0 \quad \text{(A-6)}$$

The Newton iteration scheme gives rise to:

$$R_i^{\beta,n+1}\left(x_{k,p+1}\right) = R_i^{\beta,n+1}\left(x_{k,p}\right) + \sum_k \frac{\partial R_i^{\beta,n+1}\left(x_{k,p}\right)}{\partial x_k} \left(x_{k,p+1} - x_{k,p} \right) = 0 \quad \text{(A-7)}$$

Notice here, for the above steps, the upstream weighting scheme is used for averaging relative permeability the mobility term and harmonic weighting is used for absolute permeability.

APPENDIX B
PENG-ROBINSON EQUATION OF STATE

The Peng-Robinson equation of state (PR-EOS) was developed by Dr. Ding-Yu Peng and Dr. Donald Robinson at University of Alberta to satisfy the following goals (Peng and Robinson 1976; Wikipedia 2018):

- The parameters must be expressible in terms of the acentric factor ϖ and critical properties.
- The model should have reasonable accuracy near critical point, especially for the calculation of liquid density and compressibility factor Z.
- The mixing rules should not be applied to more than a single binary interaction parameter, which is independent of composition and temperature.
- The equation should be applicable to all calculations of all fluid properties in natural gas process.

For the most part, the Peng–Robinson equation exhibits performance similar to the Soave equation, although it is generally superior in predicting the liquid densities of many materials, especially nonpolar ones (Donnez 2007). The structure and the equation of Peng-Robinson are given as follows:

$$p = \frac{RT}{V_m - b} - \frac{a\alpha}{V_m^2 + 2bV_m - b^2} \tag{B-1}$$

$$\alpha = \frac{0.457235R^2T_c^2}{P_c} \tag{B-2}$$

$$b = \frac{0.077796RT_c}{P_c} \tag{B-3}$$

$$\alpha = \left(1 + \kappa\left(1 - T_r^{0.5}\right)\right)^2 \tag{B-4}$$

$$\kappa = 0.37464 + 1.54226\varpi - 0.26992\varpi^2 \tag{B-5}$$

$$T_r = \frac{T}{T_c} \tag{B-6}$$

The polynomial form of the equation is given by:

$$A = \frac{\alpha ap}{R^2 T^2} \tag{B-7}$$

$$B = \frac{bp}{RT} \tag{B-8}$$

$$Z^3 - (1-B)Z^2 + (A-2B-3B^2)Z - (AB - B^2 - B^3) = 0 \tag{B-9}$$

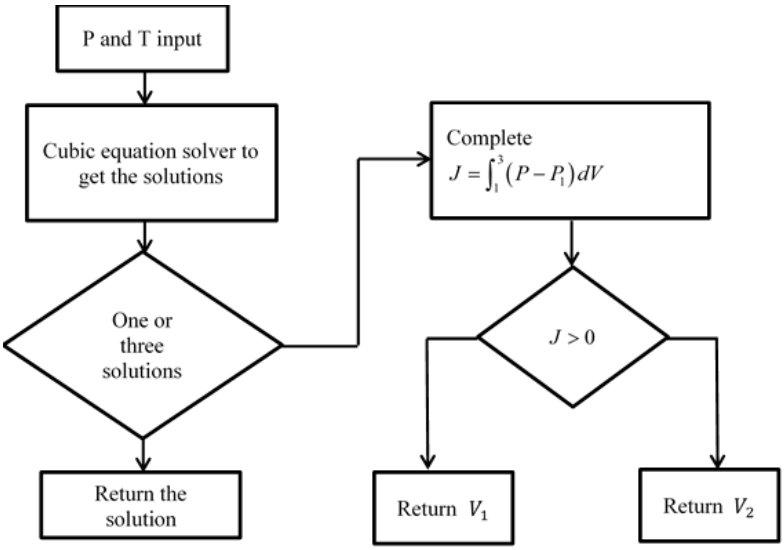

Figure B- 1 Structure Chart of Peng-Robinson EOS (Wu, 2005)

APPENDIX C
VERIFICATION RESULTS OF GRADIENT DESCENT METHOD WITH VARIOUS INITIAL POINTS

Table C-1 Result Table of initial point [400 150 5]

Hydraulic Fracture Spacing (m)	**Hydraulic Fracture Half length (m)**	**Dimensionless Fracture Conductivity**	**Gas Production (m^3)**	**#MSFLOW Called**	**Program Running Time (s)**
328.0703	170	15	5.3525E+08	8	68.38
279.1426	190	25	7.5281E+08	16	137.47
238.2461	245.6855	35	1.1578E+09	24	206.09
207.0957	271.9590	60.4824	1.5442E+09	32	269.76
180.2559	289.0488	68.3809	1.8869E+09	40	333.03
155.1719	299.9805	73.7070	2.2451E+09	48	391.52
125.7520	300	77.5938	2.8852E+09	56	427.11
98.5781	300	80.4473	3.7840E+09	64	459.46
74.5098	300	82.5078	4.9571E+09	72	491.08
54.5938	300	83.9551	6.2202E+09	80	522.83
39.6133	300	84.9590	7.2230E+09	88	554.55
29.2871	300	85.6563	7.8549E+09	96	585.85
20	300	86.1484	8.4772E+09	104	612.55
20	300	86.4512	8.4779E+09	112	639.04
20	300	86.7520	8.4787E+09	120	665.36
20	300	87.0527	8.4794E+09	128	691.60
20	300	87.3496	8.4802E+09	136	717.88
20	300	87.6465	8.4809E+09	144	744.06
20	300	87.9414	8.4816E+09	152	770.66
20	300	88.2363	8.4824E+09	160	797.09
20	300	88.5254	8.4831E+09	168	823.53
20	300	88.8145	8.4838E+09	176	851.28
20	300	89.1035	8.4845E+09	184	878.04
20	300	89.3887	8.4851E+09	192	904.67
20	300	89.6719	8.4858E+09	200	930.52
20	300	89.9531	8.4865E+09	208	956.45
20	300	90.2344	8.4871E+09	216	983.27
20	300	90.5117	8.4878E+09	224	1009.30
20	300	90.7891	8.4884E+09	232	1035.64
20	300	91.0645	8.4891E+09	240	1061.98
20	300	91.3379	8.4897E+09	248	1088.28

Table C-1 Continued

20	300	91.7656	8.4907E+09	256	1114.82
20	300	92.0371	8.4913E+09	264	1141.16
20	300	92.3066	8.4919E+09	272	1167.57
20	300	92.5742	8.4925E+09	280	1193.62
20	300	92.8418	8.4931E+09	288	1220.21
20	300	93.1074	8.4937E+09	296	1246.31
20	300	93.3730	8.4943E+09	304	1272.68
20	300	93.6328	8.4948E+09	312	1299.05
20	300	93.8926	8.4954E+09	320	1325.60
20	300	94.1523	8.4960E+09	328	1351.88
20	300	94.4121	8.4965E+09	336	1378.28
20	300	94.6680	8.4971E+09	344	1404.44
20	300	94.9238	8.4976E+09	352	1430.92
20	300	95.1758	8.4982E+09	360	1456.79
20	300	95.4297	8.4987E+09	368	1483.33
20	300	95.6797	8.4992E+09	376	1509.49
20	300	95.9297	8.4998E+09	384	1535.73
20	300	96.1777	8.5003E+09	392	1562.27
20	300	96.4238	8.5008E+09	400	1588.72
20	300	96.6680	8.5013E+09	408	1614.81
20	300	96.9141	8.5018E+09	416	1641.25
20	300	97.1563	8.5023E+09	424	1667.48
20	300	97.3984	8.5028E+09	432	1693.69
20	300	97.6406	8.5033E+09	440	1719.80
20	300	97.8809	8.5038E+09	448	1746.18
20	300	98.1191	8.5042E+09	456	1772.43
20	300	98.3555	8.5047E+09	464	1799.22
20	300	98.5918	8.5052E+09	472	1825.20
20	300	98.8281	8.5056E+09	480	1851.18
20	300	99.0625	8.5061E+09	488	1877.67
20	300	99.2969	8.5066E+09	496	1903.84
20	300	99.5293	8.5070E+09	504	1929.83
20	300	99.7539	8.5075E+09	512	1955.90
20	300	99.9258	8.5078E+09	520	1982.21
20	300	100	8.5079E+09	529	2011.80

Table C-2 Result Table of initial point [200 50 30]

Hydraulic Fracture Spacing (m)	Hydraulic Fracture Half length (m)	Dimensionless Fracture Conductivity	Gas Production (m^3)	#MSFLOW Called	Program Running Time (s)
180	70	40	5.0597E+08	8	71.37
86.2559	90	74.9043	1.4607E+09	16	140.05
20	147.6543	79.2383	4.5360E+09	24	198.57
20	159.127	79.8379	4.8542E+09	32	249.61
20	169.0391	80.3965	5.1288E+09	40	299.50
20	177.9219	80.9297	5.3752E+09	48	349.54
20	186.1172	80.1621	5.6003E+09	56	399.91
20	193.5703	80.6621	5.8068E+09	64	450.14
20	200.6875	81.1445	6.0045E+09	72	500.16
20	207.2441	81.6133	6.1861E+09	80	550.49
20	213.4277	82.0645	6.3576E+09	88	600.62
20	219.1074	82.5059	6.5165E+09	96	651.15
20	224.8184	82.9375	6.6756E+09	104	700.92
20	230.5000	83.3574	6.8360E+09	112	746.99
20	235.9844	83.7695	6.9899E+09	120	793.44
20	241.1660	84.1758	7.1335E+09	128	839.76
20	246.1953	84.5723	7.2750E+09	136	885.94
20	251.0176	84.9629	7.4105E+09	144	932.14
20	255.6523	85.3438	7.5394E+09	152	978.07
20	260.0469	85.7188	7.6652E+09	160	1023.98
20	264.2676	86.0859	7.7799E+09	168	1069.73
20	267.8496	86.4492	7.8759E+09	176	1115.66
20	271.2148	86.8066	7.9674E+09	184	1161.53
20	274.9180	87.1563	8.0595E+09	192	1207.24
20	278.4043	87.5000	8.1450E+09	200	1252.90
20	281.5879	87.8340	8.2198E+09	208	1298.50
20	284.0762	88.1602	8.2721E+09	216	1343.92
20	286.8301	88.4805	8.3310E+09	224	1387.98
20	289.0273	88.7949	8.3723E+09	232	1429.58
20	290.8379	89.1035	8.4018E+09	240	1471.33
20	292.4395	89.4082	8.4247E+09	248	1512.91
20	294.2363	89.7051	8.4503E+09	256	1554.07
20	295.7207	89.9980	8.4622E+09	264	1595.40
20	296.9688	90.2852	8.4734E+09	272	1636.06

Table C-2 Continued

20	297.5527	90.5684	8.4792E+09	280	1673.89
20	298.0254	91.7461	8.4839E+09	288	1711.75
20	298.3066	92.0195	8.4850E+09	296	1748.84
20	299.0684	92.2910	8.4902E+09	304	1786.54
20	299.6914	92.5605	8.4934E+09	312	1822.92
20	300	92.8262	8.4934E+09	358	2013.69
20	300	93.0898	8.4936E+09	366	2040.40
20	300	93.3516	8.4942E+09	374	2066.59
20	300	93.6113	8.4948E+09	382	2092.84
20	300	93.8691	8.4954E+09	390	2118.97
20	300	94.1289	8.4959E+09	398	2145.08
20	300	94.3867	8.4965E+09	406	2171.39
20	300	94.6426	8.4970E+09	414	2197.47
20	300	94.8984	8.4976E+09	422	2223.66
20	300	95.1523	8.4981E+09	430	2251.17
20	300	95.4043	8.4987E+09	438	2277.44
20	300	95.6563	8.4992E+09	446	2303.86
20	300	95.9063	8.4997E+09	454	2330.27
20	300	96.1543	8.5002E+09	462	2356.71
20	300	96.4004	8.5007E+09	470	2383.11
20	300	96.6445	8.5012E+09	478	2409.59
20	300	96.8887	8.5017E+09	486	2435.83
20	300	97.1309	8.5022E+09	494	2462.14
20	300	97.3691	8.5027E+09	502	2488.03
20	300	97.6113	8.5032E+09	510	2514.36
20	300	97.8516	8.5037E+09	518	2540.76
20	300	98.0879	8.5042E+09	526	2566.83
20	300	98.3262	8.5047E+09	534	2592.69
20	300	98.5625	8.5051E+09	542	2619.10
20	300	98.7969	8.5056E+09	550	2645.43
20	300	99.0332	8.5061E+09	558	2671.59
20	300	99.2676	8.5065E+09	566	2697.43
20	300	99.5000	8.5070E+09	574	2723.05
20	300	99.7324	8.5074E+09	582	2749.16
20	300	99.9102	8.5078E+09	590	2775.73
20	300	100	8.5079E+09	599	2805.37

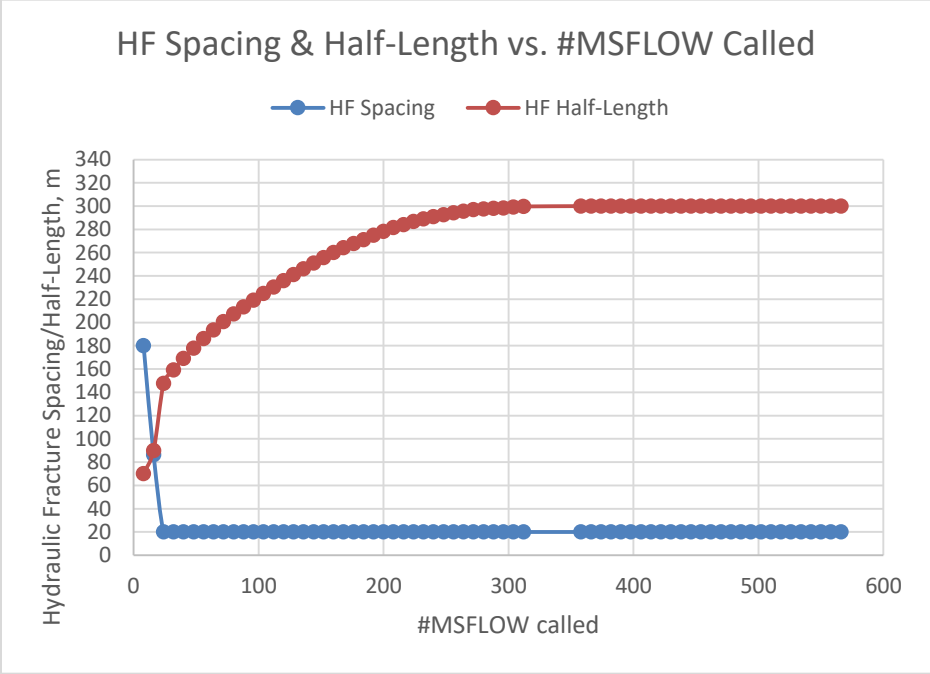

Figure C- 1 Hydraulic Fracture Spacing and Half-length vs. #MSFLOW Called when optimization starts from initial point [200 50 30]

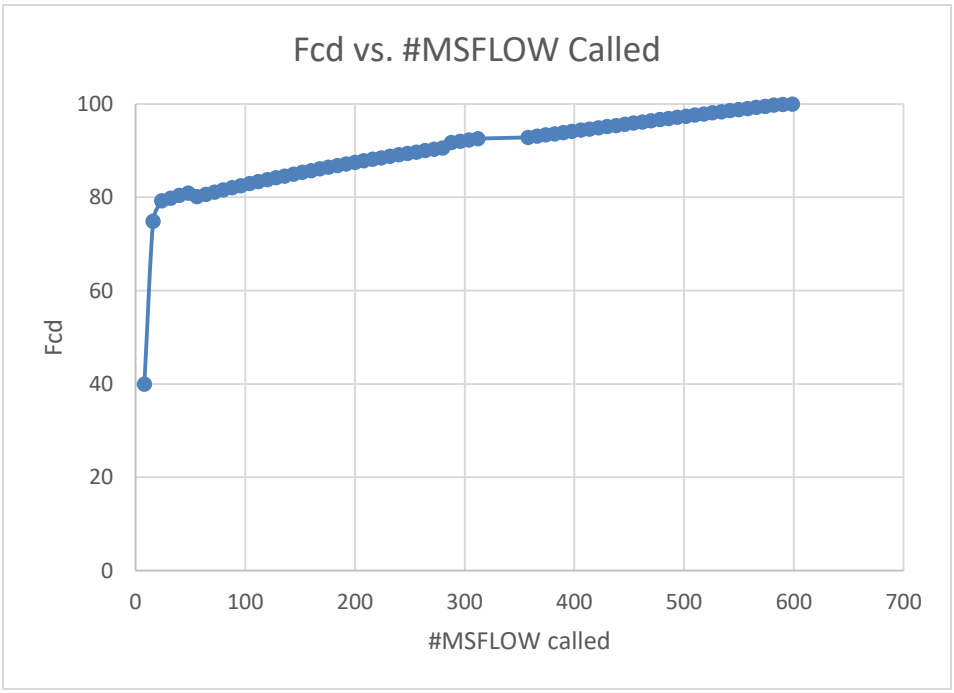

Figure C- 2 Dimensionless Fracture Conductivity vs. #MSFLOW Called when optimization starts from initial point [200 50 30]

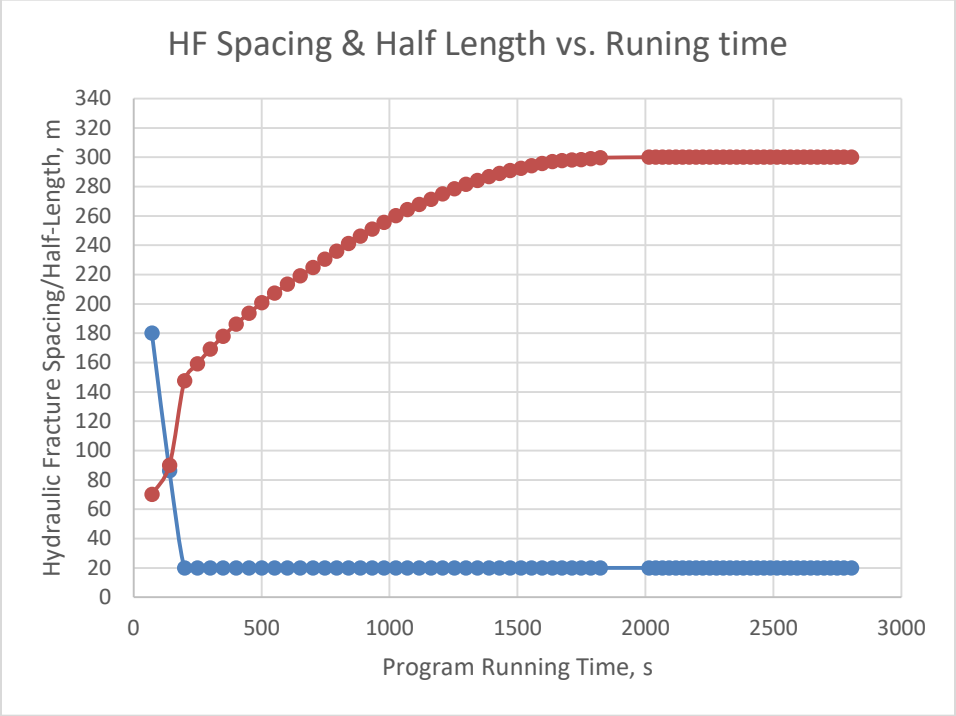

Figure C- 3 Hydraulic Fracture Spacing and Half-length vs. Optimization Program Running time when optimization starts from initial point [200 50 30]

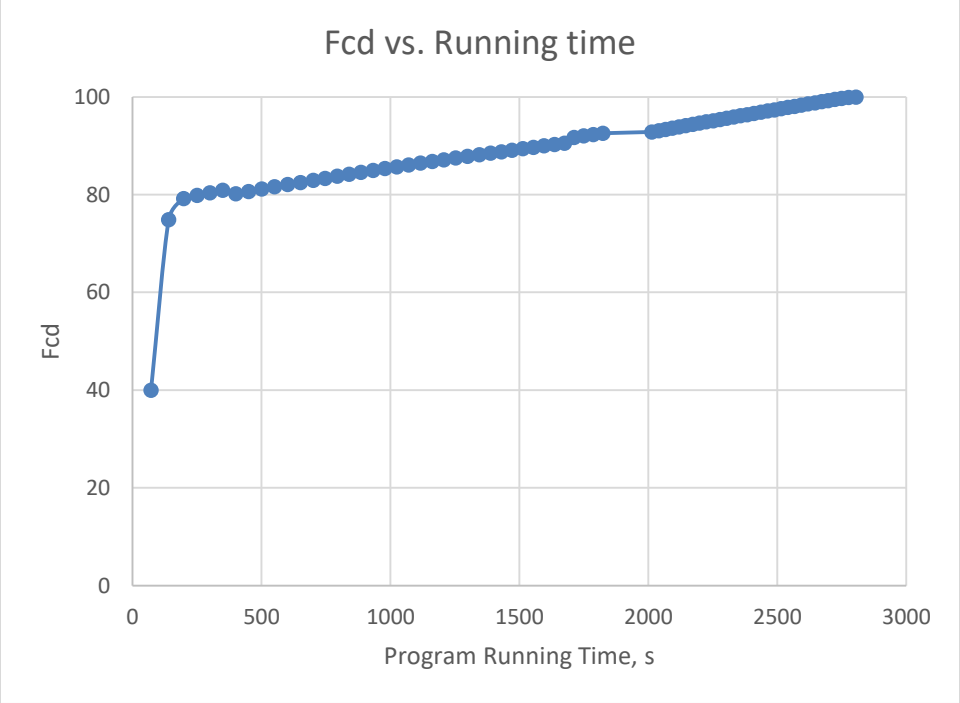

Figure C- 4 Dimensionless Fracture Conductivity vs. Optimization Program Running Time when optimization starts from initial point [200 50 30]

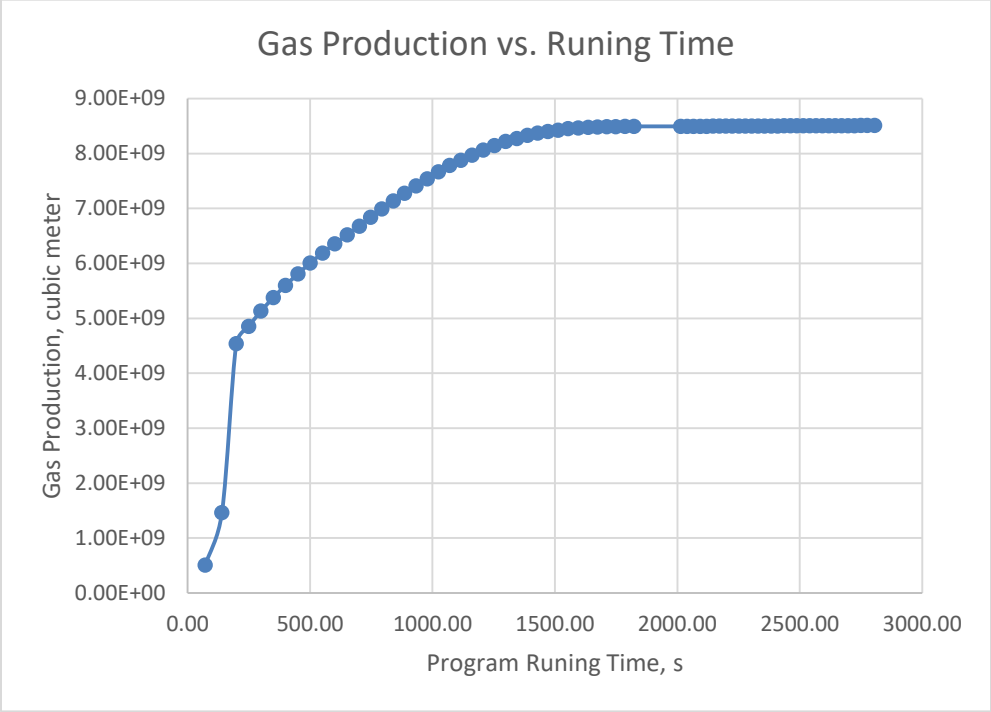

Figure C- 5 Gas Production vs. Optimization Program Running Time when optimization starts from initial point [200 50 30]

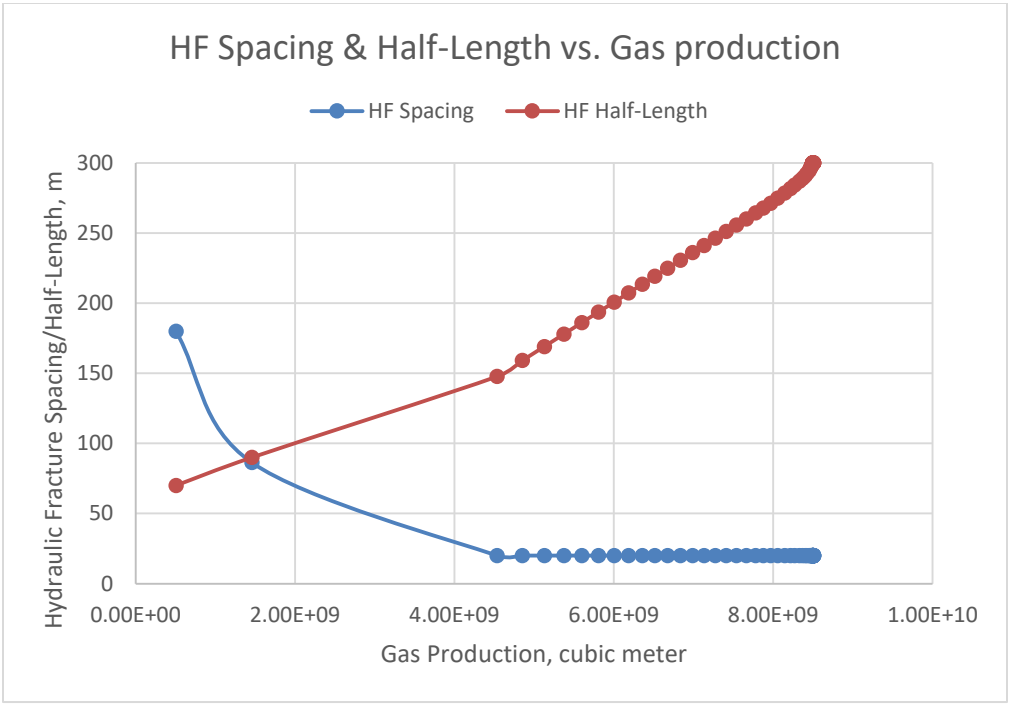

Figure C- 6 Hydraulic Fracture Spacing and Half-length vs. Gas Production when optimization starts from initial point [200 50 30]

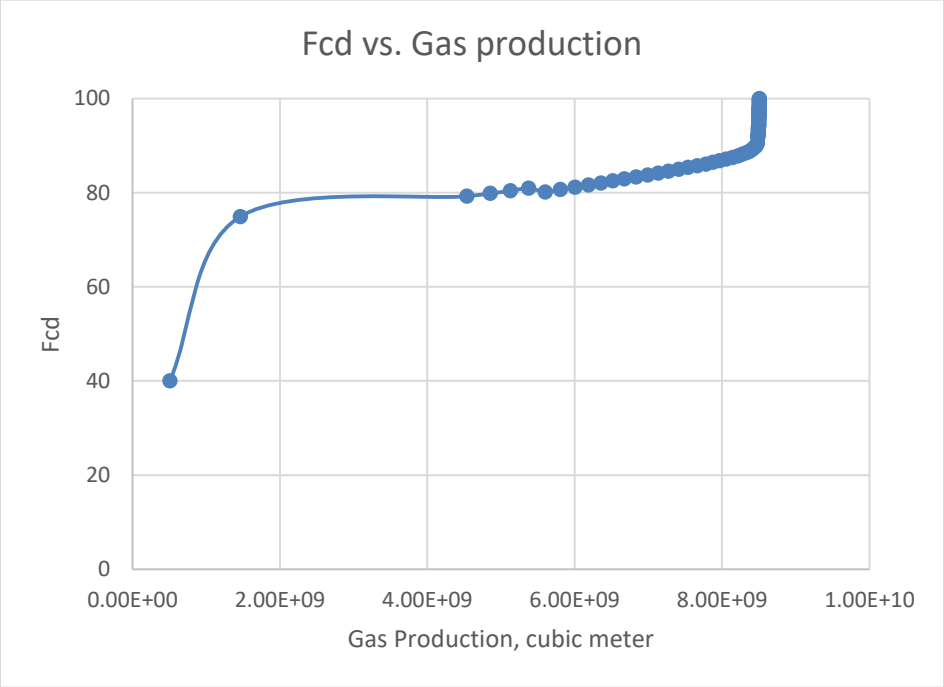

Figure C- 7 Dimensionless Fracture Conductivity vs. Gas Production when optimization starts from initial point [200 50 30]

APPENDIX D
CASE #1 RESULTS WITH VARIOUS INITIAL POINTS

Table D-1 Result Table of initial point [300 150 5]

Hydraulic Fracture Spacing (m)	Hydraulic Fracture Half length (m)	Dimensionless Fracture Conductivity	Cumulative Discounted-NPV ($)	#MSFLOW Called	Program Running Time (s)
296.4177	152.9830	15	-2.5176E+06	8	80.22
290.5732	158.5597	29.5463	-2.3190E+06	16	161.14
282.7068	166.0773	35.7556	-2.1810E+06	24	242.21
272.8642	176.2414	41.0152	-2.0071E+06	32	323.43
259.7788	187.1132	46.6371	-1.7866E+06	40	404.74
240.8244	203.8920	53.2986	-1.4271E+06	48	485.85
204.8514	233.1947	63.1841	-6.3784E+05	56	564.94
184.8514	272.8191	91.2736	1.3705E+05	64	639.99
164.8514	291.3784	96.8977	6.3544E+05	72	713.65
83.1010	297.3494	98.9330	3.4120E+06	80	778.59
61.7778	296.5268	98.9036	4.2128E+06	88	833.65
49.3912	296.2060	99.6836	4.6017E+06	96	890.69
41.4310	296.3348	100	4.7850E+06	104	948.95
36.3178	296.1260	100	4.8607E+06	112	1006.71
33.4671	295.5398	100	4.8849E+06	120	1064.86
31.9418	295.0162	100	4.8900E+06	128	1121.95
31.2260	295.3244	100	4.8939E+06	136	1177.41
29.2124	294.7526	100	4.9081E+06	144	1227.68
27.6519	294.8562	100	4.9146E+06	152	1276.66
27.8464	294.7034	100	4.9148E+06	162	1336.85
28.1374	294.3746	100	4.9133E+06	208	1591.52
27.3662	294.0345	100	4.9151E+06	216	1643.06
27.3652	294.0342	100	4.9154E+06	238	1768.48
27.2239	293.9968	100	4.9157E+06	246	1816.88
27.2238	293.9961	100	4.9158E+06	270	1953.10
26.7510	293.8279	100	4.9136E+06	316	2208.19
26.9459	293.3285	100	4.9153E+06	326	2268.19
26.9463	293.3287	100	4.9153E+06	354	2426.54
27.3395	293.5677	100	4.9147E+06	400	2681.49
27.3483	293.5547	100	4.9157E+06	410	2741.46
26.8769	293.5432	100	4.9122E+06	456	2997.38
27.2824	293.6657	100	4.9143E+06	464	3046.65

Table D-1 Continued

27.2883	293.6746	100	4.9158E+06	478	3128.22
27.2879	293.6746	100	4.9158E+06	506	3290.12
27.2877	293.6747	100	4.9158E+06	536	3458.71
26.8390	293.7453	100	4.9136E+06	582	3713.80
27.1794	293.9268	100	4.9156E+06	590	3763.13
27.1992	293.9578	100	4.9147E+06	636	4018.77
27.2094	293.9840	100	4.9142E+06	682	4274.34
27.2058	293.7087	100	4.9148E+06	692	4334.25
27.2062	293.7083	100	4.9148E+06	716	4470.19
27.2493	293.6554	100	4.9155E+06	726	4530.00
27.3071	293.7367	100	4.9147E+06	772	4785.30
27.3112	293.7680	100	4.9121E+06	818	5040.91
26.8289	293.6940	100	4.9148E+06	826	5090.08
27.2015	293.7036	100	4.9131E+06	872	5346.87
27.2516	293.6521	100	4.9145E+06	882	5406.45
27.2686	293.6698	100	4.9151E+06	894	5477.82
27.3149	293.7396	100	4.9153E+06	902	5526.60
27.3141	293.7407	100	4.9157E+06	920	5629.41
27.3139	293.7407	100	4.9157E+06	950	5797.89
26.8286	293.7710	100	4.9126E+06	996	6053.42
27.0124	293.8584	100	4.9148E+06	1006	6113.84
27.1775	293.8688	100	4.9135E+06	1052	6368.15
27.1940	293.8586	100	4.9154E+06	1064	6438.75
27.1944	293.8581	100	4.9155E+06	1084	6552.53
27.2151	293.8424	100	4.9155E+06	1094	6612.70
27.2152	293.8422	100	4.9155E+06	1118	6748.75
27.2445	293.8052	100	4.9136E+06	1164	7004.02
27.2628	292.7436	100	4.9153E+06	1174	7064.62
27.1057	292.7849	100	4.9154E+06	1186	7135.81
27.1052	292.7851	100	4.9167E+06	1214	7294.51
27.1041	292.7855	100	4.9171E+06	1240	7441.32
27.1038	292.7856	100	4.9171E+06	1270	7610.24
26.8382	292.8935	100	4.9176E+06	1280	7670.64
27.4614	293.2581	100	4.9156E+06	1326	7934.87
27.0029	293.2596	100	4.9193E+06	1336	7994.24

Table D-2 Result Table of initial point [400 20 70]

Hydraulic Fracture Spacing (m)	Hydraulic Fracture Half length (m)	Dimensionless Fracture Conductivity	Cumulative Discounted-NPV ($)	#MSFLOW Called	Program Running Time (s)
399.6424	24.3616	70.1252	-3.6150E+06	8	84.17
399.2412	28.5072	70.2827	-3.5798E+06	16	169.05
398.7623	32.6199	70.4188	-3.5458E+06	24	252.39
398.2230	36.6845	70.5624	-3.5131E+06	32	334.83
397.6219	40.7133	70.7147	-3.4814E+06	40	416.64
396.9583	44.7192	70.8764	-3.4502E+06	48	498.38
396.2301	48.7293	71.0483	-3.4194E+06	56	579.85
395.4345	52.8111	71.2312	-3.3885E+06	64	661.59
394.5680	56.8183	71.4259	-3.3584E+06	72	743.09
393.6293	60.7893	71.6323	-3.3287E+06	80	825.07
392.6157	64.8227	71.8511	-3.2987E+06	88	907.31
391.5236	68.8968	72.0836	-3.2686E+06	96	989.12
390.3676	72.9352	72.3301	-3.2388E+06	104	1070.60
389.1051	77.0600	72.5913	-3.2083E+06	112	1151.92
387.7496	81.2148	72.8683	-3.1776E+06	120	1233.35
386.2955	85.4074	73.1620	-3.1465E+06	128	1314.83
384.7365	89.6061	73.4729	-3.1152E+06	136	1396.02
382.7763	93.8470	73.8027	-3.0827E+06	144	1477.30
380.9849	98.1496	74.1524	-3.0501E+06	152	1558.44
379.0657	102.5086	74.5234	-3.0169E+06	160	1639.66
377.0096	106.8862	74.9167	-2.9830E+06	168	1721.17
374.8046	111.3594	75.3340	-2.9480E+06	176	1801.79
372.4388	115.8734	75.7767	-2.9119E+06	184	1883.33
369.8986	120.4851	76.2465	-2.8745E+06	192	1964.53
367.1655	125.1944	76.7465	-2.8355E+06	200	2046.85
364.2177	129.9876	77.3888	-2.7946E+06	208	2128.27
361.0316	134.8653	77.9547	-2.7518E+06	216	2209.04
357.5778	139.8406	78.5601	-2.7067E+06	224	2290.61
353.8322	145.0746	79.2071	-2.6580E+06	232	2372.01
349.7257	150.4840	79.9034	-2.6058E+06	240	2453.46
345.2156	156.4286	80.6533	-2.5465E+06	248	2534.55
340.2005	161.9219	81.4764	-2.4868E+06	256	2615.66
334.6280	168.6282	82.3698	-2.4138E+06	264	2697.70
328.2253	175.5477	83.3624	-2.3321E+06	272	2778.57

Table D-2 Continued

320.9500	182.9919	84.4692	-2.2372E+06	280	2860.38
312.3880	190.2596	85.7400	-2.1312E+06	288	2942.48
302.1392	199.5628	87.0458	-1.9914E+06	296	3024.15
289.1457	210.3053	88.8329	-1.8067E+06	304	3105.47
270.8322	222.2193	91.1672	-1.5425E+06	312	3185.58
242.2452	242.5544	94.6249	-1.0397E+06	320	3262.81
142.7310	282.9901	99.0265	1.2032E+06	328	3335.60
76.5768	296.3725	99.6081	3.6679E+06	336	3398.70
58.0703	296.2169	99.8500	4.3398E+06	344	3456.83
47.0407	288.8762	100	4.6495E+06	352	3515.35
39.5287	289.9114	100	4.8102E+06	360	3573.18
35.1501	290.7383	100	4.8681E+06	368	3631.72
32.7201	291.3413	100	4.8862E+06	376	3690.06
31.5541	291.6947	100	4.8913E+06	384	3747.99
30.5009	292.0129	100	4.8998E+06	392	3803.11
28.0417	292.3494	100	4.9130E+06	400	3852.58
27.0123	292.3979	100	4.9142E+06	408	3901.64
27.0016	292.3733	100	4.9149E+06	426	4005.30
26.6800	292.6128	100	4.9141E+06	472	4262.35
27.5053	292.9790	100	4.9141E+06	480	4311.37
27.5917	293.0376	100	4.9146E+06	488	4360.45
27.6091	293.0497	100	4.9154E+06	496	4409.45
27.3737	293.0493	100	4.9154E+06	508	4480.53
27.1784	293.0661	100	4.9155E+06	520	4551.92
26.5145	293.2974	100	4.9119E+06	566	4807.61
27.2687	293.6787	100	4.9152E+06	574	4856.96
27.2694	293.6782	100	4.9152E+06	594	4971.62
27.2695	293.6781	100	4.9206E+06	620	5118.65

Table D-3 Result Table of initial point [25 200 90]

Hydraulic Fracture Spacing (m)	**Hydraulic Fracture Half length (m)**	**Dimensionless Fracture Conductivity**	**Cumulative Discounted-NPV ($)**	**#MSFLOW Called**	**Program Running Time (s)**
30.9606	219.4266	90.9346	3.5440E+06	8	65.86
28.2412	231.7441	91.7481	3.8937E+06	16	122.88
27.6573	243.8327	92.3937	4.2036E+06	24	175.26

Table D-3 Continued

26.8457	252.2422	92.9422	4.3975E+06	32	227.25
27.9917	259.5069	93.4264	4.5407E+06	40	279.65
27.1993	264.9678	93.8888	4.6435E+06	48	331.33
26.1817	269.9088	94.3123	4.7223E+06	56	382.72
26.4345	274.5112	94.6962	4.7819E+06	64	433.88
25.9926	278.1385	95.0642	4.8240E+06	72	484.83
26.8259	280.8504	95.4108	4.8505E+06	80	535.93
26.1152	283.2301	95.7564	4.8681E+06	88	586.96
26.2057	285.5455	96.0812	4.8839E+06	96	637.07
26.5592	287.5444	96.3990	4.8953E+06	104	683.78
26.999	289.0431	96.7139	4.9004E+06	112	730.38
26.6734	290.0971	97.0295	4.9052E+06	120	777.20
26.5696	290.0559	97.1057	4.9059E+06	132	844.50
26.7375	291.1183	97.4094	4.9073E+06	140	890.95
26.9505	291.8023	97.7121	4.9113E+06	148	937.80
26.8032	292.3570	98.0132	4.9108E+06	194	1180.80
26.9952	292.3391	98.0875	4.9124E+06	206	1247.96
26.9939	292.3405	98.0886	4.9127E+06	230	1378.39
26.9938	292.3405	98.0886	4.9127E+06	266	1570.91
26.6537	292.6934	98.3872	4.9120E+06	312	1815.69
27.4426	293.1520	98.6786	4.9121E+06	320	1862.40
26.4946	293.6667	98.9775	4.9149E+06	328	1910.61
26.5141	293.6609	98.9863	4.9175E+06	346	2011.97
26.5144	293.6610	98.9865	4.9175E+06	376	2181.12
27.1153	293.9607	98.1057	4.9133E+06	422	2436.13
27.1238	293.9750	98.1798	4.9137E+06	434	2504.43
27.1244	293.9750	98.1845	4.9137E+06	454	2613.60
27.1563	293.9750	98.4817	4.9136E+06	500	2856.51
27.1657	293.9607	98.7765	4.9141E+06	508	2903.40
27.1660	293.9613	98.7811	4.9141E+06	528	3011.96
27.1660	293.9618	98.7856	4.9141E+06	548	3120.60
27.1731	293.9931	99.0788	4.9169E+06	556	3168.00
27.1795	293.8365	99.3702	4.9129E+06	602	3419.98
27.1963	293.8297	99.4428	4.9147E+06	614	3487.37
27.1965	293.8292	99.4440	4.9148E+06	638	3616.98
27.1965	293.8291	100	4.9155E+06	666	3767.90
27.2312	293.6882	99.7345	4.9136E+06	712	4015.41
27.2987	293.6736	99.9567	4.9155E+06	720	4061.99

Table D-3 Continued

27.3000	293.6779	99.9591	4.9190E+06	736	4150.62
27.3002	293.6776	99.9595	4.9190E+06	758	4272.91
27.3003	293.6775	99.9596	4.9190E+06	782	4406.05
27.3247	293.6444	100	4.9143E+06	828	4658.15
27.3349	293.8675	100	4.9158E+06	838	4715.20
26.3061	293.7915	100	4.9124E+06	884	4958.20
27.0478	294.1525	100	4.9127E+06	892	5004.72
27.1303	294.1072	100	4.9138E+06	900	5051.59
27.1567	294.1243	100	4.9145E+06	908	5098.32
27.1516	294.0278	100	4.9149E+06	916	5145.29
27.1708	293.0352	100	4.9153E+06	924	5192.30
27.1695	293.0363	100	4.9157E+06	946	5311.82
27.1489	293.0406	100	4.9157E+06	964	5410.39
26.5025	293.1775	100	4.9119E+06	1010	5656.20
26.7923	293.5838	100	4.9123E+06	1018	5702.90
27.2402	293.7294	100	4.9129E+06	1026	5749.29
27.3134	293.8004	100	4.9147E+06	1034	5796.09
27.6372	293.8078	100	4.9152E+06	1044	5853.07
27.6362	293.8076	100	4.9155E+06	1068	5983.12
27.6356	293.8074	100	4.9156E+06	1094	6123.20
26.9019	293.7243	100	4.9133E+06	1140	6366.97
27.2207	293.8074	100	4.9145E+06	1148	6413.74
27.2554	293.8529	100	4.9157E+06	1156	6460.32
27.2550	293.8528	100	4.9157E+06	1184	6611.03

Table D-4 Result Table of initial point [100 50 60]

Hydraulic Fracture Spacing (m)	**Hydraulic Fracture Half length (m)**	**Dimensionless Fracture Conductivity**	**Cumulative Discounted-NPV ($)**	**#MSFLOW Called**	**Program Running Time (s)**
84.9486	84.1497	61.8006	-1.0828E+06	8	70.61
43.7495	104.1497	71.3940	6.2822E+04	16	140.70
20.7915	124.1497	86.0945	5.8164E+05	24	208.31
30.7915	144.1497	94.5254	1.3588E+06	32	267.58
27.0216	164.1497	98.2028	1.9738E+06	40	327.31
34.7126	215.5328	99.7736	3.4391E+06	48	389.08
31.0258	228.8351	99.9162	3.8091E+06	56	456.02

Table D-4 Continued

27.7096	240.2930	100	4.1275E+06	64	512.08
26.5539	249.0787	100	4.3388E+06	72	566.89
26.4911	257.0880	100	4.5066E+06	80	621.28
26.8474	263.6029	100	4.6270E+06	88	675.08
26.1423	268.9796	100	4.7152E+06	96	729.24
26.8326	272.5041	100	4.7646E+06	104	784.12
26.2924	275.8788	100	4.8039E+06	112	837.97
26.1096	279.2906	100	4.8394E+06	120	891.54
26.0774	282.0726	100	4.8631E+06	128	945.29
26.6482	284.5800	100	4.8805E+06	136	998.15
26.9935	286.5435	100	4.8954E+06	144	1047.98
26.4675	288.1949	100	4.9001E+06	152	1097.61
26.8512	289.6758	100	4.9061E+06	160	1147.22
27.4597	290.6226	100	4.9106E+06	168	1197.14
27.3420	291.2862	100	4.9122E+06	176	1246.43
27.2780	291.4016	100	4.9133E+06	188	1317.68
27.2770	291.4038	100	4.9137E+06	212	1453.47
27.0384	291.9636	100	4.9117E+06	258	1709.76
26.7896	292.3693	100	4.9136E+06	266	1758.98
27.1932	292.3257	100	4.9139E+06	276	1819.34
27.1913	292.3264	100	4.9145E+06	300	1956.63
27.1373	292.3486	100	4.9148E+06	314	2038.97
26.7210	292.6654	100	4.9128E+06	360	2296.01
27.5104	293.0356	100	4.9148E+06	368	2345.27
27.5178	293.0395	100	4.9154E+06	382	2428.29
27.3797	293.0664	100	4.9127E+06	428	2684.75
27.4664	293.1466	100	4.9129E+06	438	2744.36
27.4845	293.1790	100	4.9130E+06	450	2815.00
27.5445	293.4576	100	4.9135E+06	458	2864.15
27.4801	293.8774	100	4.9147E+06	466	2912.63
27.3934	293.8149	100	4.9148E+06	476	2972.15
27.3819	293.9545	100	4.9149E+06	490	3053.83
27.3212	293.9364	100	4.9156E+06	500	3113.39
27.3205	293.9309	100	4.9157E+06	522	3237.66
27.2429	293.8293	100	4.9132E+06	568	3492.79
27.2770	293.6852	100	4.9158E+06	576	3547.09
27.2769	293.6854	100	4.9158E+06	610	3735.89
26.8369	292.2478	100	4.9145E+06	656	3990.36

Table D-4 Continued

26.8362	292.2498	100	4.9148E+06	680	4125.37
26.7907	292.3727	100	4.9151E+06	692	4196.48
26.7907	292.3727	100	4.9151E+06	728	4399.81
27.7162	291.6769	100	4.9114E+06	774	4657.62
27.0812	292.0368	100	4.9131E+06	782	4707.39
27.7711	292.4134	100	4.9137E+06	790	4756.14
27.8375	292.6237	100	4.9139E+06	798	4804.76
27.3385	292.6629	100	4.9164E+06	806	4853.86
26.6830	292.8586	100	4.9141E+06	852	5112.91
27.4270	293.1827	100	4.9150E+06	860	5161.39
27.5049	293.3059	100	4.9129E+06	906	5415.27
27.5140	293.3855	100	4.9154E+06	914	5463.68
27.5036	293.3793	100	4.9154E+06	926	5534.37
26.9968	293.3471	100	4.9148E+06	972	5791.99
27.3666	293.4631	100	4.9145E+06	1018	6050.60
27.3752	293.4605	100	4.9154E+06	1030	6123.69
27.3747	293.4605	100	4.9154E+06	1060	6308.23
26.4641	293.4438	100	4.9120E+06	1106	6595.67
27.2023	293.8013	100	4.9142E+06	1114	6649.70
27.2561	293.8540	100	4.9153E+06	1122	6704.89
27.2560	293.8517	100	4.9154E+06	1138	6808.27
27.2559	293.8504	100	4.9155E+06	1156	6924.77
27.2559	293.8500	100	4.9155E+06	1178	7058.42
27.2530	293.8025	100	4.9142E+06	1224	7316.30
27.2890	293.8503	100	4.9146E+06	1232	7364.71
27.2872	293.8427	100	4.9152E+06	1246	7445.21
27.2859	293.8390	100	4.9158E+06	1262	7536.50
26.3106	293.7671	100	4.9126E+06	1308	7788.99
26.5415	294.0050	100	4.9146E+06	1316	7837.92
27.0282	294.0439	100	4.9152E+06	1324	7886.33
27.1218	294.1074	100	4.9130E+06	1370	8139.08
27.1269	294.1087	100	4.9148E+06	1384	8219.69
27.1348	294.1188	100	4.9153E+06	1394	8279.75
27.1353	294.1002	100	4.9159E+06	1406	8351.26
27.6365	294.1120	100	4.9148E+06	1452	8608.09

APPENDIX E
CASE #2 RESULTS WITH VARIOUS INITIAL POINTS

Table E-1 Result Table of initial point [250 50 50]

Hydraulic Fracture Spacing (m)	Hydraulic Fracture Half length (m)	Dimensionless Fracture Conductivity	Cumulative Discounted-NPV ($)	#MSFLOW Called	Program Running Time (s)
215.8607	70	49.9873	6.1116E+06	8	155.13
193.4052	102.3289	49.9750	6.1830E+06	16	305.58
172.9058	118.6250	49.9595	6.1986E+06	24	455.97
158.6873	103.2815	49.9175	6.2240E+06	32	605.51
146.2449	88.6700	49.8816	6.2437E+06	40	750.70
131.0742	96.4299	49.8585	6.2579E+06	48	878.46
132.1685	85.6584	49.829	6.2615E+06	56	1006.26
120.6859	82.6910	49.8071	6.2723E+06	64	1133.91
112.3411	84.7458	49.7859	6.2765E+06	72	1261.59
112.3265	84.7799	49.7858	6.2765E+06	96	1617.55
106.2534	94.0340	49.7633	6.2705E+06	142	2289.54
96.5511	68.4243	49.7376	6.2779E+06	150	2417.78
105.1661	70.7801	49.7300	6.2781E+06	160	2576.30
104.4142	69.1770	49.7262	6.2784E+06	172	2763.21
105.6815	69.8677	49.7244	6.2786E+06	186	2979.59
101.8915	73.9888	49.7201	6.2792E+06	198	3167.35
101.9017	73.8825	49.7196	6.2802E+06	216	3438.14
102.3743	73.9481	49.7191	6.2806E+06	234	3708.21
102.3839	73.9726	49.7189	6.2809E+06	256	4036.09
102.3844	73.9735	49.7189	6.2809E+06	294	4592.22
115.6939	101.1576	49.7016	6.2634E+06	340	5260.44
112.9025	86.7927	49.6684	6.2759E+06	348	5387.88
112.9120	86.8090	49.6683	6.2762E+06	374	5771.68
120.6564	93.8667	49.6450	6.2684E+06	420	6442.20
109.1038	85.9746	49.6166	6.2776E+06	428	6574.88
109.1044	85.9743	49.6166	6.2776E+06	464	7108.07
119.6507	81.3182	49.5937	6.2731E+06	510	7776.44
119.9899	83.9777	49.5912	6.2732E+06	524	7988.24
113.8366	69.4518	49.5699	6.2745E+06	532	8115.32
114.4260	69.9611	49.5686	6.2746E+06	546	8327.64
114.5188	69.7842	49.5681	6.2746E+06	564	8598.76
105.3111	72.9441	49.5484	6.2788E+06	572	8729.81

Table E-1 Continued

106.9725	71.9044	49.5462	6.2794E+06	586	8944.34
106.9435	71.7820	49.5459	6.2794E+06	606	9246.68
106.9420	71.7843	49.5459	6.2795E+06	636	9688.74
103.8236	76.5596	49.5293	6.2802E+06	644	9818.64
103.8918	75.2943	49.5121	6.2803E+06	652	9947.30
103.4539	75.3246	49.5116	6.2803E+06	670	10218.24
115.8174	74.0473	49.4923	6.2754E+06	716	10886.86
107.6228	78.5145	49.4743	6.2783E+06	724	11015.21
108.4898	80.2985	49.4721	6.2787E+06	738	11228.80
101.1887	79.2318	49.4615	6.2797E+06	748	11385.65
101.1272	77.4979	49.4592	6.2806E+06	762	11605.97
128.8205	86.8830	49.4405	6.2642E+06	808	12276.18
119.5369	73.4340	49.4139	6.2712E+06	816	12403.34
109.3206	77.2717	49.3956	6.2790E+06	824	12530.77
105.4868	77.0783	49.3933	6.2799E+06	838	12742.24
105.3603	73.8345	49.3911	6.2803E+06	852	12955.19
116.2404	66.6652	49.3746	6.2720E+06	898	13622.20
117.7052	84.0773	49.3599	6.2745E+06	906	13749.65
117.0574	85.0748	49.3570	6.2746E+06	920	13961.54
115.5083	78.2367	49.3510	6.2750E+06	932	14145.04
108.7103	77.5727	49.3325	6.2789E+06	940	14272.20
106.2916	78.1554	49.3122	6.2800E+06	948	14399.31
106.2924	78.1547	49.3122	6.2801E+06	984	14924.34
105.9773	76.9141	49.3099	6.2806E+06	998	15136.48
116.4185	62.6023	49.2911	6.2670E+06	1044	15803.66
96.3053	76.9000	49.2784	6.2779E+06	1052	15942.63
96.6590	78.4334	49.2774	6.2788E+06	1068	16185.73
102.2466	73.5036	49.2571	6.2797E+06	1076	16313.78
102.9212	73.3237	49.2561	6.2810E+06	1092	16555.85
118.2444	72.7992	49.2374	6.2736E+06	1138	17225.27
107.8761	67.0034	49.2191	6.2764E+06	1146	17354.55
105.2712	76.1633	49.2118	6.2797E+06	1156	17510.63
100.9338	76.9959	49.1947	6.2800E+06	1164	17639.00
101.0760	76.4464	49.1941	6.2804E+06	1182	17910.97
101.0892	76.4590	49.1941	6.2804E+06	1212	18349.48
100.6251	76.0122	49.1935	6.2806E+06	1230	18620.12
100.6269	76.0138	49.1935	6.2807E+06	1264	19117.67
100.6274	76.0142	49.1935	6.2808E+06	1302	19671.93

Table E-1 Continued

116.6682	88.8410	49.1749	6.2722E+06	1348	20337.71
113.9164	82.5983	49.1503	6.2761E+06	1356	20464.32
114.5895	80.7962	49.1476	6.2761E+06	1370	20677.83
114.7452	80.7882	49.1468	6.2765E+06	1388	20947.64
114.6117	80.9719	49.1466	6.2765E+06	1410	21273.42
114.9603	80.7197	49.1453	6.2768E+06	1426	21514.93
107.7519	83.2595	49.1403	6.2787E+06	1438	21699.66
106.3557	76.5944	49.1180	6.2790E+06	1446	21830.85
98.7251	72.1544	49.1085	6.2801E+06	1456	21990.06
98.7352	72.1904	49.1084	6.2804E+06	1482	22378.87

Table E-2 Result Table of initial point [100 200 35]

Hydraulic Fracture Spacing (m)	**Hydraulic Fracture Half length (m)**	**Dimensionless Fracture Conductivity**	**Cumulative Discounted-NPV ($)**	**#MSFLOW Called**	**Program Running Time (s)**
104.7970	141.5707	34.7404	6.1915E+06	8	107.89
109.0336	112.4690	34.6843	6.2502E+06	16	215.98
111.6548	94.9783	34.6504	6.2705E+06	24	324.23
107.9502	86.5065	34.6237	6.2765E+06	32	432.88
107.9516	86.5061	34.6237	6.2766E+06	66	856.12
110.8037	82.6857	34.6179	6.2774E+06	78	1013.26
108.2968	85.0873	34.6123	6.2776E+06	90	1170.35
109.3753	80.9506	34.5894	6.2781E+06	98	1279.56
109.9536	80.7271	34.5882	6.2783E+06	114	1484.89
109.8923	80.7573	34.5881	6.2786E+06	138	1787.07
109.9534	80.7290	34.5879	6.2789E+06	160	2079.72
109.9524	80.7295	34.5879	6.2790E+06	196	2552.36
94.2482	88.1010	34.5688	6.2666E+06	242	3154.60
92.1462	64.7681	34.5454	6.2750E+06	250	3267.90
97.0500	61.7590	34.5422	6.2765E+06	262	3428.74
93.9205	63.9081	34.5392	6.2766E+06	274	3586.93
96.4686	64.4808	34.5326	6.2776E+06	284	3720.34
96.4632	64.4838	34.5326	6.2784E+06	314	4097.65
97.9562	70.1617	34.5188	6.2794E+06	322	4207.08
98.4892	70.7124	34.5139	6.2795E+06	334	4364.63
98.9711	70.2253	34.5132	6.2797E+06	352	4595.48

Table E-2 Continued

98.9804	70.2551	34.5131	6.2802E+06	374	4874.62
97.6871	73.6882	34.4946	6.2795E+06	420	5457.13
97.6402	73.6914	34.4946	6.2800E+06	444	5769.08
97.9149	73.7517	34.4943	6.2800E+06	464	6031.45
102.1862	73.3744	34.4898	6.2806E+06	476	6193.08
102.1879	75.5155	34.4707	6.2782E+06	522	6777.15
105.5519	79.4501	34.4660	6.2788E+06	534	6939.09
106.2965	80.3210	34.4648	6.2792E+06	550	7150.39
102.9763	78.4254	34.4619	6.2795E+06	564	7344.76
102.9953	78.2327	34.4613	6.2802E+06	582	7583.21
102.9762	77.7894	34.4589	6.2806E+06	596	7771.52
102.9898	77.4024	34.4583	6.2809E+06	614	8008.67
128.6312	99.5478	34.4389	6.2596E+06	660	8595.66
101.2206	97.4026	34.4091	6.2671E+06	668	8706.31
107.7097	79.2419	34.3791	6.2788E+06	676	8815.44
107.7411	79.1311	34.3789	6.2788E+06	698	9094.46
106.2113	83.5262	34.3689	6.2789E+06	708	9227.72
106.1201	75.5374	34.3586	6.2791E+06	718	9360.84
102.3308	78.9875	34.3536	6.2792E+06	730	9518.79
104.2165	78.8372	34.3523	6.2796E+06	746	9752.36
104.2074	77.0130	34.3429	6.2807E+06	756	9971.97
104.2080	77.0121	34.3429	6.2807E+06	792	10583.32
91.4958	85.8718	38.7381	6.2718E+06	838	11357.73
103.0322	75.8740	38.7155	6.2797E+06	846	11489.34
103.0261	75.8756	38.7155	6.2800E+06	876	11926.90
103.0269	75.8757	38.7155	6.2801E+06	914	12444.71
103.4694	75.8472	38.7152	6.2807E+06	934	12699.40
103.4680	75.8473	38.7152	6.2807E+06	968	13122.82
93.3381	76.4495	38.6960	6.2770E+06	1014	13699.47
100.7414	74.4217	38.6775	6.2802E+06	1022	13815.16
100.1086	73.6081	38.6765	6.2802E+06	1038	14025.72
101.1444	74.5158	38.6754	6.2803E+06	1054	14235.43
101.1452	74.5165	38.6754	6.2804E+06	1090	14692.77
101.2715	74.7091	38.6753	6.2812E+06	1112	14972.99
101.2720	74.7094	38.6753	6.2812E+06	1150	15456.79
115.3406	83.2388	38.6589	6.2751E+06	1196	16036.73
109.7623	80.5027	38.6383	6.2775E+06	1204	16145.32
110.8766	81.9905	38.6357	6.2783E+06	1218	16328.20

Table E-2 Continued

107.7340	80.9214	38.6155	6.2787E+06	1226	16436.66
108.9277	82.0391	38.6128	6.2789E+06	1240	16618.66
106.6959	78.8446	38.5916	6.2801E+06	1248	16727.54
106.6961	78.8443	38.5916	6.2801E+06	1286	17200.35
114.3063	66.0148	38.5716	6.2728E+06	1332	17769.64
106.1230	86.3173	38.5637	6.2770E+06	1340	17878.86
106.3066	86.4278	38.5634	6.2774E+06	1360	18132.54
109.0355	77.0310	38.5517	6.2785E+06	1370	18265.90
108.8494	76.6760	38.5468	6.2785E+06	1382	18424.27
108.4621	79.5351	38.5446	6.2791E+06	1396	18606.16
108.7398	79.4411	38.5440	6.2793E+06	1414	18835.77
108.8859	79.4103	38.5437	6.2794E+06	1434	19090.41
101.2294	77.2453	38.5335	6.2797E+06	1444	19223.41
98.4269	73.2843	38.5289	6.2798E+06	1456	19381.45
100.0047	72.6887	38.5209	6.2804E+06	1466	19515.59
100.0052	72.6943	38.5209	6.2806E+06	1496	19892.32
100.0308	73.0919	38.5203	6.2807E+06	1514	20122.88
117.9976	90.8863	38.5021	6.2711E+06	1560	20693.93
118.0726	90.9622	38.5018	6.2715E+06	1580	20950.90
115.1210	75.5608	38.4891	6.2744E+06	1590	21086.91
115.8838	76.1620	38.4850	6.2755E+06	1602	21246.75

Table E-3 Result Table of initial point [400 120 22]

Hydraulic Fracture Spacing (m)	**Hydraulic Fracture Half length (m)**	**Dimensionless Fracture Conductivity**	**Cumulative Discounted-NPV ($)**	**#MSFLOW Called**	**Program Running Time (s)**
371.1194	138.3497	21.9901	5.8600E+06	8	149.51
346.8715	127.1157	21.8965	5.9086E+06	16	292.03
307.1521	131.6348	21.8475	5.9832E+06	24	434.49
286.5270	123.1832	21.8179	6.0248E+06	32	575.12
270.4653	122.6998	21.7815	6.0526E+06	40	717.02
247.2357	116.3789	21.7385	6.0944E+06	48	859.74
230.6906	112.7621	21.6925	6.1231E+06	56	1004.38
208.4912	111.0486	21.6509	6.1582E+06	64	1146.41
190.0012	110.1415	21.6451	6.1844E+06	72	1288.41
175.3381	102.7169	21.6093	6.2069E+06	80	1431.06
159.8914	111.0677	21.5555	6.2180E+06	88	1577.76

Table E-3 Continued

148.1099	114.4841	31.5555	6.2272E+06	96	1719.98
127.4913	90.9150	31.5143	6.2649E+06	104	1844.15
111.4448	83.3639	41.5143	6.2764E+06	112	1970.71
110.2450	80.7552	41.4933	6.2774E+06	120	2095.35
111.5858	80.3088	41.4907	6.2778E+06	134	2302.86
109.5203	81.8438	41.4882	6.2781E+06	148	2507.75
109.8547	81.7760	41.4878	6.2782E+06	168	2791.68
102.4621	80.8343	41.4776	6.2782E+06	178	2939.18
105.8705	75.9331	41.4726	6.2787E+06	190	3115.14
98.6845	80.8782	41.4627	6.2788E+06	200	3261.99
102.8733	83.0218	41.4574	6.2789E+06	212	3436.29
106.5601	80.4143	41.4361	6.2788E+06	258	4078.45
99.3377	72.7915	41.4271	6.2798E+06	268	4218.78
99.5189	69.4180	41.4252	6.2800E+06	282	4415.04
99.4188	69.5629	41.4250	6.2803E+06	304	4711.67
87.8635	87.2181	41.4136	6.2669E+06	350	5330.53
118.1022	89.1337	41.3900	6.2722E+06	358	5451.02
112.2720	69.6982	41.3623	6.2753E+06	366	5571.78
112.3074	69.6361	41.3622	6.2755E+06	388	5873.89
102.6354	73.2129	41.3509	6.2800E+06	398	6020.47
102.5749	73.3569	41.3499	6.2805E+06	414	6245.98
102.9797	73.9334	41.3457	6.2805E+06	426	6432.89
103.0045	73.9115	41.3457	6.2807E+06	452	6801.87
114.7577	73.2280	41.3268	6.2752E+06	498	7437.14
100.3144	76.2617	41.3176	6.2787E+06	508	7586.78
97.5696	71.9231	41.3132	6.2795E+06	520	7762.85
97.7941	71.9459	41.3122	6.2796E+06	536	7993.14
97.9800	71.8416	41.3117	6.2798E+06	554	8249.03
98.3618	71.9705	41.3098	6.2799E+06	568	8452.40
98.3855	71.9539	41.3096	6.2802E+06	590	8766.23
98.3860	71.9538	41.3096	6.2802E+06	622	9214.01
100.4240	71.3460	41.2950	6.2784E+06	668	9852.61
100.5144	74.0534	41.2910	6.2800E+06	680	10026.93
103.5861	77.5915	41.2862	6.2807E+06	692	10204.60
103.5850	77.5902	41.2862	6.2809E+06	722	10604.83
103.5831	77.5914	41.2862	6.2809E+06	756	11026.01
103.5841	77.5905	41.2862	6.2810E+06	792	11470.20
89.5969	87.8492	41.2671	6.2670E+06	838	12036.33
111.9802	98.3108	41.2555	6.2678E+06	848	12169.04
86.9538	76.7288	41.2276	6.2723E+06	856	12277.41

Table E-3 Continued

116.1563	89.0481	41.2077	6.2730E+06	864	12386.35
111.2035	83.7408	41.1827	6.2765E+06	872	12494.61
108.1474	70.4571	41.1601	6.2785E+06	880	12602.63
101.6917	74.7060	41.1408	6.2800E+06	888	12710.76
101.6740	74.6984	41.1408	6.2803E+06	914	13037.14
101.8769	74.9292	41.1405	6.2803E+06	934	13290.86
101.8306	74.9336	41.1405	6.2807E+06	958	13592.27
115.7205	75.5850	41.1209	6.2757E+06	1004	14160.97
130.0544	79.7014	41.1058	6.2638E+06	1050	14726.60
118.6381	72.5091	41.0855	6.2731E+06	1058	14835.15
108.9942	68.9340	41.0698	6.2771E+06	1066	14944.27
102.9423	75.7652	41.0506	6.2797E+06	1074	15053.23
99.6132	75.5186	41.0461	6.2805E+06	1086	15210.24
100.5890	76.2686	41.0448	6.2806E+06	1102	15415.02
99.2182	73.9650	41.0428	6.2809E+06	1116	15596.64
100.7716	75.5512	41.0406	6.2810E+06	1130	15778.11
114.4951	86.4622	41.0228	6.2748E+06	1176	16345.08
98.4619	77.8271	41.0002	6.2790E+06	1184	16453.73
98.9476	78.6503	40.9979	6.2791E+06	1198	16634.62
103.2813	74.2050	40.9930	6.2795E+06	1210	16791.10
101.6903	74.2201	40.9906	6.2799E+06	1224	16972.68
105.0536	76.7127	40.9863	6.2801E+06	1236	17129.39
105.0300	76.7617	40.9858	6.2805E+06	1254	17358.77
105.0320	76.7585	40.9858	6.2807E+06	1286	17763.02
102.9106	75.1456	40.9834	6.2808E+06	1300	17945.48
118.4832	89.3067	40.9667	6.2718E+06	1346	18513.66
112.6183	72.5852	40.9410	6.2768E+06	1354	18621.76
114.2698	76.8710	40.9359	6.2773E+06	1366	18777.86
114.2776	76.8823	40.9359	6.2773E+06	1396	19150.79

Table E-4 Result Table of initial point [310 250 1]

Hydraulic Fracture Spacing (m)	**Hydraulic Fracture Half length (m)**	**Dimensionless Fracture Conductivity**	**Cumulative Discounted-NPV ($)**	**#MSFLOW Called**	**Program Running Time (s)**
273.7632	173.0963	0.8120	5.9786E+06	8	116.92
255.8926	136.7469	0.7205	6.0667E+06	16	242.31
245.7074	130.0309	0.6934	6.0898E+06	24	368.76

Table E-4 Continued

229.6116	143.4449	0.6593	6.0961E+06	32	494.11
208.6206	129.4178	0.5984	6.1437E+06	40	619.17
189.2686	115.4514	0.5378	6.1825E+06	48	744.34
169.1147	99.9159	0.5153	6.2147E+06	56	869.80
153.4004	94.7904	0.4901	6.2351E+06	64	991.44
128.3107	82.2441	0.4901	6.2670E+06	72	1074.38
136.0155	92.5825	0.4901	6.2571E+06	118	1608.37
125.1470	75.1283	0.4901	6.2677E+06	126	1691.90
124.5405	73.9815	0.4901	6.2679E+06	138	1822.68
124.4162	87.5267	0.4901	6.2682E+06	146	1905.98
124.4852	88.4431	0.4901	6.2684E+06	160	2060.28
114.9227	93.5249	0.4901	6.2704E+06	168	2359.93
116.1443	92.9438	0.4901	6.2718E+06	184	2552.56
99.9092	70.1118	0.4901	6.2795E+06	192	2637.47
96.9540	74.6263	0.4901	6.2797E+06	204	2855.23
105.9324	75.9220	0.4901	6.2798E+06	214	2963.00
105.8738	75.9756	0.4901	6.2802E+06	238	3238.67
104.9433	75.1925	0.4901	6.2803E+06	254	3420.03
105.2910	75.1603	0.4901	6.2803E+06	272	3622.89
105.2937	75.1574	0.4901	6.2804E+06	304	3992.02
105.2944	75.1582	0.4901	6.2804E+06	340	4415.29
116.3859	75.5788	0.4901	6.2752E+06	386	4976.93
96.6457	82.3366	0.4901	6.2760E+06	394	5066.30
106.1034	85.9536	0.4901	6.2767E+06	404	5180.23
104.6063	87.0311	0.4901	6.2771E+06	418	5343.66
104.6007	87.0349	0.4901	6.2773E+06	448	5710.97
104.6012	87.0352	0.4901	6.2774E+06	486	6181.55
121.1340	96.3388	0.4901	6.2663E+06	532	6739.37
115.0924	84.6305	0.4901	6.2753E+06	540	6822.94
101.0867	83.7575	0.4901	6.2775E+06	550	6930.27
103.6843	73.6186	0.4901	6.2795E+06	560	7037.73
99.7935	74.4239	0.4901	6.2803E+06	572	7170.04
99.7998	74.4308	0.4901	6.2804E+06	602	7518.61
100.7735	75.3762	0.4901	6.2807E+06	618	7697.66
114.6686	87.2921	0.4901	6.2737E+06	664	8274.73
115.0983	87.0180	0.4901	6.2748E+06	680	8468.90
98.8045	81.9588	0.4901	6.2765E+06	688	8562.67
96.3438	80.5337	0.4901	6.2780E+06	700	8718.02

Table E-4 Continued

81.2138	77.0679	0.4901	6.2642E+06	746	9354.94
102.5155	87.9494	0.4901	6.2757E+06	754	9456.02
97.0911	84.5914	0.4901	6.2763E+06	764	9580.47
103.6265	76.0125	0.4901	6.2810E+06	772	9675.20
120.2485	82.9762	0.4901	6.2729E+06	818	10306.47
114.478	82.5102	0.4901	6.2755E+06	826	10405.62
97.6692	79.1240	0.4901	6.2772E+06	834	10504.94
102.7348	81.5201	0.4901	6.2776E+06	846	10660.56
97.0360	79.3920	0.4901	6.2780E+06	856	10783.16
108.1337	76.8226	0.4901	6.2797E+06	866	10896.29
95.2676	65.7925	0.4901	6.2768E+06	912	11480.56
98.3453	73.6061	0.4901	6.2794E+06	920	11567.84
97.6063	72.7970	0.4901	6.2798E+06	938	11779.07
98.9737	72.8125	0.4901	6.2803E+06	948	11889.79
101.0487	74.2277	0.4901	6.2806E+06	962	12050.29
101.5841	74.5050	0.4901	6.2808E+06	980	12260.80
115.4044	89.2822	0.4901	6.2730E+06	1026	12816.57
110.8636	81.3657	0.4901	6.2783E+06	1034	12904.36
106.8510	80.9508	0.4901	6.2793E+06	1046	13041.25
115.4189	88.9951	0.4901	6.2721E+06	1092	13600.67
98.6289	80.2205	0.4901	6.2780E+06	1100	13687.72
103.4522	81.8008	0.4901	6.2784E+06	1112	13823.90
102.7319	81.5409	0.4901	6.2789E+06	1128	14009.27
106.2915	76.5201	0.4901	6.2792E+06	1140	14147.22
106.1159	78.0259	0.4901	6.2792E+06	1154	14308.72
105.9738	78.8072	0.4901	6.2796E+06	1170	14495.02
106.0819	78.8719	0.4901	6.2798E+06	1192	14757.07
104.1979	72.8711	0.4901	6.2807E+06	1202	14885.94
104.3506	76.6430	0.4901	6.2800E+06	1248	15505.24
128.8560	52.1163	0.4901	6.2354E+06	1294	16090.30
109.4668	72.1120	0.4901	6.2768E+06	1302	16182.15
104.8109	74.2236	0.4901	6.2789E+06	1310	16273.08
107.6404	76.6715	0.4901	6.2790E+06	1322	16415.11
105.2470	75.3598	0.4901	6.2798E+06	1330	16506.24
103.5387	76.9128	0.4901	6.2801E+06	1344	16674.33
100.3855	74.2790	0.4901	6.2804E+06	1352	16765.21
100.3877	74.2773	0.4901	6.2804E+06	1386	17192.61

Table E-4 Continued

100.3870	74.2765	0.4901	6.2805E+06	1422	17652.98
100.3868	74.2762	0.4901	6.2805E+06	1462	18172.66